

Histidine phosphorylation in proteins -  
A characterization of phosphohistidines in  
the bacterial transcription factor GlcT of  
*Bacillus subtilis*

**I n a u g u r a l d i s s e r t a t i o n**

zur  
Erlangung des akademischen Grades  
doctor rerum naturalium (Dr. rer. nat.)  
an der Mathematisch-Naturwissenschaftlichen Fakultät  
der  
Ernst-Moritz-Arndt-Universität Greifswald

vorgelegt von  
Sebastian Himmel  
geboren am 30.03.1982  
in Beeskow

Greifswald, April 2011

Dekan: .....Prof. Dr. K. Fesser.....

1. Gutachter: .....Prof. Dr. K. Weisz.....

2. Gutachter: .....Prof. Dr. H. Oschkinat.....

Tag der Promotion: .....13. Juli 2011.....

**Results of my work were published or contributed to publications:**

D. D. Rodríguez, C. Grosse, S. Himmel, C. González, I. M. de Ilarduya, S. Becker, G. M. Sheldrick, I. Usón "Crystallographic *ab initio* protein structure solution below atomic resolution", Nature Methods, Vol. 6, No. 9, 651-653 (2009)

S. Himmel, S. Wolff, S. Becker, D. Lee, C. Griesinger "Detection and Identification of Protein-Phosphorylation Sites in Histidines through HNP Correlation Patterns", Angewandte Chemie Intern. Ed., Vol. 49, No. 47, 8971-8974 (2010)

S. Himmel, S. Wolff, S. Becker, D. Lee, C. Griesinger "Nachweis und Identifizierung von Protein- Phosphorylierungen in Histidinen mithilfe von HNP-Korrelationen", Angewandte Chemie, Vol. 122, No. 47, 9155-9158 (2010)

# Table of Contents

<b>1</b>	<b>Introduction</b>	<b>7</b>
1.1	Histidine phosphorylation in proteins . . . . .	7
1.2	The bacterial sugar Phosphotransferase System (PTS) and the role of a transcriptional antiterminator: GlcT . . . . .	8
1.3	Characteristics of phosphohistidines . . . . .	11
1.4	Detection of histidine phosphorylation . . . . .	12
1.5	Goal of this dissertation . . . . .	14
<b>2</b>	<b>Materials &amp; Methods</b>	<b>16</b>
2.1	General materials . . . . .	16
2.1.1	Important chemicals . . . . .	16
2.1.2	Important materials & Enzymes . . . . .	18
2.1.3	Software . . . . .	20
2.1.4	Growth media & Antibiotics . . . . .	20
2.1.5	Vectors . . . . .	22
2.2	General methods . . . . .	23
2.2.1	DNA plasmid purification & Sequencing . . . . .	23
2.2.2	PCR: DNA cloning primers . . . . .	23
2.2.3	PCR: Cloning & Mutagenesis . . . . .	25
2.2.4	DNA agarose gel electrophoresis . . . . .	26
2.2.5	Plasmid transformation . . . . .	27
2.2.6	Denaturing SDS-PAGE . . . . .	27
2.2.7	Determination of protein concentration . . . . .	29
2.3	Protein sequence . . . . .	29
2.4	Protein constructs . . . . .	29
2.5	Protein expression & Purification . . . . .	31
2.5.1	Cell lysis . . . . .	31
2.5.2	Nucleic acid precipitation by polyethylenimine (PEI) . . . . .	31
2.5.3	Nickel-nitrilotriacetic acid (Ni-NTA) agarose affinity chromatography . . . . .	32
2.5.4	Purification of GST-fusion proteins . . . . .	33
2.5.5	Proteolytic cleavage with TEV-protease . . . . .	33
2.5.6	Concentrating of proteins . . . . .	34



2.5.7	Size exclusion chromatography (gel filtration)	34
2.5.8	PRDI	34
2.5.9	PRDII	36
2.5.10	RBD-PRDI	39
2.5.11	Enzyme I (EI)	41
2.5.12	Enzyme II-AB (EII-AB)	42
2.5.13	HPr	43
2.6	Specialized methods	45
2.6.1	Phosphoramidate (PA) synthesis	45
2.6.2	Analytical gel filtration & Sample preparation	45
2.6.3	Mass spectrometry & Sample preparation	45
2.6.4	RNA synthesis (RAT RNA)	47
2.6.5	Electrophoretic mobility shift assay (EMSA)	48
2.6.6	Nuclear magnetic resonance spectroscopy (NMR)	49
<b>3</b>	<b>The new HNP-experiment</b>	<b>51</b>
3.1	Summary	57
<b>4</b>	<b>The PRDI of the antiterminator GlcT</b>	<b>58</b>
4.1	Composition of the PRDI phosphorylation mix	59
4.2	Regiochemistry of PRDI phosphohistidines	62
4.3	Sample optimization for mass spectrometry	63
4.4	Quantification of PRDI phosphorylation	64
4.5	Histidine phosphorylation sites in PRDI	66
4.6	Specificity of PRDI phosphorylation	71
4.7	Summary	76
<b>5</b>	<b>The PRDII of the antiterminator GlcT</b>	<b>77</b>
5.1	Regiochemistry of PRDII phosphohistidines	78
5.2	Quantification of PRDII phosphorylation	81
5.3	Histidine phosphorylation sites in PRDII	84
5.4	Specificity of PRDII phosphorylation	85
5.5	Summary	91
<b>6</b>	<b>1,3-diphosphohistidines in proteins</b>	<b>92</b>
<b>7</b>	<b>Discussion and comparison between PRDI and PRDII</b>	<b>94</b>
7.1	Conclusion	99
<b>8</b>	<b>References</b>	<b>102</b>
<b>9</b>	<b>Appendix</b>	<b>112</b>
<b>10</b>	<b>Curriculum Vitae</b>	<b>127</b>
<b>11</b>	<b>Acknowledgement</b>	<b>128</b>

# Abbreviations

<b>1-phosphohistidine</b>	N <sup>δ1</sup> phosphorylated histidine
<b>1,3-diphosphohistidine</b>	N <sup>δ1</sup> and N <sup>ε2</sup> phosphorylated histidine
<b>3-phosphohistidine</b>	N <sup>ε2</sup> phosphorylated histidine
<b>Ac</b>	Acetate
<b>ATP</b>	Adenosine triphosphate
<b>BglG</b>	β-glucoside specific antiterminator protein in <i>Escherichia coli</i> (transcription factor)
<b>CAT</b>	co-antiterminator
<b>EI</b>	first member of the PTS: Enzyme I (part of the general PTS)
<b>EII<sub>Glc</sub> / EII</b>	carbohydrate specific member of the PTS: Enzyme II (part of the specific PTS); the AB fragment was used in this work
<b>GlcT</b>	Glucose specific antiterminator protein in <i>Bacillus subtilis</i> (transcription factor, member of the BglG family)
<b>GST</b>	Glutathione S-transferase
<b>HNP-NMR</b>	Nuclear Magnetic Resonance correlation spectroscopy combining <sup>1</sup> H, <sup>15</sup> N and <sup>31</sup> P nuclei
<b>HPr</b>	second member of the PTS: histidine containing phosphocarrier protein (part of the general PTS)
<b>LicT</b>	β-glucoside specific antiterminator protein in <i>Bacillus subtilis</i> (transcription factor, member of the BglG family)
<b>NMR</b>	Nuclear Magnetic Resonance spectroscopy
<b>OD</b>	optical density (measured at 600 nm)
<b>PA</b>	Phosphoramidate
<b>PEP</b>	Phosphoenolpyruvate
<b>PRD</b>	PTS regulation domain
<b>PTS</b>	Phosphoenolpyruvate: sugar phosphotransferase system (bacterial system to transport carbohydrates)
<b>ptsGHI</b>	operon induced by glucose and controlled by the GlcT protein, encoding EII <sub>Glc</sub> , EI and HPr
<b>RAT</b>	Ribonucleic antiterminator
<b>RBD</b>	RNA-binding domain (N-terminal domain of antiterminator proteins)
<b>SacY</b>	sucrose specific antiterminator protein (transcription factor, member of the BglG family)
<b>TEV protease</b>	tobacco etch virus protease
<b>UV</b>	ultraviolet electromagnetic radiation ranging from 10 to 400 nm

# 1 Introduction

## 1.1 Histidine phosphorylation in proteins

Phosphorylation is defined as "the addition of a phosphate ( $\text{PO}_4$ ) group" to a target molecule<sup>1</sup>. Small molecules such as adenosine triphosphate (ATP), phosphoramidate (PA) and phosphoenolpyruvate (PEP) are various phosphate donor molecules, which often phosphorylate proteins. In general, protein phosphorylation is wide spread and is considered as an essential posttranslational modification. This modification involves the modulation of the biological activity, subcellular location, half life and docking with other proteins [Cohen, 2000]. Although one of the common targets for such phosphorylations are histidine amino acids [Attwood *et al.*, 2007], histidine phosphorylation was neglected for quite a long time because of the difficulties in phosphohistidine detection [Klumpp and Krieglstein, 2002]. Recently, histidine phosphorylation has been found to be involved in many biological processes and thus investigation of histidine phosphorylated proteins has become an emerging interest [Puttick *et al.*, 2008].

Over decades, histidine phosphorylation was assumed to occur only in prokaryotic cells [Parkinson, 1993, Thomason and Kay, 2000]. Two prominent examples are the prokaryotic two component cell signalling system [Robinson and Stock, 1999] and the bacterial sugar phosphotransferase system (PTS) [Meadow *et al.*, 1990], which will be described in the following section. However, histidine phosphorylation has also been found among eukaryotic cells [Thomason and Kay, 2000, Steeg *et al.*, 2003].

---

<sup>1</sup><http://en.wikipedia.org/wiki/Phosphorylation>

## 1.2 The bacterial sugar Phosphotransferase System (PTS) and the role of a transcriptional antiterminator: GlcT

The bacterial phosphotransferase system (PTS) is a paramount example of histidine phosphorylation. It well illustrates that the phosphorylation of histidines plays a fundamental role in the uptake and utilization of carbohydrates for the glycolysis in prokaryotes. As shown in Figure 1.1 a) phospho(enol)pyruvic acid (PEP) transfers a phosphate to Enzyme I (EI) and this phosphate is cascaded sequentially to the histidine-containing phosphocarrier protein (HPr), Enzyme II (EII) and glucose, through histidine phosphorylations.

This PTS is also regulated by histidine phosphorylation on the transcriptional level through antiterminator proteins (for reviews see [van Tilbeurgh and Declerck, 2001, Deutscher *et al.*, 2006]). One of the first identified antiterminator proteins was BglG which regulates the uptake of  $\beta$ -glucosides in *Escherichia coli* [Amster-Choder and Wright, 1992, Amster-Choder and Wright, 1997]. Another well known antiterminator protein (LicT), which regulates the  $\beta$ -glucoside metabolism in *Bacillus subtilis*, was biochemically and structurally studied in the recent years [Declerck *et al.*, 1999, van Tilbeurgh *et al.*, 2001, Graille *et al.*, 2005]. A variety of homologous antiterminators of different specificities have been identified [Greenberg *et al.*, 2002]. Among them, our model system GlcT specifically regulates the uptake of glucose in *Bacillus subtilis*, which is the preferred carbon and energy source for these bacteria.

The GlcT antiterminator protein acts as a transcription factor, which modulates the expression level of the PTS gene products encoded by the ptsGHI operon [Bachem and Stülke, 1998]. "ptsG", "ptsH" and "ptsI" encode the glucose specific EII, EI and HPr proteins, respectively. The function of GlcT in the context of the PTS is summarized and shown in Figure 1.1.

GlcT is a 288 amino acids protein comprising three domains, which are common for proteins of the BglG family of transcriptional antiterminators. The N-terminus starts with the RNA-binding domain (RBD), followed by two PTS regulation domains (PRDs) known as PRDI and PRDII. In the presence of glucose, GlcT forms a dimer to bind its RNA-binding motif and stabilizes the specific RNA antiterminator target structure formed by this motif (RAT; Figure 1.1 a). In the absence of glucose the constitutive stable terminator motif causes efficient termination of the transcription (Figure 1.1 b) because GlcT forms an inactive

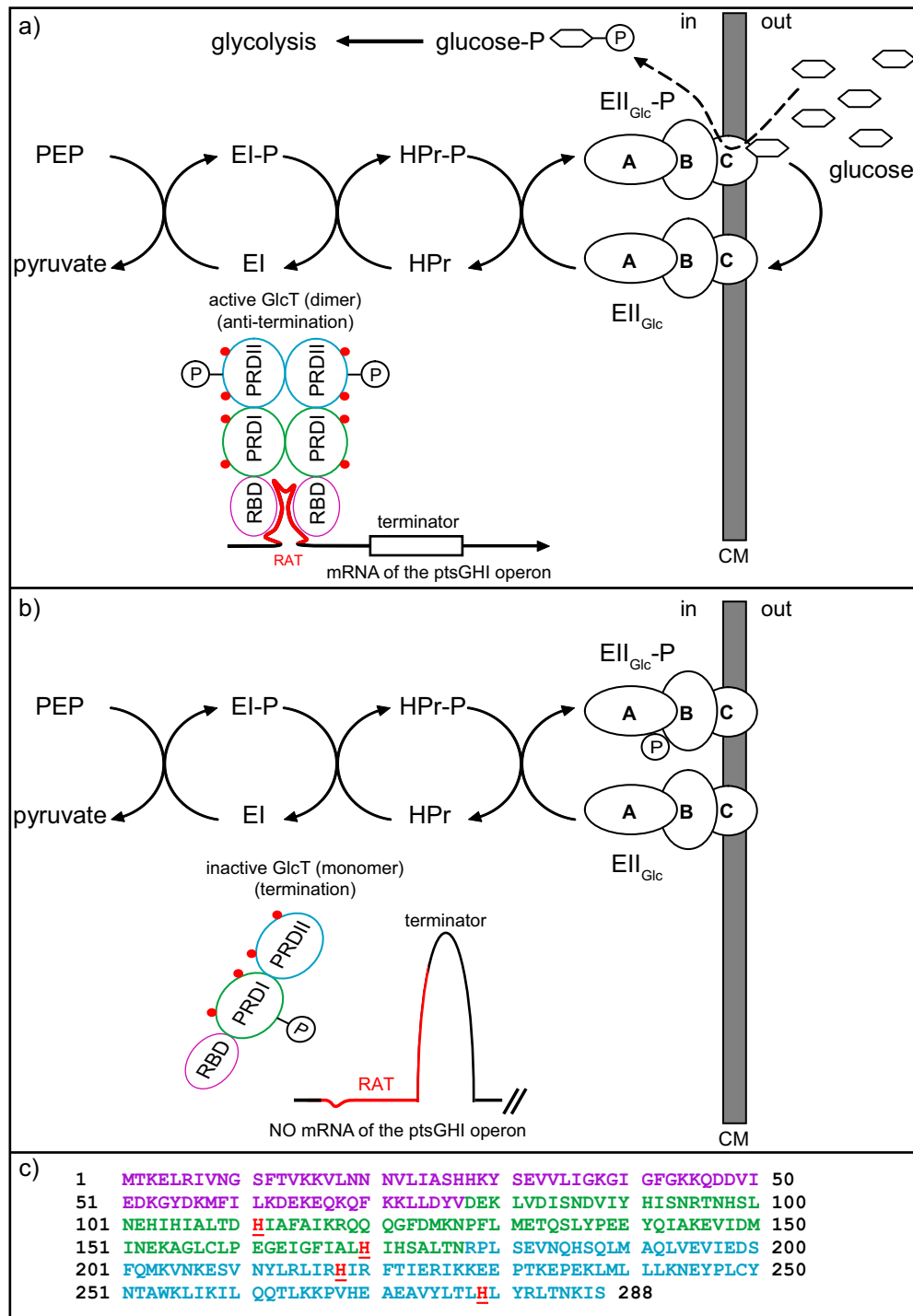


**Figure 1.1:** GlcT and its regulatory function in a) the presence of glucose and b) the absence of glucose. The full length sequence of GlcT is shown in c) (section: 2.3). A colour code is used to highlight domain boundaries as follows: purple = RBD (RNA-binding domain), green = PRDI (PTS regulation domain I) and blue = PRDII (PTS regulation domain II). The same colour code is used in a) and b). CM indicates the cell membrane. Conserved histidine residues are underlined and highlighted in red in c). In a) and b) these conserved histidines are illustrated as red dots and phosphate groups are drawn only schematically. In the presence of glucose (a) the dimeric transcription factor GlcT binds to its RAT (Ribonucleic Antiterminator Target; shown in red in a and b) motif to prevent transcriptional termination. Consequently, mRNAs of EII<sub>Glc</sub>, EI and HPr are synthesized. In the absence of glucose (b) the phosphorylation of the PRDI domain of GlcT leads to an inactive monomeric state not capable to bind the RAT motif. Hence, the transcriptional terminator is active.

monomer upon PRDI phosphorylation. Only upon binding of dimeric GlcT to its RAT motif this RAT structure is stabilized and hence, the terminator is destabilized which causes *ptsGHI* transcription (Figure 1.1 a). Thus, the process of termination/antitermination requires binding of dimeric GlcT and consequently leads to a protein-dependent riboswitch mechanism, which is based on the existence of alternative, mutually exclusive RNA structures [Schilling *et al.*, 2004]. One of these structures is the transcriptional terminator, whereas the alternative structure (RAT) prevents the formation of the terminator and allows transcription elongation to proceed. The RAT sequence (shown in red in Figure 1.1 a and b) is part of the terminator region, which constitutes the protein-dependent riboswitch [Schilling *et al.*, 2004].

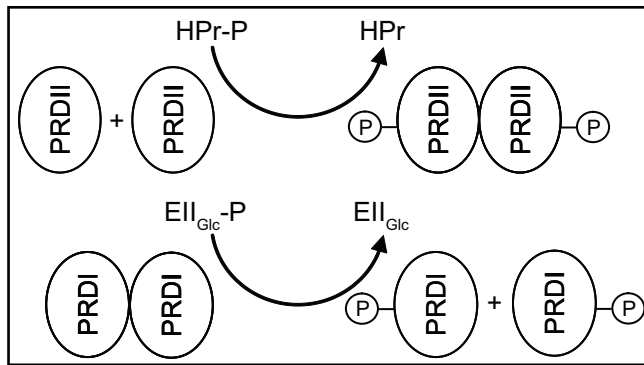


**Figure 1.2:** Phosphorylation states of PRDI and PRDII of GlcT and their aggregation behaviour. Dimerization of PRDII is triggered by HPr-dependent phosphorylation of monomeric PRDII whereas inactivation of GlcT is achieved upon phosphorylation of dimeric PRDI. This PRDI phosphorylation leads to GlcT monomerization and is driven by  $EII_{Glc}$ -dependent phosphorylation in the absence of glucose.

$EII_{Glc}$  (Enzyme II) is a three domain enzyme, which has a membrane integrated 'C'-domain to incorporate glucose from the outer environment (Figure 1.1). EI and HPr are considered as general members of the PTS because their presence is needed for even more regulatory processes. Hence, the expression level of those two proteins is controlled by additional promoter elements forming a constitutive *ptsHI* operon [Stülke *et al.*, 1997].

Interestingly, homology studies revealed that antiterminator proteins usually comprise four highly conserved histidine

residues, two in each of the two PRDs [Greenberg *et al.*, 2002]. It is proposed and generally accepted that these conserved residues are essential in the regulatory processes leading to active or inactive states of GlcT upon their phosphorylation. In GlcT these conserved histidines are residues 111 and 170 in PRDI and 218 and 279 in PRDII (Figure 1.1 c).

In the absence of glucose PRDI is phosphorylated by the carbohydrate specific Enzyme II (EII) whereas PRDII is phosphorylated by HPr [Schmalisch *et al.*, 2003]. The latter HPr-dependent phosphorylation of PRDII is not as manda-

tory as for homologous proteins, such as LicT or BglG [Schmalisch *et al.*, 2003]. Interestingly, the phosphorylation of histidines in both PRDs results in opposite effects. Whereas PRDI phosphorylation leads to the inactive monomeric form of GlcT, phosphorylation of PRDII stabilizes the dimer. Thus, different members of the PTS are involved in the antagonistic regulation pathway of transcriptional antitermination. In Figure 1.2 the consequences upon PRDI and PRDII phosphorylation are summarized. The non-phosphorylated PRDI and the phosphorylated PRDII strongly favour the dimeric aggregation state of GlcT. The formation of the RNA-protein complex is supposed to take place only upon binding to dimeric GlcT [Schmalisch *et al.*, 2003].

The specific characteristics of phosphorylated histidines are discussed in the following section.

### 1.3 Characteristics of phosphohistidines

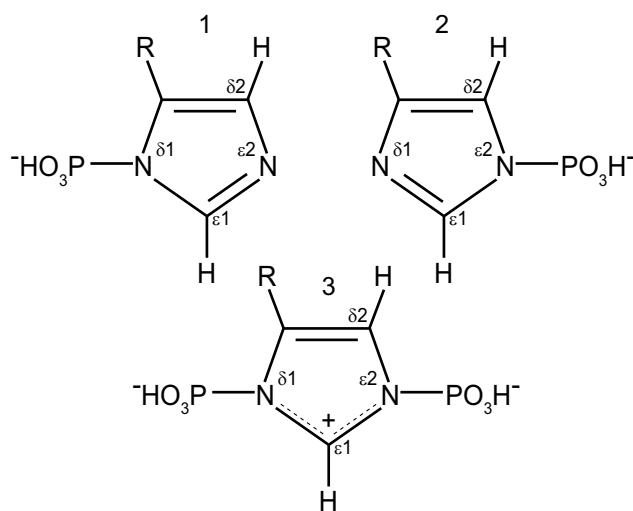


**Figure 1.3:** Illustration of all possible histidine phosphorylation states: 1) 1-phosphohistidine ( $\delta 1$ -phosphorylation), 2) 3-phosphohistidine ( $\epsilon 2$ -phosphorylation), 3) 1,3-diphosphohistidine ( $\delta 1$ ,  $\epsilon 2$ -diphosphorylation).

Unlike well studied phosphoserine, phosphothreonine and phosphotyrosine, which contain phosphoester bonds, phosphohistidines form a covalent phosphoramidate bond between the phosphorus and the imidazole nitrogen atoms (N-PO<sub>3</sub>). Phosphoramidates are significantly different compared to phosphoester bonds (O-PO<sub>3</sub>). Hydrolysis of P-N bonds of histidines in proteins release a higher energy ( $\Delta G^\circ = -12$  to  $-14$  kcal mol<sup>-1</sup>) than phosphoester bonds ( $\Delta G^\circ = -6.5$  to  $-9.5$  kcal mol<sup>-1</sup>) pointing already to the ability of an efficient phosphate transfer to other target molecules [Besant and Attwood, 2009].

Also, a clear difference in pH stability is observed between phosphoramidates and phosphoesters. Whereas phosphoester bonds are stable under acidic conditions phosphoramidates undergo rapid hydrolysis and are stabilized under basic pH conditions. The loss of stability at low pH is a main reason that the detection and characterization of phosphohistidines in proteins was difficult for quite a long time. Since most techniques, such as mass spectrometry, require or at least prefer acidic conditions (which are suitable to detect phosphoesters), histidine phosphorylations were left undiscovered and unnoticed [Macek *et al.*, 2007].

Another difference between phosphoramidates and phosphoesters is the regiochemistry of phosphorylation. Phosphoester of serine, threonine or tyrosine are restricted to their specific functional hydroxyl groups of these amino acids. The imidazole of histidines provides two nitrogen atoms called  $\delta 1$  and  $\epsilon 2$  which are the potential phosphorylation targets. In Figure 1.3 all possible phosphorylation states and their nomenclature are summarized.

The following labelling schemes are known:  $\delta 1$ -phosphorylation which is also known as 1-phosphohistidine,  $\epsilon 2$ -phosphorylation (3-phosphohistidine) and  $\delta 1$ -,  $\epsilon 2$ -diphosphorylation (1,3-diphosphohistidine). The two nitrogen phosphorylation sites are significantly different in their stability. Over the entire pH range 1-phosphohistidine is more labile and has a shorter half life time than 3-phosphohistidine [Hultquist *et al.*, 1966, Hultquist, 1968]. This reduced half life time is caused by the  $\alpha$ -amino group of histidine, which has a destabilizing effect on the  $\delta 1$ -phosphorylation site and, hence, promotes the hydrolysis of 1-phosphohistidine.

Due to their chemical nature the detection of phosphohistidines is challenging and will be explained in the following section.

## 1.4 Detection of histidine phosphorylation

All attempts to characterize phosphohistidines involve very time consuming and cumbersome methods. First of all two main issues can be identified: i) to prove the presence of a phosphorylated histidine and ii) which nitrogen site is phosphorylated, addressing the question of the regiochemistry. Further questions arise for proteins comprising several histidine residues. In this situation experiments are needed to identify how many and which histidines are phosphorylated in the protein sequence. The characteristics of phosphohistidines can be used to identify histidine phosphorylation. pH- and temperature dependent hydrolysis studies have



revealed whether the phosphate bond is sensitive to certain pH conditions, allowing to distinguish between phosphoesters and phosphoramidates [Amster-Choder and Wright, 1997]. The regiochemistry of histidine phosphorylation can be determined by comparing the pH- and temperature-dependent hydrolysis rates of the N-P bond to free phosphohistidines [Hultquist *et al.*, 1966]. This allows to distinguish between  $\delta 1$ - and  $\epsilon 2$  phosphorylation sites. However, hydrolysis rates of phosphohistidines in proteins can differ compared to free phosphohistidines due to the protein environment. In addition, pH- and/or temperature-dependent titration series can often convert proteins from a folded into a partially or even totally unfolded state, which most likely affects hydrolysis rates. Furthermore, denaturation and precipitation of a target protein leads to the loss of the sample, which hinders a complete data accumulation through the experiment [Dooijewaard *et al.*, 1979]. Another practical problem is that hydrolysed phosphate needs to be separated from the protein sample and quantified. In order to achieve this separation, additional chromatographic methods such as reverse phase thin layer chromatography (RP-TLC) need to be performed. Frequently, radioactively labelled  $^{32}\text{P}$ -phosphate is used to detect and quantify phosphorylations [Waygood *et al.*, 1985, Besant *et al.*, 1998, Besant *et al.*, 2000].

Free phosphohistidines are often deployed as reference compounds for phosphorylated histidines in proteins. Similar to hydrolysis studies,  $^{31}\text{P}$  NMR was used for chemical shift comparisons [Bock and Sheard, 1975, Fujitaki *et al.*, 1981, Vogel *et al.*, 1982, Brauer and Sykes, 1984, James, 1985, James, 1985, Vogel *et al.*, 1989]. Due to  $^{31}\text{P}$  phosphorus's favourable properties for NMR, no isotope enrichment is necessary to carry out  $^{31}\text{P}$  NMR experiments. NMR spectroscopy also allows to perform experiments under conditions appropriate for the target protein (e. g. pH).  $^{31}\text{P}$  chemical shifts of phosphorylated histidines were measured in 1D NMR experiments to distinguish between all phosphorylation states in order to identify and verify histidine phosphorylation in proteins [Surette *et al.*, 1996]. However, individual chemical shift variations due to the protein environment might arise and, eventually, data interpretation becomes difficult or even impossible to specify the regiochemistry of the phosphohistidine. The low dispersion of  $^{31}\text{P}$  chemical shifts of all species of phosphohistidines (ranging from approx. 0 to -10 ppm) makes it more likely that chemical shifts obtained from a phosphoprotein do not agree with the chemical shifts gained from free phosphohistidines. In one instance the regiochemistry of an unfolded phosphoprotein could be only determined by  $^{31}\text{P}$  NMR using short reference peptides instead of free phosphohistidines [Lecroisey *et al.*, 1995].

Histidine phosphorylations can be indirectly observed by  $^{15}\text{N}$  chemical shift effects in long range 2D  $^1\text{H}$ ,  $^{15}\text{N}$ -correlation spectra [Pelton *et al.*, 1993, Zhou and

Dahlquist, 1997]. Those  $^{15}\text{N}$  chemical shifts of phosphohistidines, which are ranging approx. from 200 to 210 ppm, also show low dispersion similar to the  $^{31}\text{P}$  chemical shifts. Unfortunately, various reasons can cause additional chemical shift differences such as pH, temperature or solvent effects. Hence, both 1D  $^{31}\text{P}$  and 2D  $^1\text{H}, ^{15}\text{N}$ -spectra fail to give a direct and reliable proof of phosphorylated histidines, especially in proteins. However, 2D  $^1\text{H}, ^{15}\text{N}$ -long range experiments are preferred and necessary in order to determine  $\text{pK}_a$  values and to study the tautomeric conditions of histidines, since chemical shifts are sensitive to the protonation of imidazole nitrogen atoms [Pelton *et al.*, 1993, Zhou and Dahlquist, 1997, Garrett *et al.*, 1998].

Another important biophysical method to investigate phosphohistidines is mass spectrometry. In recent years proteins have been successfully investigated to identify histidine phosphorylations [Zu *et al.*, 2007]. The process of collision-induced dissociation (CID), commonly used to generate peptide fragments during tandem mass spectrometry (MS-MS), may result in a loss of phosphate, depending on the residue and the collision energy used. The loss of 80 Da, which results from the loss of a phosphate group ( $\text{HPO}_3$ ), is characteristic for phosphoramidates in phosphohistidines [Ross, 2007]. Commonly, a tryptic proteolysis and subsequent enrichment of the peptides is performed to improve the sensitivity for mass spectrometric experiments. Hence, sample conditions for such experiments (pH, temperature and time) need to be adjusted in order to preserve the stability of phosphoramidates. However, despite all the recent advancements in sample preparation and method optimization the characteristic loss of 80 Da does not allow to distinguish between both nitrogen sites in the imidazole of phosphohistidines.

Other experimental approaches, such as native gel analysis often need very specialized experimental conditions (e. g. regarding pH, buffer composition and gel preparation) [Niepmann, 2007]. Observed bands are often blurred and other conditions affecting the migration process can be observed and need to be correctly interpreted. At best, a qualitative proof of general phosphorylation can be seen in combination with radioactively labelled  $^{32}\text{P}$ . However, no direct evidence of phosphates, which are attached to histidine sidechains is supplied. Furthermore, no information regarding the regiochemistry is provided.

## 1.5 Goal of this dissertation

A combined technique giving both the evidence of phosphohistidines and providing regiochemistry information of phosphorylated histidines is still in need. A spec-

troscopic method, which does not rely on radioactively labelled material or time consuming titration series is highly desired. My goal was to develop and establish a new Nuclear Magnetic Resonance (NMR) spectroscopy technique to address the issue of histidine phosphorylation in proteins and its regiochemistry. By applying this new NMR technique, I wanted to gain new insight in the regulatory histidine phosphorylation of the bacterial antiterminator protein GlcT from *Bacillus subtilis*. The GlcT-dependence of the PTS is a fundamental regulatory pathway of glucose utilization and depends on histidine phosphorylation. Hence, it was my goal to study and characterize the phosphohistidines in each regulatory domain (PRDI, PRDII) individually.

This goal included determining the number of phosphate groups, which are involved in the phosphorylation process of each domain. I wanted to optimize the sample conditions for mass spectrometry in order to detect the phosphoprotein within a complex phosphorylation mix of three enzymes (Enzyme I, HPr and the target protein). It was further my goal to combine NMR and mass spectrometry to specify, which histidine(s) is (are) phosphorylated in the protein sequence. Finally, I wanted to study differences in the aggregation states upon phosphorylation by analytical gel filtration to validate possible functional consequences.

It has been proposed that both PRDs are specialized in the choice of their phosphorylation partners [Schmalisch *et al.*, 2003]. Hence, by applying the methods mentioned above, I wanted to gain insight into why PRDI interacts with Enzyme II and PRDII with HPr.

## 2 Materials & Methods

In this chapter a summary of the used materials, chemicals and methods is given. Detailed descriptions can be found in textbooks such as [Lottspeich, Zorbas; Bioanalytik; Spektrum Verlag].

### 2.1 General materials

#### 2.1.1 Important chemicals

Compound	Supplier
1,4-Dithio-D,L-Threitol (DTT)	Gerbu Biotechnik GmbH
2-Methyl-2,4-pentanediol (MPD)	Fluka
2-propanol	Merck
Acrylamide (Rotiphorese Gel 30, 37.5:1)	Carl Roth
Acrylamide bis, ready to use solution 40 % (19:1)	Merck
Agar	AppliChem
Agarose (Electrophorese Grade)	Invitrogen
Ammonia solution 25 %	Merck
Ammonium- <sup>15</sup> N chloride ( <sup>15</sup> NH <sub>4</sub> Cl)	isotec
Ammonium acetate (NH <sub>4</sub> Ac)	Merck
Ammonium chloride (NH <sub>4</sub> Cl)	Carl Roth
di-Ammonium hydrogen phosphate (NH <sub>4</sub> ) <sub>2</sub> HPO <sub>4</sub>	Fluka
Ammonium peroxodisulphate (APS)	Carl Roth
Ampicillin Sodium salt	Carl Roth
Bromophenol blue Sodium salt	Carl Roth
Chloramphenicol	ICN Biomedicals Inc.
Complete (EDTA / EDTA free)	Roche
Coomassie Brilliant Blue G 250	Carl Roth
Dodecylsulfate Sodium salt	Serva
Ethidium bromide (10 mg/ml solution)	Carl Roth

Compound	Supplier
Ethylenediamine tetraaceticacid (2x Na <sup>+</sup> , 2x H <sub>2</sub> O) (EDTA)	Carl Roth
Gentamycin sulfate	Carl Roth
Glacial acetic acid	Merck
<sup>13</sup> C <sub>6</sub> -D-Glucose	Spectra Stable Isotopes
D(+)-Glucose monohydrate	Merck
Glutathione Sepharose 4B	GE Healthcare
Glycerol	Merck
Glycine	Merck
HEPES	Carl Roth
<sup>15</sup> N <sub>3</sub> -histidine	isotec
Imidazole <sup>15</sup> N <sub>2</sub>	isotec
Imidazole	Carl Roth
Isopropyl-β-D-thiogalactopyranosid (IPTG)	AppliChem
Kanamycin sulfate	Carl Roth
Magnesium chloride hexahydrate (MgCl <sub>2</sub> 6x H <sub>2</sub> O)	Carl Roth
Magnesium sulfate heptahydrate (MgSO <sub>4</sub> 5x H <sub>2</sub> O)	Merck
Ni-NTA Agarose	Qiagen
Pefabloc (protease inhibitor)	Carl Roth
Phenylmethylsulfonyl fluoride (PMSF)	Carl Roth
Phospho(enol)pyruvic acid tri(cyclohexylammonium) salt	Sigma
Phospho(enol)pyruvic acid trisodium salt	Sigma
Phospho(enol)pyruvic acid monopotassium salt	Sigma
Phosphoramidate (PA)	this work
Poly (ethyleneimine) solution (50 %) (PEI)	Sigma
Polyethylene glycol 3350 (PEG 3350)	Hampton Research
Potassium chloride (KCl)	Merck
Potassium dihydrogen phosphate (KH <sub>2</sub> PO <sub>4</sub> )	Carl Roth
Sodium chloride (NaCl)	Merck
Sodium dihydrogen phosphate (NaH <sub>2</sub> PO <sub>4</sub> )	Merck
di-Sodium hydrogen phosphate (Na <sub>2</sub> HPO <sub>4</sub> )	Merck
Sodium hydroxide (NaOH)	Merck
Sodium iodide (NaI)	Fluka
N,N,N',N'-Tetramethylethylenediamine (TEMED)	Sigma
Thiamine chloride hydrochloride	Merck
Tris(hydroxymethyl)aminomethane (Tris)	VWR
Triton X-100	Merck
Tryptone / Pepton from casein	Carl Roth
Yeast extract	Carl Roth

**Table 2.1:** List of relevant chemicals used during this work in alphabetical order.

## 2.1.2 Important materials & Enzymes

Name	Product & Supplier
Balances	Bp 3100 S; Sartorius A 210 S; Sartorius
Centrifuges	Avanti J-20 & J-30I; Beckmann-Coulter rotors: JLA 8.100, JLA 9.100, JLA 16.250, JA 25.50 Ti, JA 30.50 Ti; Beckmann-Coulter 5415D; Eppendorf 5804; Eppendorf 5415C; Eppendorf
Concentrators	Vivaspin 2, 6, 20 ml, MWCO: 5,000 & 10,000; Sartorius
Dialysis	Tube-O-DIALYZER ( 1K MWCO, Micro); G-Bioscience Spectra / Por membranes; Carl Roth
DNA-kits	midi prep: Nucleo Bond PC 100; Macherey-Nagel plasmid purification: Nucleo Spin Plasmid; Macherey-Nagel
Electrophoresis	SDS-PAGE: Mini-PROTEAN 3 Cell; BioRad Agarose gel: Sub-Cell GT Mini; BioRad Power Pac 300; BioRad
Freezer	VIP series -86°C MDF-U71V; SANYO Hera freeze -80°C; Heraeus Instr. Comfort -20°C; Liebherr
Filtration	Rotilabo steril filters 0.22 $\mu$ m; Carl Roth
FPLC	Äkta prime, basic, purifier; GE Healthcare Superdex 75 (16/60); GE Healthcare Superdex 75 (10/300); GE Healthcare
Imaging (gels)	DC120 zoom, digital science; Kodak TFX-20M Transilluminator, life Technologies
Incubator	Multitron HT; Infors AG Certomat R; B. Braun Biotech Intern. B6 function line; Hereaus Instr.
Lyophilisation	Christ Alpha 2-4; B. Braun Biotech Intern.
Marker (DNA)	$\lambda$ / <i>HindIII</i> (2); Fermentas $\phi$ X 174 DNA/ BsuRI ( <i>HaeIII</i> ) (9); Fermentas
Marker (protein)	BenchMark protein ladder 10747-012; Invitrogen
Mass spectrometry	Micromass ZQ 4000; Waters

Name	Product & Supplier
NMR	AVANCE I 400; Bruker AVANCE I 600 cryo; Bruker AVANCE III 600; Bruker AVANCE I 700 cryo; Bruker AVANCE III 700; Bruker (Oxford magnet) AVANCE III 800; Bruker AVANCE I 900; Bruker NMR sample tubes 5 mm; Hilgenberg NMR Shigemi tubes 5 mm; Shigemi Corp.
PCR	Phusion, High-Fidelity PCR Master Mix; New England Biolabs Quickchange II Site-Directed Mutagenesis Kit; Stratagene Hot Star Taq; Qiagen
pH Meter	PB11 + PY-P10; Sartorius SevenEasy; Mettler Toledo Spintrode pH NMR electrode; Hamilton
Protein purification	5 ml / 10 ml single use plastic column, PIERCE
Restriction enzymes	Fermentas & New England Biolabs (NdeI, BamHI, EcoRI, SalI)
Sonication	SONOPULS HD 2200 + UW 2200; Bandelin SONOPULS GM 3100 + UW 3100; Bandelin
thermocycler	HYBIAD PCR sprint; Perkin Elmer
UV/VIS spectroscopy	UV/VIS spectrometer; Hewlett-Packard DU-70 spectrophotometer; Beckman

**Table 2.2:** List of relevant materials and enzymes used during this work in alphabetical order.

### 2.1.3 Software

Software	Provider	Reference
Cara (1.8.4)	<a href="http://cara.nmr.ch/doku.php">http://cara.nmr.ch/doku.php</a>	
Igor Pro (4.04)	<a href="http://www.wavemetrics.com/">http://www.wavemetrics.com/</a>	
NmrPipe/NmrDraw	<a href="http://spin.niddk.nih.gov/bax/software/NMRPipe/info.html">http://spin.niddk.nih.gov/bax/software/NMRPipe/info.html</a>	[Delaglio <i>et al.</i> , 1995]
pyMOL (0.99rc6)	<a href="http://pymol.org/">http://pymol.org/</a>	
swiss-PdbViewer (4.01)	<a href="http://www.expasy.org/spdbv/">http://www.expasy.org/spdbv/</a>	
TOPSPIN (2.0/2.1)	Bruker <a href="http://www.bruker-biospin.com/nmr.html">http://www.bruker-biospin.com/nmr.html</a>	
Vector NTI 8	InforMax, Inc.; Invitrogen, <a href="http://www.invitrogen.com/site/us/en/home/LINNEA-Online-Guides/LINNEA-Communities/Vector-NTI-Community/vector-nti-software.html">http://www.invitrogen.com/site/us/en/home/LINNEA-Online-Guides/LINNEA-Communities/Vector-NTI-Community/vector-nti-software.html</a>	

**Table 2.3:** List of special software, which was used in this work.

### 2.1.4 Growth media & Antibiotics

Name	Chemical	Amount	Remarks
M9 minimal medium	ddH <sub>2</sub> O	758 ml	autoclaved
	Trace elements	10 ml	filtered
	Thiamine HCl (5mg ml <sup>-1</sup> )	6 ml	filtered
	CaCl <sub>2</sub> (2 M)	50 µl	filtered
	MgSO <sub>2</sub> (1 M)	2 ml	filtered
	Glucose (4 g l <sup>-1</sup> )	20 ml	filtered
	NH <sub>4</sub> Cl (1 g l <sup>-1</sup> )	1 ml	filtered
	M9 salts (5x)	200 ml	autoclaved
M9 salts (5x)	Na <sub>2</sub> HPO <sub>4</sub>	33.9 g	final pH 7.4
	KH <sub>2</sub> PO <sub>4</sub>	15.0 g	
	NaCl	2.5 g	
	ddH <sub>2</sub> O	add to 1 L	
Trace elements	FeSO <sub>4</sub> 7x H <sub>2</sub> O	0.6 g	important order



Name	Chemical	Amount	Remarks
Trace elements	MnCl <sub>2</sub> 4x H <sub>2</sub> O	0.115 g	
	CoCl <sub>2</sub> 6x H <sub>2</sub> O	0.08 g	
	ZnSO <sub>4</sub> 7x H <sub>2</sub> O	0.07 g	
	CuCl <sub>2</sub> 2x H <sub>2</sub> O	0.03 g	
	H <sub>3</sub> BO <sub>4</sub>	0.002 g	
	(NH <sub>4</sub> ) <sub>6</sub> Mo <sub>7</sub> O <sub>24</sub> 4x H <sub>2</sub> O	0.025 g	
	ddH <sub>2</sub> O	add to 100 ml	filter the mixture
LB(lysogeny broth) medium	Tryptone	10 g	final pH 7.2
	Yeast extract	5 g	[Bertani, 1951]
	NaCl	10 g	[Bertani, 2004]
	ddH <sub>2</sub> O	add to 1 L	autoclave the mixture
2x YT	Tryptone	16 g	
	Yeast extract	10 g	
	NaCl	5 g	
	ddH <sub>2</sub> O	add to 1 L	autoclave the mixture
Ampicillin (stock)	Ampicillin (sodium salt)	25 mg ml <sup>-1</sup>	in H <sub>2</sub> O
Kanamycin (stock)	Kanamycin	70 mg ml <sup>-1</sup>	in H <sub>2</sub> O
IPTG (stock)	Isopropyl- $\beta$ -D-thiogalactopyranosid	1 M	in H <sub>2</sub> O
Agar plates	Agar	3 g	[Hitchens and Leikind, 1939]
	LB medium	200 ml	

**Table 2.4:** List of compounds used for media preparation and antibiotics. The media were supplemented with appropriate amounts of antibiotics prior to the expression. For liquid media ampicillin was diluted 1:500, for agar plates 1:250. Kanamycin was diluted 1:1000 for both liquid media as well as for agar plates.

### 2.1.5 Vectors

The protein constructs, which are listed in Table 2.10 were cloned into the expression vectors that are shown in Figure 2.1.

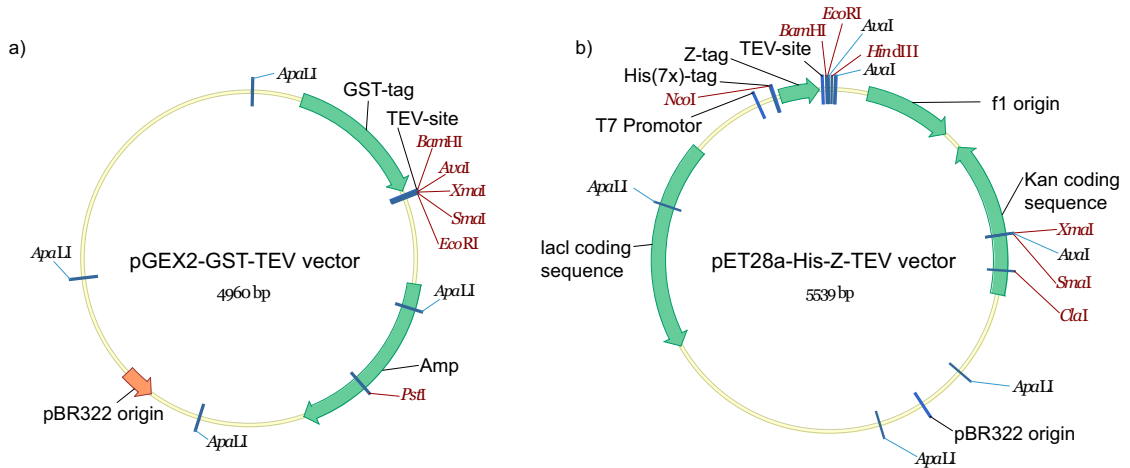


**Figure 2.1:** Two expression vectors were mainly used for protein overexpression during this work. In a) the pGEX vector is shown, which was used for the overexpression of PRDI. This vector encodes an N-terminal GST fusion protein (in the figure: GST-tag). In b) the pET28a vector is shown, which encodes a hepta-histidine tag (in the figure: His(7x)-tag) fused to the Z-domain (in the figure: Z-tag). This vector was used for the overexpression of PRDII and RBD-PRDI. Specific restriction sites are indicated. Genes, encoding for antibiotic resistance are indicated by Amp (ampicillin) and Kan (kanamycin). In both vectors there is a TEV cleavage site between the fusion tag and the target protein (in the figure: TEV-site).

## 2.2 General methods

### 2.2.1 DNA plasmid purification & Sequencing

DNA plasmid purification was carried out using the "Nucleo Bond midi prep kit" (Macherey-Nagel) following the protocol of the supplier. After DNA purification, final UV absorption was measured at 260 and 280 nm UV wavelength and multiplied by a factor of 50 to obtain approximately the plasmid concentration in  $\mu\text{g ml}^{-1}$ .

DNA sequencing was done by the Seqlab company (Göttingen)<sup>2</sup>. For successful sequencing the  $A_{260}/A_{280}$  ratio is recommended to be 1.6 or higher. Samples for sequencing were prepared as follows: approx. 600 ng of plasmid DNA were mixed with 2  $\mu\text{l}$  of sequencing primers (10  $\mu\text{M}$ ) and ddH<sub>2</sub>O was added to a final volume of 7  $\mu\text{l}$ .

### 2.2.2 PCR: DNA cloning primers

DNA cloning primers were purchased from Invitrogen and IBA GmbH<sup>3</sup>. The melting temperatures ( $T_m$ ) of the PCR cloning primers were calculated according to the following formula [Marmur and Doty, 1962]:  $T_m = 69.3 + 41(\frac{G+C}{N}) - (\frac{650}{N})$  where N is the primer length in bases and G+C the summation of guanine and cytosine bases within the sequence. PCR was carried out according to section 2.2.3.

Mutagenesis primers were designed following the formula for  $T_m$  calculation:  $T_m = 81.5 + 41(\frac{G+C}{N}) - (\frac{675}{N}) - \%mismatch$  where "%mismatch" is given in whole numbers reflecting the number of mutated bases based on the primer length. Detailed information is given in the instruction manual of the mutagenesis kit.

Cloning and mutagenesis primers are listed in Table 2.5.

---

<sup>2</sup><http://www.seqlab.de/>

<sup>3</sup><http://www.iba-go.com/index.html>

Name.	5' - 3' Sequence	Construct	Remarks
PRD3	CGA CAT ATG GGA TCC CGT CCG CTG TCC GAG GTC	(GlcT) PRDII	forw., into pGEX2TEV (BamHI & NdeI)
PRD4	GGA AAG CTT GAA TTC TCA TTG GTT AAT CGG TAT CAG ATG AAG C	(GlcT) PRDII	rev., into pGEX2TEV (EcoRI & HindIII)
PRD7	CGA CAT ATG GGA TCC AAG CTC CTT GAC TAT GTT GAT GAA AAG C	(GlcT) PRDI	forw., into pGEX-2TEV (BamHI & NdeI)
PRD8	GGA AAG CTT GAA TTC CTG ATT GAC CTC GGA CAG CG	(GlcT) PRDI	rev., into pGEX2TEV (EcoRI & HindIII)
PRD9	CGA GGA TCC CAT ATG GCA CAA AAA ACA TTT AAA GTA ACT GCA G	(HPr) full	forw., into pET16bTEV (BamHI & NdeI)
PRD10	CGG GAA TTC GGA TCC TCA CTC GCC GAG TCC TTC GCT T	(HPr) full	rev., into pET16bTEV (BamHI & EcoRI)
PRD18	CGA GGA TCC CAT ATG ACA AAG GAG CTG AGG ATC GTG	(GlcT) RBD	forw., into pGEX2TEV (BamHI & NdeI)
PRD21	GGA AAG CTT GAA TTC TCA CTG ATT GAC CTC GGA CAG CG	(GlcT) PRDI <sub>185</sub>	rev., into pGEX2TEV (EcoRI & HindIII)
PRD22	GGA AAG CTT GAA TTC TCA GTT TGT CAA CGC TGA ATG GAT ATG C	(GlcT) PRDI <sub>177</sub>	rev., into pGEX2TEV (EcoRI & HindIII)
PRD24	CAT ATG GGA TCC GAT GAA AAG CTC GTT GAT ATT TCA AAC G	(GlcT) PRDI <sub>178</sub>	forw., into pGEX2TEV (BamHI & NdeI)
PRD25	C GCT CTG CAT ATC GCT TCA GCG TTG ACA AAC TGA G	(GlcT) PRDI	mutagenesis primer H172A (forw.)
PRD26	C TCA GTT TGT CAA CGC TGA AGC GAT ATG CAG AGC G	(GlcT) PRDI	mutagenesis primer H172A (rev. complement)
PRD29	CTA TTT GCG GCT GAT CAG GGA TAT CAG ATT TAC AAT AGA AAG	(GlcT) PRDII	mutagenesis primer H218D (forw.)
PRD30	CTT TCT ATT GTA AAT CTG ATA TCC CTG ATC AGC CGC AAA TAG	(GlcT) PRDII	mutagenesis primer H218D (rev. complement)
PRD31	GCG GTT TAT CTG ACG CTT GAT CTG TAC CGA TTA ACC	(GlcT) PRDII	mutagenesis primer H279D (forw.)
PRD32	GGT TAA TCG GTA CAG ATC AAG CGT CAG ATA AAC CGC	(GlcT) PRDII	mutagenesis primer H279D (rev. complement)
PRD33	CAC ATT GCG TTG ACA GAC GAC ATC GCA TTT GCG ATC	(GlcT) PRDI	mutagenesis primer H111D (forw.)
PRD34	GAT CGC AAA TGC GAT GTC GTC TGT CAA CGC AAT GTG	(GlcT) PRDI	mutagenesis primer H111D (rev. complement)
PRD35	G ATT GGT TTT ATC GCT CTG GAC ATC CAT TCA GCG TTG AC	(GlcT) PRDI	mutagenesis primer H170D (forw.)
PRD36	GT CAA CGC TGA ATG GAT GTC CAG AGC GAT AAA ACC AAT C	(GlcT) PRDI	mutagenesis primer H170D (rev. complement)

**Table 2.5:** A selection of PCR primers used for cloning and mutagenesis. All sequences are given in 5' to 3' direction.

### 2.2.3 PCR: Cloning & Mutagenesis

The polymerase chain reaction (PCR) is a molecular biology tool for efficient DNA amplification [Saiki *et al.*, 1988]. For DNA amplification 100 ng template DNA were mixed with 2  $\mu$ l (10  $\mu$ M) primer solution (forward and reverse) and 20  $\mu$ l "Phusion" master mix solution, containing buffer, polymerase and dNTP's (New England-BioLabs, "Phusion" kit). ddH<sub>2</sub>O was added up to a final volume of 40  $\mu$ l.

"QuickChange II Site-Directed Mutagenesis Kit" (Stratagene) was used for site directed mutagenesis. 20 ng of template DNA were mixed with 5  $\mu$ l 10x reaction buffer, 125 ng of each mutagenesis primer (forward and reverse), 1  $\mu$ l dNTP's and 1  $\mu$ l *PfuUltra* HF DNA polymerase. The final volume of 50  $\mu$ l was adjusted by adding ddH<sub>2</sub>O.

Experimental conditions for all PCR experiments are summarized in Table 2.6.

Step	Temperature	Time	Cycles	Remarks
initial denaturation	98°C	30 sec	1	
denaturation	98°C	20 sec		
annealing	55°C	30 sec	25	
extension	72°C	30 sec		15-30 sec/kb
final extension	72°C	10 min	1	

**Table 2.6:** The table shows the PCR parameters for the amplification using plasmid DNA as template. For the amplification using genomic DNA (*Bacillus subtilis*) the initial denaturation time was prolonged to 2 min, the annealing time was set to 20 seconds and the number of amplification cycles was increased to 28. For site directed mutagenesis experiments all denaturation steps were performed at 95°C and the denaturation length in each cycle was set to 30 sec. The annealing time was increased to 1 min at 55°C and the extension was carried out with 1 min per kb of plasmid length at 68°C. For single base mutations the number of cycles was 16.

The PCR fragments were digested with restriction enzymes (Fermentas, NEB) and purified by agarose gel electrophoresis (for further information see section: 2.2.4). After the electrophoresis the "Nucleo Spin Plasmid Kit" (Macherey-Nagel) was used for the purification according to the protocol of the supplier.

The ligation into host plasmid DNA was carried out by mixing the vector DNA with an excess of target DNA. 1  $\mu$ l T4-ligase, 1.5  $\mu$ l 10x ligase buffer and ddH<sub>2</sub>O were added for a final volume of 15  $\mu$ l. The ligation was performed overnight

in a 14°C water bath. After ligation the plasmid DNA was transformed into XL2blue host cells (see section: 2.2.5). These cells were spread onto LB agar plates containing appropriate antibiotics and were incubated overnight at 37°C. Colony PCR (Hot Star Taq polymerase; Qiagen) was used to confirm the presence of the insert. Colonies were picked and mixed with 2.5 µl 10x PCR buffer, 0.2 µl dNTP's (25 mM), 1 µl of forward and reverse primers (10 µM), 0.125 µl polymerase and 20.2 µl ddH<sub>2</sub>O. 1 ml 2x YT medium was heated to 37°C and mixed with 3 µl of the PCR mixture to start cell growth. The amplified fragments were analysed by agarose gel electrophoresis (see section: 2.2.4).

Plasmids, mutated by site directed mutagenesis, were directly transformed into XL2blue host cells without further plasmid purification. Prior to transformation *Dpn I* restriction enzyme was used to digest parental template DNA for one hour at 37°C.

Colonies, verified by DNA sequencing, were stored at -80°C. For this purpose 150 µl 50 % glycerol were mixed with 350µl of cells grown at 37°C in 2x YT medium for several hours.

## 2.2.4 DNA agarose gel electrophoresis

Agarose gel electrophoresis was used to separate mixtures of DNA molecules and/or to estimate the size of such fragments [Brody and Kern, 2004]. Agarose gels were prepared as follows: 0.4 g agarose was dissolved in 40 ml 1x Tris-EDTA-Borate (TBE) buffer by heating the solution to 100°C for a few minutes. 1 µl of Ethidium bromide was added after the solution was cooled down to about 40°C. Gels were prepared in BioRad gel boxes. Electrophoresis was performed at room temperature for 30 to 120 minutes with constant 60 mV in 1x TBE buffer. A DNA ladder (Fermentas) was used as molecular weight standard. Gel pictures were taken with the "DC120 zoom, digital science" camera from Kodak.

Name	Chemicals	Amounts
5x TBE	Tris	445 mM (54 g)
	Boric acid	445 mM (27.5 g)
	EDTA	0.01 mM (20 ml 0.5 mM stock)
	ddH <sub>2</sub> O	add to 1 L

**Table 2.7:** Chemical composition used for one liter of 5x TBE buffer.

### 2.2.5 Plasmid transformation

Plasmids verified by DNA sequencing were transformed into *E. coli* strains. XL2blue host cells were used for DNA preparation and BL21 strains for high yield protein overexpression. A summary of host strains is given in Table 2.8. Plasmid transformation was performed by heat shock. 0.5 to 1  $\mu$ g of purified plasmid DNA were incubated on ice along with an aliquot of competent host cells for 30 minutes, followed by 40 seconds of heat shock at 42°C and another two minutes incubation on ice. Cells were mixed with one ml of 2x YT medium (37°C) and incubated at 37°C for 60 to 120 minutes. Grown cells were centrifuged at room temperature (1500 *ref*, 4 minutes) and spread onto LB agar plates, containing appropriate antibiotics, for overnight incubation (37°C).

Strain	Genotype	Reference
XL2blue	recA1 endA1 gyrA96 thi-1 hsdR17 supE44 relA1 lac [F'proAB lacI <sup>q</sup> Z $\Delta$ M15Tn10 (Tet <sup>r</sup> ) Amy Cam <sup>r</sup> ]	Stratagene
BL21 (DE3)	F <sup>-</sup> , <i>ompT</i> , <i>hsdS</i> <sub>B</sub> ,( <i>r</i> <sub>B</sub> <sup>-</sup> , <i>m</i> <sub>B</sub> <sup>-</sup> ), <i>dcm</i> , <i>gal</i> $\lambda$ (DE3)	[Grodberg and Dunn, 1988]
BL21	F <sup>-</sup> , <i>ompT</i> , <i>hsdS</i> <sub>B</sub> ,( <i>r</i> <sub>B</sub> <sup>-</sup> , <i>m</i> <sub>B</sub> <sup>-</sup> ), <i>dcm</i> , <i>gal</i>	[Grodberg and Dunn, 1988]

**Table 2.8:** List of bacterial strains used in this work.

### 2.2.6 Denaturing SDS-PAGE

Sodium dodecylsulfate polyacrylamide gel electrophoresis (SDS-PAGE) was used to verify and analyse proteins by their molecular weight [Laemmli *et al.*, 1970]. For this purpose separating and stacking gels containing 12 to 15 % and 3 % acrylamide were used, respectively. A list of buffers and solutions is shown in Table 2.9. The electrophoresis was performed at room temperature and with constant 25 mA per gel in a BioRad gel chamber. An appropriate molecular weight protein ladder (BenchMark protein ladder 10747-012; Invitrogen) was used as molecular weight marker (Figure 2.2). Pictures were taken with the "DC120 zoom, digital science" camera from Kodak.

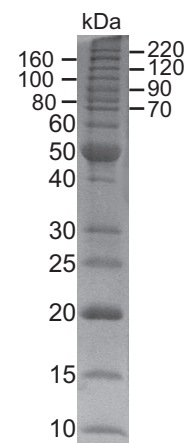


**Figure 2.2:** The 10747-012 molecular weight ladder (Invitrogen)

Name	Chemicals	Amounts	Remarks
Stacking gel	acrylamide	0.5 ml	(Rotiphorese)
	ddH <sub>2</sub> O	3.76 ml	
	Tris HCl 1M	0.626 ml	pH 6.8
	APS (10 %)	50 $\mu$ l	stored at - 20°C
	SDS (10 %)	50 $\mu$ l	
	TEMED	4 $\mu$ l	stored at - 4°C
Separation gel	acrylamide	4.3 ml	(Rotiphorese)
	ddH <sub>2</sub> O	3 ml	
	Tris HCl 1M	2.5 ml	pH 8.8
	APS (10 %)	100 $\mu$ l	stored at - 20°C
	SDS (10 %)	100 $\mu$ l	
	TEMED	4 $\mu$ l	stored at - 4°C
Coomassie staining solution	Coomassie blue G250	2.2 g	
	ddH <sub>2</sub> O	650 ml	
	glacial acetic acid	100 ml	
	2-propanol	250 ml	
sample buffer (4 x)	SDS (10 %)	8.5 ml	
	Tris HCl 1M	3.75 ml	pH 6.8
	glycerol	11.5 ml	
	bromophenol blue	25 mg	
	ddH <sub>2</sub> O	25 ml	
Running buffer (10 x)	Tris	151.5 g (1.25 M)	
	Glycine	720.5 g (9.6 M)	
Electrophoresis buffer	SDS	0.9 g	
	running buffer (10 x)	90 ml	
	ddH <sub>2</sub> O	add to 900 ml	

**Table 2.9:** List of chemicals and solutions used for SDS-PAGE. The amounts refer to two gels. The sample buffer was prepared without 2-mercaptoethanol for long time storage at -20°C. Prior to use 10  $\mu$ l of 2-mercaptoethanol were added to 1 ml of sample buffer.



### 2.2.7 Determination of protein concentration

Protein concentrations were determined by UV absorption at 280 nm based on extinction coefficient calculation [Gill and Hippel, 1989]. The extinction coefficient  $A_{280}$  is available from analytical tools such as Protparam within the Expasy internet portal<sup>4</sup>.

The concentration of proteins containing no tryptophane (W), tyrosine (Y) and cysteine (C) residues can be determined by measuring UV absorption at 205 and 280 nm. The calculation of the concentration was performed as follows:  $A_{205}(1mg/ml) = 27 + 120(A_{280}/A_{205})$  as described previously [Scopes, 1974].

A brief overview about both methods is given by [Kelly *et al.*, 2005].

## 2.3 Protein sequence

All constructs listed in Table 2.10 were derived from the GlcT full length protein sequence, which is shown in Figure 1.1 c)<sup>5</sup>. Plasmid DNA and genomic DNA of *Bacillus subtilis* were provided by the group of Prof. Dr. Jörg Stülke, Department of General Microbiology, University of Göttingen.

## 2.4 Protein constructs

Protein constructs that were designed and used in this study are listed in Table 2.10. All constructs were stored at -20°C.

Different PRDI constructs were designed according to Table 2.10 to optimize the spectral quality of NMR experiments. The length of PRDI constructs varied between 100 and 114 amino acids.

---

<sup>4</sup><http://www.expasy.org/tools/protparam.html>

<sup>5</sup>[http://srs.ebi.ac.uk/srsbin/cgi-bin/wgetz?-e+\[EMBLCDS:CAB13261\]+-newId](http://srs.ebi.ac.uk/srsbin/cgi-bin/wgetz?-e+[EMBLCDS:CAB13261]+-newId)

Name	Length	Vector	Tag	Restrict. Sites	M [Da]
HP <sub>r</sub> <sup>6</sup>	1-88	pET16bTEV	His	NdeI & BamHI	9383.5 / 11353.6
RBD-PRDI	1-177	pET28aZ2TEV	His-Z	BamHI & EcoRI	20606.6
PRDI	78-177				11586.1
PRDI	72-185				13946.8
PRDI H172A	78-185	pGEX2TEV	GST	BamHI & EcoRI	12444.0
PRDI H111D	78-177				11564.0
PRDI H170D	78-177				11564.0
PRDII					13431.8 / 23581.8
PRDII H218D					
PRDII H279D	178-288	pET28aZ2TEV	His-Z	BamHI & SalI	23559.7
PRDII H218D, H279D					23537.7

**Table 2.10:** Protein constructs used or designed for experimental work. All sequences were derived from *Bacillus subtilis*. Mutations are indicated by their one-letter code and its positions. Values given in the "Length" column are based on the full length coding sequence (Figure 1.1 c). Relevant protein masses for mass spectrometry are given. Protein masses comprising the purification tag are given as additional values in the last column. For PRDI, constructs of different lengths were designed and used.

<sup>6</sup>[http://www.subtiwiki.uni-goettingen.de/wiki/index.php/HP\\_r](http://www.subtiwiki.uni-goettingen.de/wiki/index.php/HP_r)

## 2.5 Protein expression & Purification

All proteins were expressed either in LB (for mass spectrometry or analytical gel filtration) or in M9 minimal medium (for uniformly isotope enriched NMR samples). Cells were grown for 4 to 5 hours at 37°C in 1 ml of 2x YT medium. 50  $\mu$ l were transferred into 20 ml of either LB or M9 media for overnight cultivation (37°C). The overnight culture was added to 1 L of LB or M9 media. The GlcT-domains were expressed overnight at 22°C. For this purpose, the temperature was lowered to 22°C after an optical density (OD<sub>600</sub>) of 0.5 to 0.6 was reached. Protein overexpression was induced by adding isopropyl  $\beta$ -D-1-thiogalactopyranoside (IPTG; final concentration: 0.3 to 0.5 mM). HPr, Enzyme I (EI) and the AB-fragment of Enzyme II (EII) were either overexpressed at 37°C approx. for 12 hours or overnight at 22°C. Upon reaching stationary phase (OD<sub>600</sub>: approx. 2.0) the cells were harvested by centrifugation (7500 rcf, 20 to 30 minutes at 4°C) and either directly lysed for protein purification or stored at -80°C.

### 2.5.1 Cell lysis

Cell pellets were thawed on ice and resuspended in approx. 40 ml of lysis buffer (His-tagged proteins; Table 2.11) or 1x PBS buffer (GST-fusion proteins; Table 2.12). Protease inhibitors (PMSF, Carl Roth; Complete TM, Roche) were used optionally. The resuspended cells were sonicated 8 to 9 times for 20 seconds (80 to 90 % of the maximal output). The lysate was centrifuged for 45 to 60 minutes at 48,000 rcf (4°C).

### 2.5.2 Nucleic acid precipitation by polyethylenimine (PEI)

Proteins containing the RNA binding domain (RBD) were treated with polyethylenimine (PEI) to remove unspecifically bound nucleic acids. On ice, PEI was added to a final concentration of 0.2 % (stock: 10 %) to the supernatant obtained after the cell lysis. The soluble fraction was separated by centrifugation for 45 to 60 minutes at 48,000 rcf (4°C).

### 2.5.3 Nickel-nitrilotriacetic acid (Ni-NTA) agarose affinity chromatography

Enzyme I, Enzyme II and HPr were purified as His(7x)-tagged proteins. In the case of PRDII and RBD-PRDI a His(7x)-Z fusion protein was attached to the N-terminus to improve the protein expression and protein stability. The Z-tag comprises 58 amino acids (approx. 6 kDa) and is derived from the B domain of protein A from *Staphylococcus aureus* [Chen *et al.*, 2006]. To purify PRDII and RBD-PRDI the His(7x)-tag was used as described in this section.

Proteins containing a His-tag were purified by Ni<sup>2+</sup> chelating affinity chromatography. For this purpose the supernatant (after cell lysis or nucleic acid precipitation) was incubated (one hour at 4°C) with 3 to 4 ml of Ni-NTA agarose (Qiagen) for 1 L of cell culture. Prior to incubation Ni-NTA agarose was equilibrated with lysis buffer (Table 2.11). The agarose resin loaded with the protein was washed first with 5 to 10 ml of lysis buffer (5 mM imidazole) followed by 5 to 10 ml wash buffer (20 mM imidazole; optional for HPr purification). The elution was carried out by adding stepwise 5 ml elution buffer (4 to 5 times; 250 mM imidazole). The eluted protein was either used for proteolytic TEV cleavage or concentrated using Vivaspin concentrators (Sartorius; section: 2.5.6).

Name	Chemicals	Amounts	Remarks
Lysis buffer	Tris HCl	20 mM	pH 7.9
	NaCl	300 mM	
	Imidazole	5 mM	
	PMSF	330 µl/100 ml	optional
	Complete	1 tablet/100 ml	optional
Wash buffer	Tris HCl	20 mM	pH 7.9
	NaCl	300 mM	
	Imidazole	20 mM	
	PMSF	330 µl/100 ml	optional
	Complete	1 tablet/100 ml	optional
Elution buffer	Tris HCl	20 mM	pH 7.9
	NaCl	300 mM	
	Imidazole	250 mM	
	PMSF	330 µl/100 ml	optional
Gel filtration buffer	Tris HCl	50 mM	pH 7.4
	NaCl	200 mM	
	MgCl <sub>2</sub>	5 mM	optional
	DTT	2 mM	

**Table 2.11:** List of buffers used for the purification of His-tagged proteins.

### 2.5.4 Purification of GST-fusion proteins

Glutathione S-transferase (GST) is approx. a 26 kDa protein and provides rapid protein purification of high yield [Frangioni and Neel, 1993]. In this work PRDI was overexpressed as GST fusion protein.

The purification of GST-PRDI was based on the protocol for His-tagged proteins. 4 ml Glutathione Sepharose 4B (GE Healthcare) were used for 1 L of cell culture. The protein was washed on column with gel filtration buffer (Table 2.12). Proteolytic TEV-cleavage was performed as described in the next section. After TEV digestion the flowthrough was pooled and concentrated for gel filtration.

Name	Chemicals	Amounts	Remarks
1 x PBS	NaCl	140 mM	pH 7.3
	KCl	2.7 mM	
	Na <sub>2</sub> HPO <sub>4</sub>	10 mM	
	KH <sub>2</sub> PO <sub>4</sub>	1.8 mM	
Gel filtration buffer	Tris HCl	50 mM	pH 7.4
	NaCl	200 mM	optional
	MgCl <sub>2</sub>	5 mM	
	DTT	2 mM	

**Table 2.12:** List of buffers used for the purification of GST-fusion proteins. The PBS buffer was prepared as 10x stock solution.

### 2.5.5 Proteolytic cleavage with TEV-protease

The specific cleavage site for the TEV protease is ENLYFQG, with the proteolytic cleavage site between Q and G.

The proteolytic cleavage of His-tagged proteins was carried out during protein dialysis at room temperature. After the elution of the protein, the sample was dialysed overnight against gel filtration buffer (Table 2.11). The TEV cleavage was performed using 200 to 300  $\mu$ l TEV-protease (1 mg/ml) for 1 L of cell culture. In rare cases His-tagged proteins were digested on column prior to protein elution by using STREP-TEV-protease. This TEV protease comprises a N-terminal peptide of eight amino acids (STREP tag: Trp-Ser-His-Pro-Gln-Phe-Glu-Lys) instead of a histidine tag. The STREP tag prevents the immobilization of the TEV protease to

the Ni<sup>2+</sup> chelating NTA. Prior to TEV digestion the resin was thoroughly washed with gel filtration buffer.

GST-fusion proteins were digested overnight on column using 200 to 300  $\mu$ l TEV-protease (1 mg/ml) for 1 L of cell culture.

### 2.5.6 Concentrating of proteins

Proteins were concentrated at 4°C using Vivaspin concentrators (Sartorius) of appropriate molecular cut off.

### 2.5.7 Size exclusion chromatography (gel filtration)

Äkta chromatography systems (Äkta basic, Äkta purifier; GE Healthcare) equipped with Superdex 75 (16/60) gel filtration columns were used for preparative size exclusion chromatography. The gel filtration buffers are listed in Tables 2.11 and 2.12. The flow rate was 1 ml min<sup>-1</sup>.

### 2.5.8 PRDI

PRDI has a molecular weight of 11 to 14 kDa and was purified according to section 2.5.4 using the GST-fusion tag. In Figure 2.3 the purification of wild type PRDI is shown. After proteolytic TEV digestion, which was carried out overnight on column, PRDI was efficiently eluted (Figure 2.3 a). In Figure 2.3 b) the UV spectrum of purified and concentrated PRDI is shown. This spectrum was measured after the preparative gel filtration was performed, which is shown in Figure 2.3 c). This preparative gel filtration (Superdex 75 16/60, GE Healthcare) was performed in two different buffers. The solid line shows the chromatogram of PRDI, which was purified in 200 mM NaCl, 50 mM Tris HCl, 2 mM DTT, pH 7.4 whereas the dashed line shows purification in 200 mM ammonium acetate, 2 mM DTT, pH 7.4. The ammonium acetate purification was carried out to prepare samples for mass spectrometric experiments. In both chromatograms a single peak can be seen for PRDI.

Different PRDI constructs of various lengths (100-114 amino acids) were designed and purified to optimize the quality of PRDI NMR spectra (Table 2.10).

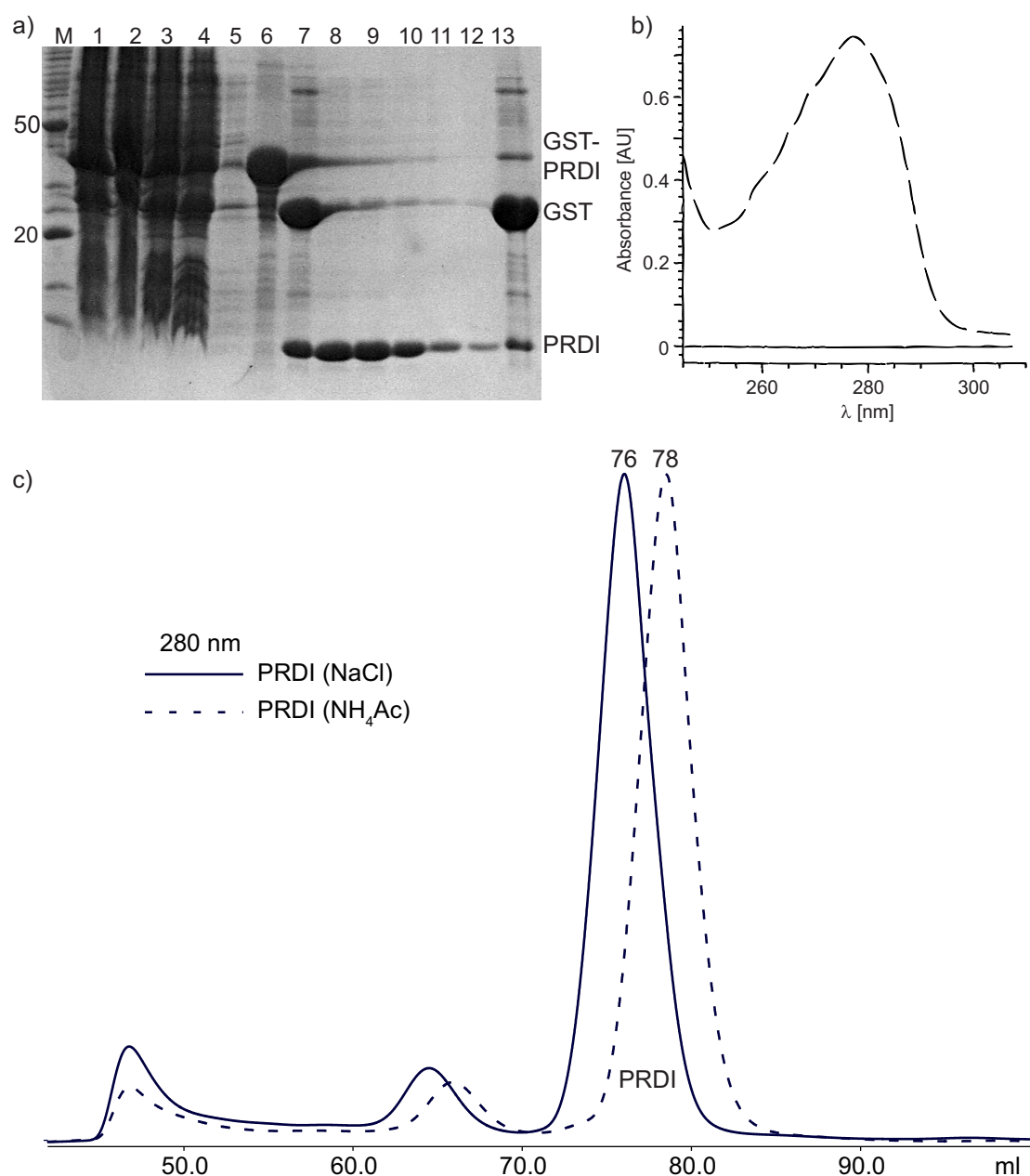


**Figure 2.3:** The purification of a GST-PRDI fusion protein is shown. In a) the SDS-PAGE gel shows all purification steps before gel filtration was applied. The lanes are read as follows: 1: before sonication; 2: after sonication; 3: supernatant; 4: flowthrough; 5: wash (gel filtration buffer); 6: resin before TEV protease overnight digestion; 7: resin after TEV protease digestion; 8: flow through; 9-12: wash fractions 1-4 (2 ml); 13: final resin. M stands for the molecular weight marker. The example shows the complete digestion of the fusion protein and the almost quantitative "elution" of PRDI. In b) a UV spectrum of purified and concentrated PRDI is shown after preparative gel filtration (shown in c). A 280/260 ratio of 1.8 indicates well purified protein. Superimposed gel filtration chromatograms (280 nm UV absorption) of two PRDI purifications are shown in c). The solid line indicates the protein purification in 200 mM NaCl, 50 mM Tris HCl, 2 mM DTT, pH 7.4 whereas the dashed line stands for protein, which was purified in 200 mM ammonium acetate, 2 mM DTT, pH 7.4 for mass spectrometric experiments. The numbers on top of both peaks correspond to the retention volumes, which are given along the x-axis.

### 2.5.9 PRDII

PRDII was purified according to section 2.5.3 using the His-Z-fusion tag. The molecular weight of GlcT PRDII is 13 kDa. Upon phosphorylation, carried out in the temperature range between 22 - 30°C, PRDII showed severe precipitation. In order to avoid this precipitation, phosphorylation of PRDII was carried out maintaining the His-Z-fusion tag (His-Z-PRDII). Hence, the molecular weight of His-Z-PRDII is 23.6 kDa.

As shown in Figure 2.4 the PRDII fusion protein can be expressed and purified in high amounts.

In Figure 2.5 two superimposed gel filtration chromatograms of PRDII are shown (Superdex 75 16/60, GE Healthcare), which was purified in two different buffers. The solid line shows PRDII purified in 200 mM ammonium acetate, 2 mM DTT, pH 7.4 for mass spectrometric experiments whereas the dashed line shows protein purified in 200 mM NaCl, 50 mM Tris HCl, 2 mM DTT, pH 7.4. Both chromatograms show that PRDII eluted in three peaks and SDS-PAGE analysis

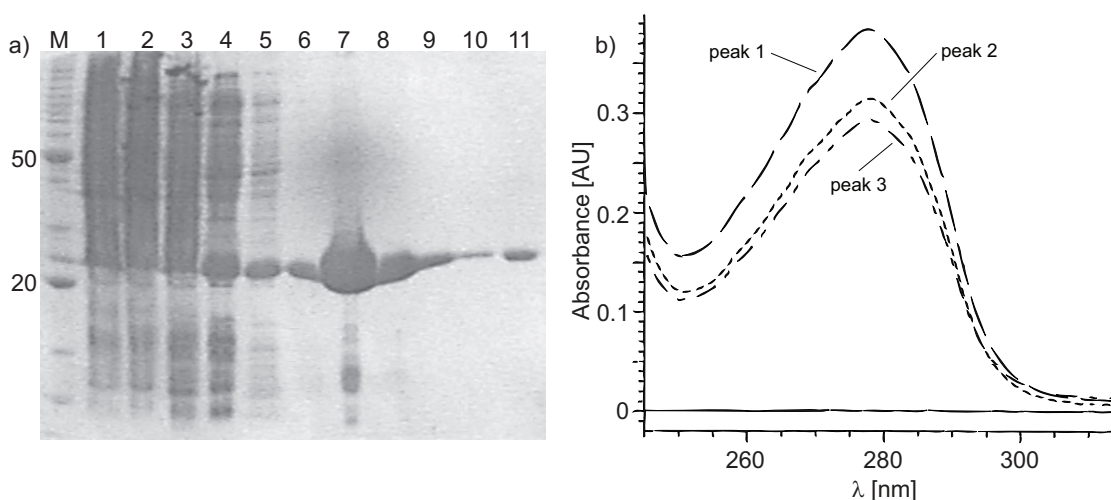


**Figure 2.4:** The purification of PRDII is shown. No TEV protease cleavage was applied to PRDII to maintain the His-Z-fusion tag for better protein stability upon phosphorylation. In a) the PRDII purification steps are shown on SDS-PAGE and the lanes are read as follows: 1: before sonication; 2: after sonication; 3: supernatant; 4: flow through; 5: wash (5 mM imidazole); 6: wash (20 mM imidazole); 7-10: elution steps 1-4 (1 ml each); 11: final resin. In b) the UV spectrum is shown for all three concentrated peaks, which are present after preparative gel filtration as seen in Figure 2.5 (solid line). Each peak contains purified PRDII protein of good quality indicated by 280/260 nm UV ratios of 1.7 to 1.8.



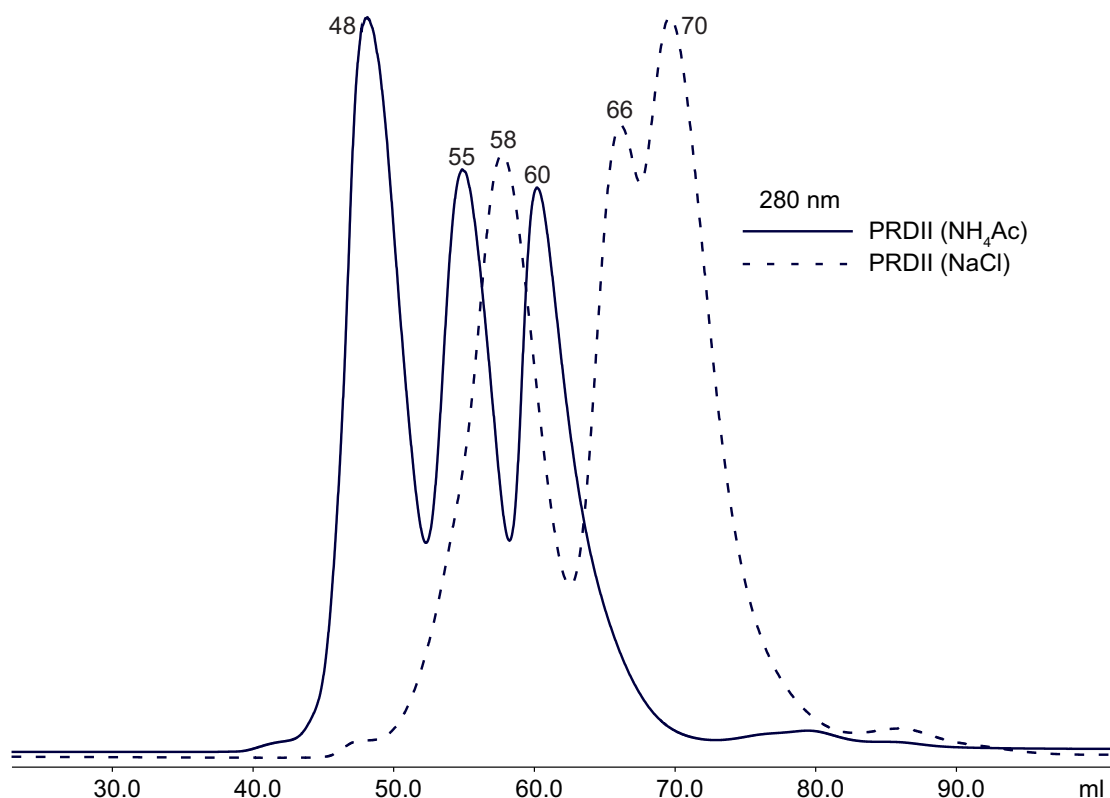


**Figure 2.5:** Superimposed gel filtration chromatograms of PRDII purified in different gel filtration buffers. Three peaks can be clearly seen after each protein purification. The solid line (PRDII (NH<sub>4</sub>Ac)) indicates PRDII, which was purified in 200 mM ammonium acetate, 2 mM DTT, pH 7.4 for mass spectrometric experiments whereas the dashed line stands for protein purified in 200 mM NaCl, 50 mM Tris HCl, 2 mM DTT, pH 7.4. The numbers on top of the peaks correspond to the retention volumes, which are indicated at the x-axis. In both purification runs three PRDII species can be seen: monomer (70 and 60 ml), dimer (66 and 55 ml) and a higher PRDII aggregate (58 and 48 ml).

confirmed that each peak contained the target protein in roughly equal amounts (data not shown). These three peaks can be assigned to the monomer, dimer and a higher aggregation state of PRDII. Figure 2.4 b) shows the UV spectrum of each PRDII peak (purified for mass spectrometry; solid line). A 280/260 nm ratio of 1.7 - 1.8 was obtained for all three PRDII species.

Three PRDII mutants were designed (summarized in Table 2.10). Two single aspartate mutants, (PRDII H218D and PRDII H279D) and a double mutant (PRDII H218D H279D) were purified in ammonium acetate for mass spectrometric experiments but were also used for analytical gel filtration. The preparative gel filtration chromatograms of PRDII H218D and PRDII H279D are shown in Figure 2.6.

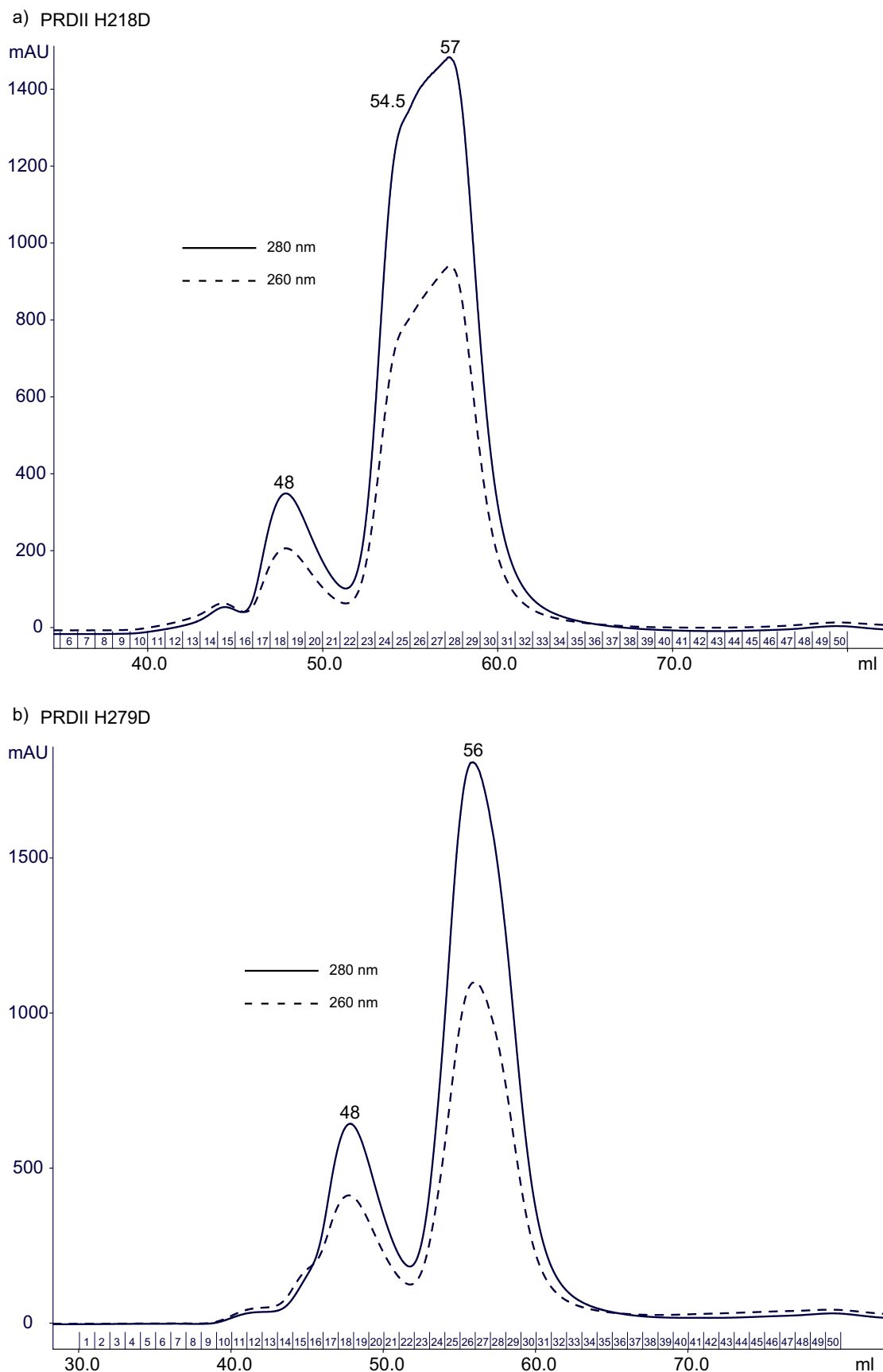


**Figure 2.6:** Gel filtration chromatograms of PRDII H218D (a) and PRDII H279D (b) purifications, which were performed in 200 mM ammonium acetate, 2 mM DTT, pH 7.4 for mass spectrometric experiments, are shown. In a) and b) a broadened peak can be seen approx. between 52 and 61 ml for both mutants. The numbers on top of the peaks correspond to the retention volumes, which are given along the x-axis.

As shown in Figure 2.6 a) a broad peak appeared between 52 and 61 ml after preparative gel filtration of PRDII H218D. Compared to the chromatogram of the wild type PRDII only a minor peak at 48 ml was observed, which indicates that the amount of the higher aggregate of PRDII is significantly reduced in PRDII H218D. The same effect can be observed for PRDII H279D (Figure 2.6 b). However, in both chromatograms the monomeric PRDII, which was assigned to the peak at 60 ml (Figure 2.5) in the chromatogram of the wild type PRDII, is not as clearly separated from the dimer as in the case of the wild type protein. This could be explained by a dimer-monomer equilibrium, which seems to be more pronounced in PRDII H218D than in PRDII H279D. However, the gel filtration runs indicate that the formation of the dimeric form of both single aspartate mutants seems to be favoured. A very similar preparative gel filtration chromatogram was observed for the double aspartate mutant (PRDII H218D H279D) where an intense peak was equally observed at 55 ml (data not shown).

### 2.5.10 RBD-PRDI

GlcT comprises three domains. A RNA binding domain (RBD) forms the very N-terminus of the protein followed by two regulatory domains (PRDI and PRDII; Figure 1.1). The RBD-PRDI fragment comprises 180 amino acids with a molecular weight of approx. 20.6 kDa. Recombinant RBD-PRDI was expressed as a His-Z fusion protein. The protein was purified using  $\text{Ni}^{2+}$  chelating affinity chromatography (section: 2.5.3), which was performed similar to the purification of PRDII (section: 2.5.9).

In Figure 2.7 a) and b) the SDS-PAGE gels show the purification steps before the preparative gel filtration was carried out (Figure 2.7 c). The precipitation of nucleic acids and the proteolytic TEV digestion were performed according to the sections 2.5.2 and 2.5.5.

In Figure 2.7 c) the preparative gel filtration chromatogram of RBD-PRDI is shown (Superdex 75 16/60, GE Healthcare). The chromatographic run was performed in 200 mM NaCl, 10 mM Tris HCl, 2 mM DTT, pH 8.0. Fractions were checked on SDS-PAGE to validate the purity of the protein. The first protein peak, identified as RBD-PRDI by SDS-PAGE analysis, eluted at 67 ml, whereas the free His-Z domain eluted at 84 ml. As shown in section 4.6 (Figure 4.8) RBD-PRDI formed dimers, which is in agreement with what was reported for RBD-PRDI of the homologous LicT, which also exists as homodimer in solution [Ducat *et al.*, 2002, Ducat *et al.*, 2006].

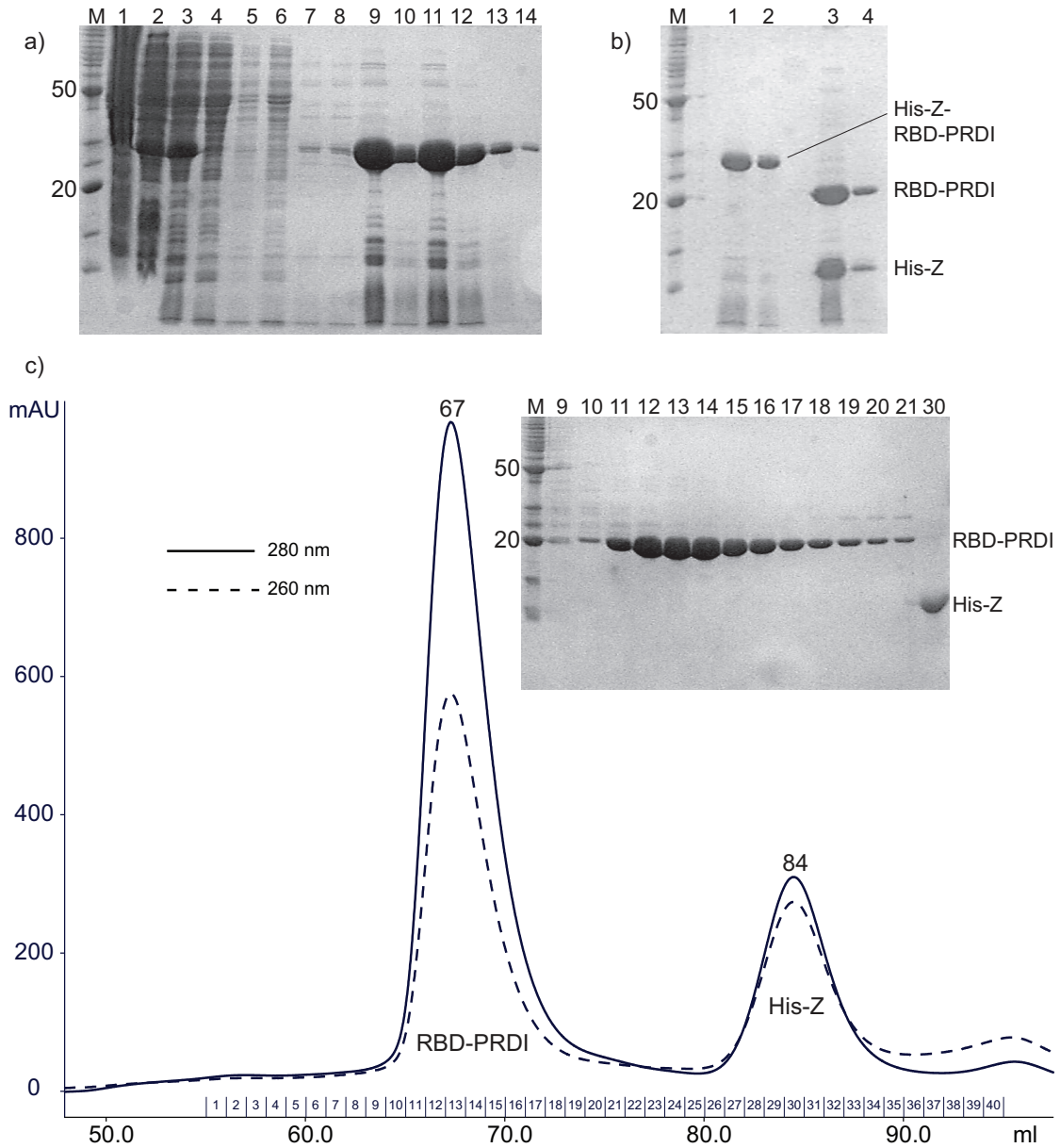


**Figure 2.7:** Purification of RBD-PRDI. In a) the purification steps are shown until TEV cleavage was carried out. The lanes are numbered as follows (several samples are shown twice): 1: after sonication; 2: supernatant; 3: supernatant after PEI precipitation; 4: flow through; 5, 6: wash (5 mM imidazole); 7, 8: wash (20 mM imidazole); 9, 10: elution step 1 (250 mM imidazole); 11, 12: elution step 2 (250 mM imidazole); 13, 14: final resin after elution. In b) the TEV cleavage is emphasized as follows: 1, 2: His-Z-RBD-PRDI before TEV cleavage in solution; 3, 4: after TEV cleavage. The gel filtration chromatogram and subsequent SDS-PAGE analysis of RBD-PRDI is shown in c). The numbers on top of each peak represent the specific retention volumes of the peaks (in ml). Selected fractions are shown on the SDS-PAGE gel. M stands for the molecular weight marker and the numbers that are given for each lane correspond to the fraction numbers in the chromatogram of RBD-PRDI, which are indicated at the x-axis. The gel filtration run was carried out in 200 mM NaCl, 10 mM Tris HCl, 2 mM DTT, pH 8.0.

### 2.5.11 Enzyme I (EI)

Enzyme I (EI) is the first member of the general PTS (Figure 1.1). The expression construct for EI was provided by Prof. Stülke's lab (University of Göttingen). The His-tagged protein was expressed and purified according to sections 2.5 and 2.5.3. In Figure 2.8 a preparative gel filtration chromatogram (Superdex 75 16/60, GE Healthcare) of Enzyme I is shown.

The molecular weight of EI is approx. 64 kDa. Since EI is one of the biggest proteins in the phosphorylation cascade of the PTS its retention volume after preparative gel filtration is relatively small compared to other protein members (e. g. HPr: 88 ml, PRDI: 78 ml, EII: 66 ml; Superdex 75 16/60, GE Healthcare). As shown in the chromatogram, EI eluted approx. at 54 ml. Enzyme I is capable of reversibly forming monomers as well as dimers [LiCalsi *et al.*, 1991] and the dimeric structure was recently published [Schwieters *et al.*, 2010]. As seen in Figure 2.8 and shown by SDS-PAGE analysis the dimeric fraction can be seen at 45 ml.

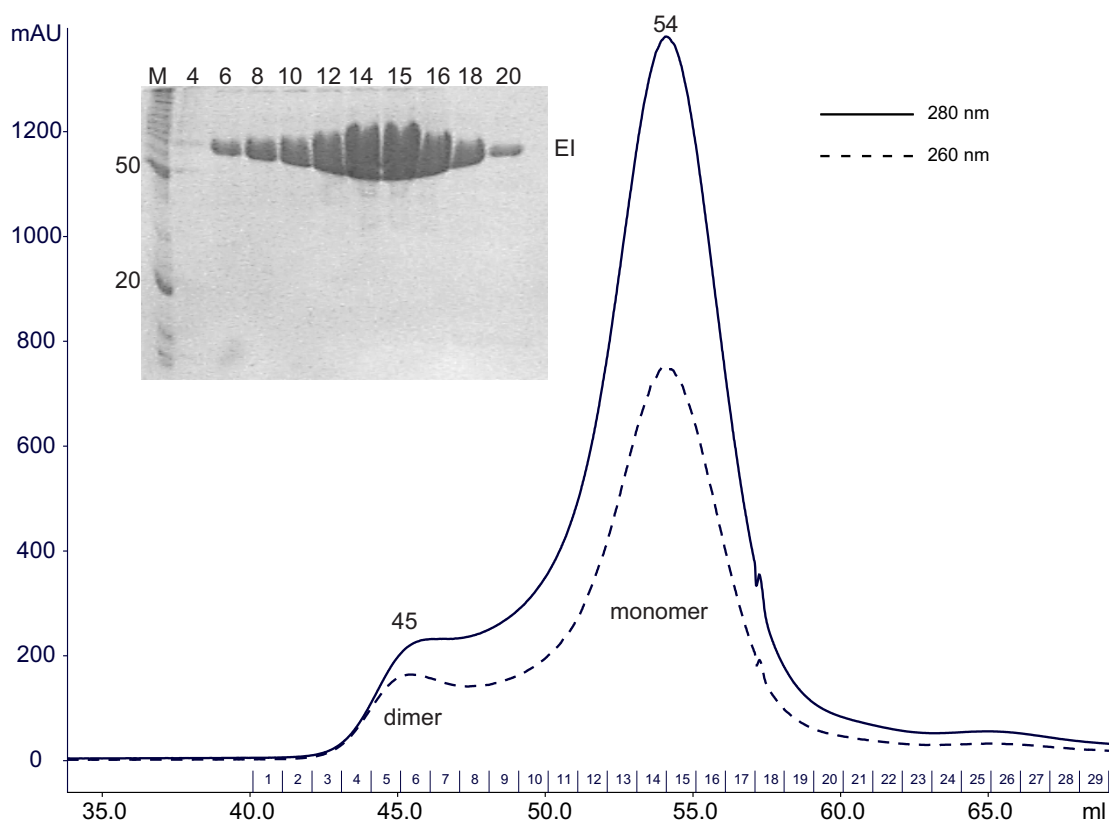


**Figure 2.8:** Gel filtration chromatogram and SDS-PAGE analysis of purified Enzyme I (EI). The purification was carried out in 200 mM ammonium acetate, 2 mM DTT, pH 7.4 for mass spectrometric experiments. The SDS gel shows selected fractions after the gel filtration was carried out. M stands for the molecular weight marker and the numbers that are given for each lane correspond to the fraction numbers in the chromatogram, which are indicated at the x-axis. The numbers on top of the peaks correspond to the retention volume (in ml).

### 2.5.12 Enzyme II-AB (EII-AB)

The His-tagged Enzyme II (EII) contains only the soluble AB domain without the membrane bound C-domain (for further information see section: 1.2). The expression clone was provided by Prof. Stülke's lab (University of Göttingen). The molecular weight of EII is approx. 31 kDa. EII was overexpressed and purified according to sections 2.5 and 2.5.3. The preparative gel filtration chromatogram (Superdex 75 16/60, GE Healthcare) and the SDS-PAGE gel are shown in Figure 2.9.

The chromatogram shows the elution of EII at 66 ml and clearly indicates that the UV absorbance at 260 nm is significantly higher than at 280 nm. This can be explained by the absence of tryptophans in the protein sequence of EII and the presence of only one tyrosine and one cysteine. These three amino acids (primarily tryptophan) are responsible for the absorption at 280 nm in a UV spectrum. As a consequence, the protein concentration of EII was determined at 205 nm (according to section: 2.2.7). SDS-PAGE analysis clearly showed a large amount of well purified EII-AB with its characteristic molecular weight of 31 kDa.

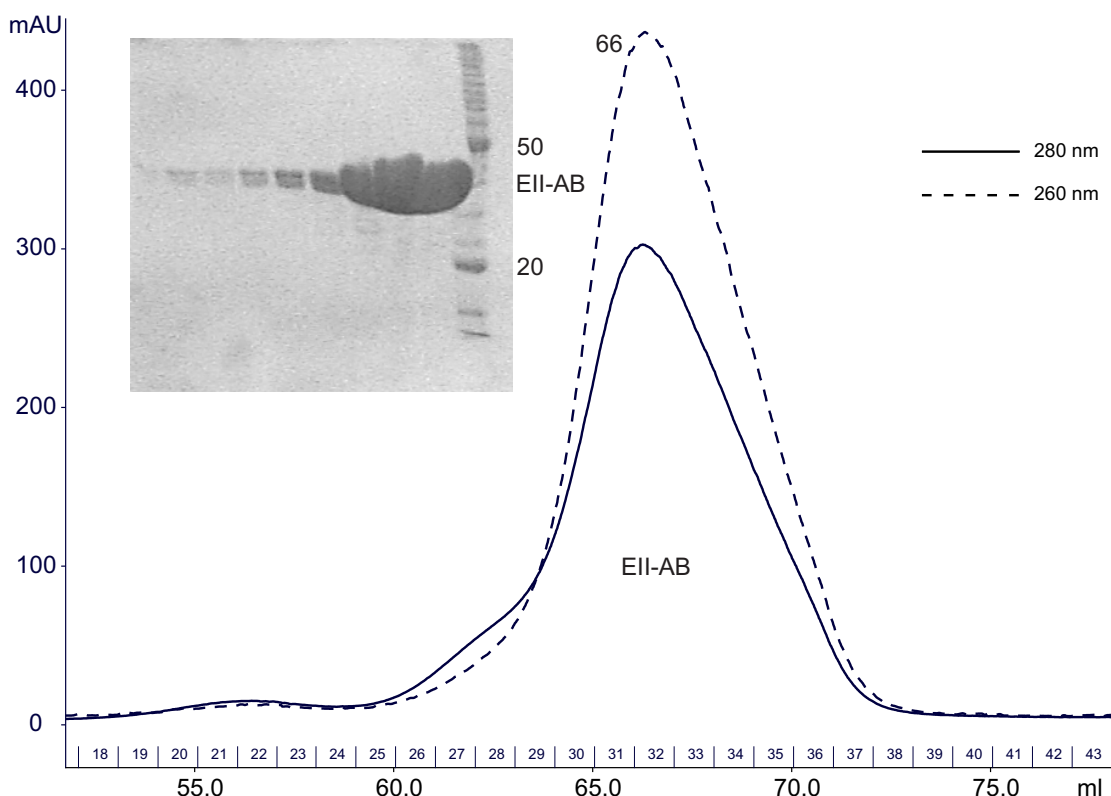


**Figure 2.9:** Gel filtration chromatogram and SDS-PAGE analysis of the Enzyme II-AB fragment (EII). The purification was carried out in 200 mM ammonium acetate, 2 mM DTT, pH 7.4 for mass spectrometric experiments. EII-AB eluted at 66 ml as indicated by the number on top of the peak. The SDS-PAGE gel shows selected fractions after preparative gel filtration. However, no information are available, which fractions are shown on the gel.

### 2.5.13 HPr

HPr is the second member of the general PTS (Figure 1.1) and is strongly involved in the transfer of phosphate groups within the PTS. HPr was cloned into the pET16bTEV expression vector, which encodes a N-terminal His(7x)-tag and a TEV cleavage site between His-tag and HPr. The overexpression and purification was carried out according to sections 2.5 and 2.5.3. Figure 2.10 a) shows a SDS-PAGE gel of all purification steps before the preparative gel filtration (Figure 2.10 b) was carried out. The gel shows one additional washing step with 40 mM imidazole (lane 7), which is not mentioned in the protein purification protocol (section: 2.5.3). Only the 5 mM imidazole washing step is essential since most HPr protein started to elute upon higher imidazole concentrations (20 and 40 mM imidazole). A preparative gel filtration chromatogram (Superdex 75 16/60, GE Healthcare) of HPr is shown in Figure 2.10 b) and HPr eluted at 88 ml. A characteristic UV spectrum of concentrated HPr is shown in Figure 2.10 c).

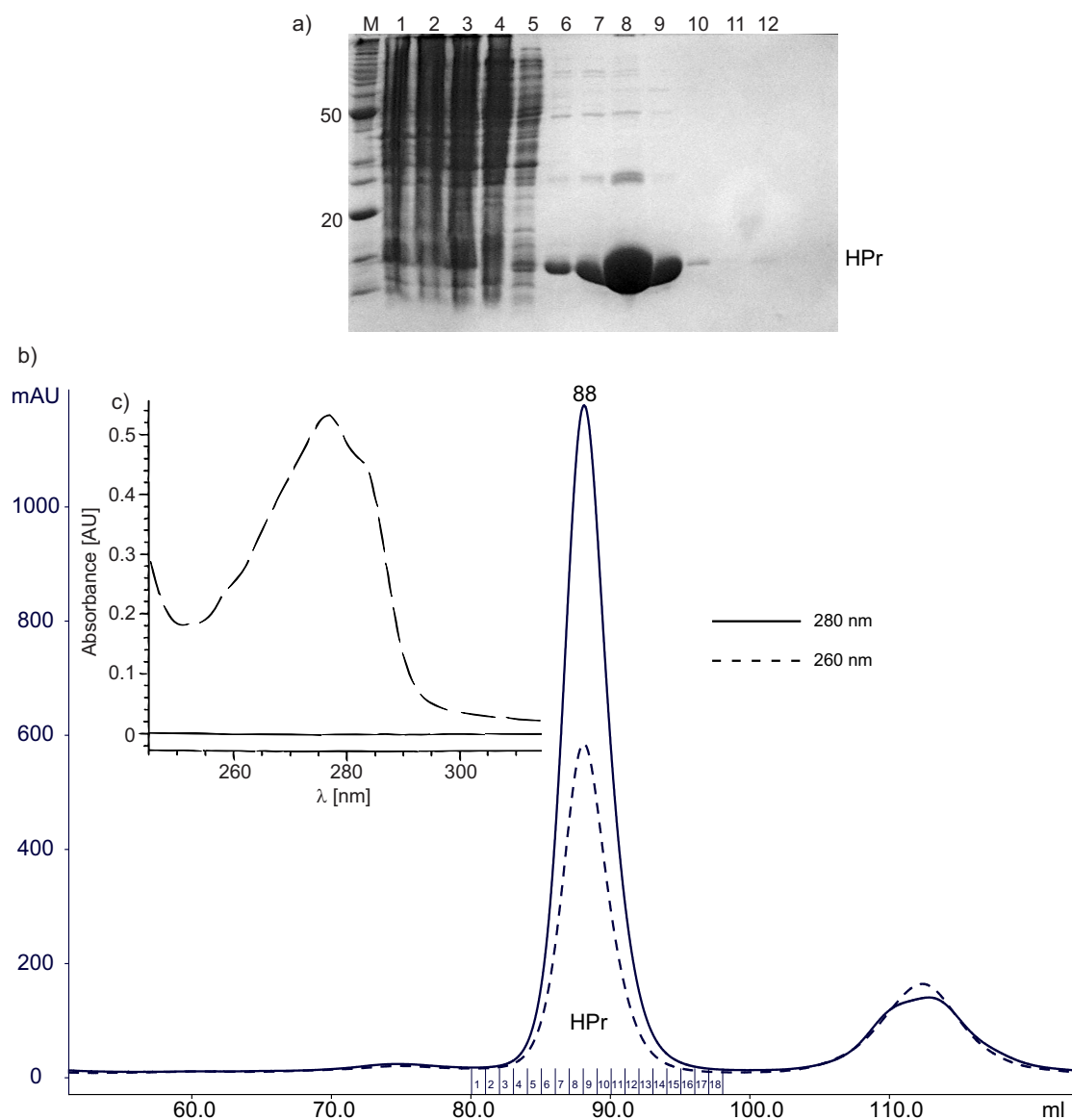


**Figure 2.10:** Purification of HPr. In a) a coomassie blue stained SDS-PAGE gel of a HPr purification is shown before preparative gel filtration was performed. The lanes are labelled as follows: 1: before sonication; 2: after sonication; 3: supernatant; 4: flow through; 5: wash (5 mM imidazole); 6: wash (20 mM imidazole); 7: wash (40 mM imidazole); 8-11: elution fractions 1-4 (250 mM imidazole); 12: final resin after elution. The preparative gel filtration chromatogram of HPr is shown in b). The presence of the protein was monitored by measuring the 280 and 260 nm UV wavelength. HPr eluted at 88 ml in 200 mM NaCl, 50 mM Tris HCl, 2 mM DTT, pH 7.4. The UV spectrum of HPr after gel filtration is shown in c) with a 280/260 ratio of 1.9. HPr shows a characteristic bump in its UV spectrum around 280 nm.



## 2.6 Specialized methods

### 2.6.1 Phosphoramidate (PA) synthesis

Phosphoramidate is a high energy phosphate donor molecule that can be used for the chemical phosphorylation of free histidine and proteins. PA was synthesized as previously described [Buckler and Stock, 2000].

### 2.6.2 Analytical gel filtration & Sample preparation

Size exclusion chromatography and in particular analytical gel filtration was used to analyse the aggregation states of GlcT domains upon phosphorylation. The samples were prepared as follows: 15 to 25 nmol of the target protein (considered as monomer) were mixed with HPr in an equimolar, Enzyme I in a 1/30 molar ratio and phospho(enol)pyruvic acid trisodium salt (PEP) in a 50 to 100 fold excess. The final sample volume did not exceed 50 to 70  $\mu$ l (injection loop: 100  $\mu$ l). The phosphorylation was carried out at 37°C for 60 to 120 min prior to the sample injection.

Gel filtration runs were performed with Superdex 75 (10/300, 24 ml volume; GE Healthcare) gel filtration columns for all proteins except for PRDI (Superdex 75 (16/60, 120 ml volume)). Both runs were significantly different in their duration (Superdex 75, 10/300: approx. 30 minutes; Superdex 75, 16/60: approx 100 minutes). The gel filtration buffer was composed of 200 mM NaCl, 50 mM Tris HCl, 5 mM MgCl<sub>2</sub> (optional) and 2 mM DTT at pH 7.4.

### 2.6.3 Mass spectrometry & Sample preparation

Electrospray ionization mass spectrometry (ESI-MS) was used to verify the correct molecular weight of proteins and to detect protein phosphorylation. For this purpose preparative gel filtration (section: 2.5.7) of the proteins was performed in 200 mM ammonium acetate, 2 mM DTT and pH 7.4. 10 nmol of target protein was mixed with the phosphorylation proteins as follows: Enzyme I in a 1/30 molar ratio, HPr in a equimolar (PRDI) or 1/8 molar ratio (PRDII) and Phospho(enol)pyruvic acid tri(cyclohexylammonium) salt in a 50 fold excess. The pH

of the reaction buffer (40 mM ammonium acetate, 2 mM DTT, pH 7.4) used for mass spectrometry was adjusted by using liquid ammonia (25 %). The final sample volume was 100  $\mu$ l. The phosphorylation was achieved prior to the measurements by incubation at 37°C for 60 to 120 min and analysed by mass spectrometry.

The analytical internet tool Protparam (Expasy)<sup>7</sup> was used determining theoretical protein masses.

Sample preparation and tandem mass experiments (MS-MS and MS-MS-MS), carried out with PRDI, were performed in the lab of Dr. Henning Urlaub (MPI for Biophysical Chemistry). Prior to mass spectrometric experiments PRDI was phosphorylated as described in this section. The phosphorylated PRDI was digested by trypsin and, afterwards, phosphopeptides were enriched by immobilized metal-ion affinity chromatography (IMAC) [Andersson and Porath, 1986, Ross, 2007].

Tandem mass spectrometry is used to generate fragments of a peptide or protein. For this purpose, usually, two mass analysers are separated by a collision cell into which an inert gas (e.g. argon, helium or xenon) is admitted to collide with the selected sample ions and bring about their fragmentation (CID = collision-induced dissociation).<sup>8</sup> This dissociation is commonly used to generate peptide fragments during MS-MS experiments [Ross, 2007]. However, depending on the amino acid and the collision energy the loss of protein modifications, such as phosphate groups, can be observed without generating additional fragments of the peptide. In case of PRDI, MS-MS experiments were used to identify histidine phosphorylated peptides of PRDI, which show a significant loss in mass of approx. 80 Da upon tandem mass analysis [Ross, 2007] (section: 4.5). In order to interpret the results, the theoretical masses of the peptides with and without phosphorylation need to be known.

Upon further modulation of the collision energy, fragments of PRDI were generated (MS-MS-MS or MS3). Such MS3 spectra allow to derive structural and sequential information. In case of PRDI such spectra were primarily used to validate the correct peptide sequence to avoid matching to other peptides of identical masses. The fragmentation of peptides is well documented [Johnson and Biemann, 1989] and can occur between three different bonds along the peptide backbone: the NH-CH, CH-CO, and CO-NH bonds. As a result, after each fragmentation two species are observed. One fragment is without charge, whereas the other one is charged and can be observed in a mass spectrum. This charge can stay on

---

<sup>7</sup><http://www.expasy.org/tools/protparam.html>

<sup>8</sup><http://www.astbury.leeds.ac.uk/facil/MStut/mstutorial.htm>

either of the two fragments. Fragments, which have the charge retained on the N-terminal end are usually labelled with b, whereas fragments having the charge retained on the C-terminal end are labelled with y. This labelling scheme refers to the most common cleavage site at the CO-NH bond and was also observed in the MS3 spectrum of PRDI, where peptide fragments (b and y) with single, double and triple charges were detected (Figure 4.5). The length of the fragments is usually indicated by subscripted numbers. After CID fragmentation, ions from peptide fragments are often present due to the loss of ammonia, water, or carbon monoxide [Johnson and Biemann, 1989, Papayannopoulos, 1995]. Thus, these losses need to be considered in the calculation of the masses.

## 2.6.4 RNA synthesis (RAT RNA)

RNA synthesis and RNA band shift assays (section: 2.6.5) were carried out in our department by C. Schwiebk.

The GlcT specific RAT RNA sequence used in our studies was ggACGUGU-UACUGAUUCGAUCAGGCAUGAGUcc [Schilling *et al.*, 2004]. The flanking nucleotides (gg-cc) were proposed and designed to stabilize the RAT RNA (RAT sequence is highlighted in capital letters) by palindromization. The palindromized RAT sequence was provided by Prof. Stülke's group, Department of General Microbiology, University of Göttingen and is supposed to form the secondary structure of a loop [Schilling *et al.*, 2004].

The RAT RNA sequence was converted into a DNA sequence and was cloned into a pUC19 vector by artificially introduced restriction sites flanking both ends. The plasmid was transformed into XL2blue host strains for DNA preparation (1L LB, 37°C, 5 to 7 hours). The plasmid DNA was isolated in preparative amounts and linearised by 3' cleavage (PstI) for in vitro amplification. The reaction mix (20 ml) containing template DNA, transcription buffer (1x), MgCl<sub>2</sub> (20 mM), DTT (5 mM), PEG 8000 (32 µl; stock: 0.5 g/ml), NTP's (ribonucleotide triphosphates: 10 mM final concentration each), T7 RNA polymerase and ddH<sub>2</sub>O was incubated for amplification for 5 to 8 hours at 37°C. The composition of the transcription buffer is shown in Table 2.13.

The target RNA was separated from the protein fraction by mixing the solution in a 1:1 ratio (final volume 40 ml) with phenol solution (water saturated) to precipitate proteins. The RAT RNA remains in the aqueous phase only under constant pH conditions (approx. pH 7). In a second step the aqueous phase was

Name	Chemicals	Amounts	Remarks
10x RNA transcription buffer	Tris HCl	400 mM	pH 8.0
	Spermidine	10 mM	
	DTT	50 mM	
	Triton X-100	0.1 %	

**Table 2.13:** 10x RNA transcription buffer composition, which was used for in vitro RAT RNA synthesis.

extracted and RNA was precipitated by adding NaCl (300 mM final concentration) and mixed in a 1:1 ratio with 2-propanol (final volume again approx. 40 ml). The precipitated RNA was centrifuged for 30 to 60 minutes at 70,000 rcf. A further washing step was applied by redissolving the RNA pellet in 10 to 20 ml 70 % ethanol followed by another centrifugation step (30 to 60 minutes at 70,000 rcf) to spin down the RNA. A "speed vac" system was used to remove all traces of ethanol. A preparative denaturing polyacrylamide gel (15 %) was used to separate RNA of correct size from other RNA fragments (N+1, N-1 etc.). After gel purification RNA bands of desired size were cut out and eluted (electroelution, S & S ELUTRAP; Schleicher & Schuell). 2-propanol precipitation (300 mM NaCl), ethanol purification and "speed vac" drying were carried out twice and the isolated and lyophilized RNA was stored at -80°C.

### 2.6.5 Electrophoretic mobility shift assay (EMSA)

Protein-RNA interactions were studied by electrophoretic mobility shift assays (EMSA or band shift assay) [Garner and Revzin *et al.*, 1981]. For this purpose the RAT RNA was reannealed for two minutes at 85 to 88°C and equilibrated for 10 to 30 minutes at room temperature prior to binding experiments. Protein and RNA were mixed in desired molecular ratios (1:9 or 1:13 for RBD-PRDI; section: 4.6) and portions of 20  $\mu$ l were incubated for one hour on ice. 10  $\mu$ l portions were mixed with 5  $\mu$ l loading buffer and used for electrophoresis with 10 % polyacrylamide native gels to perform RNA band shift assays. 40 % Acrylamide/Bis-Acrylamide (19:1) was used for gel preparation. 100 V were applied for approximately four hours (1-8 V cm<sup>-1</sup>; depending on the room temperature). RNA was detected by Ethidium bromide staining and visualized on an UV screen.

## 2.6.6 Nuclear magnetic resonance spectroscopy (NMR)

Nuclear magnetic resonance spectroscopy (NMR) and x-ray crystallography are the major techniques to determine structures of macromolecules at atomic level. Besides structure determination, NMR provides a broad variety of applications to investigate further dynamic processes such as molecular interactions and kinetics [Cavanagh; Protein NMR Spectroscopy; Elsevier Academic Press]. In this study NMR was used to study the regiochemistry of histidine phosphorylated proteins (chapter: 3).

### Sample preparation

Samples for NMR spectroscopy were dialysed against 40 mM sodium phosphate, 5 mM  $\text{MgCl}_2$ , 2 mM DTT and pH 7.4. The final sample concentrations were between 1 and 6 mM depending on the proteins, their stabilities and the desired NMR experiments. The samples were measured in 90 %  $\text{H}_2\text{O}$ /10 %  $\text{D}_2\text{O}$  unless indicated otherwise. The final sample volume was 200 - 250  $\mu\text{l}$ .

Name	Chemicals	Amount	Remarks
NMR buffer	Sodium phosphate	40 mM	pH 7.3 to 7.4
	( $\text{Na}_2\text{HPO}_4$ )	(4.01 g )	
	( $\text{NaH}_2\text{PO}_4$ )	(1.62 g )	
	$\text{MgCl}_2$	5 mM (1.02 g)	
	DTT	2 mM (0.31 g)	

**Table 2.14:** Buffer composition which was used for NMR experiments (amounts in g are for 1 L of buffer).

Samples for HNP experiments (chapter: 3) were prepared by mixing the phosphorylation enzymes in a molar ratio as follows (PRDs were considered as monomers):  $\text{PRDI} : \text{HPr} : \text{EI} : \text{PEP} = 1 : 1 : 1/30 : 100$ ;  $\text{PRDII} : \text{HPr} : \text{EI} : \text{PEP} = 1 : 1/8 : 1/30 : 100$ . Phosphorylation enzymes were purified and dialysed against NMR buffer except for EI, which was only purified in ammonium acetate. The sample was concentrated to 200 - 250  $\mu\text{l}$ . The mixture was phosphorylated prior to the measurement by adding phospho(enol)pyruvic acid trisodium salt (PEP), followed by 60 to 120 minutes of incubation at 37°C.

### pH-titration of phosphohistidines

To determine the pH dependence of  $^1\text{J}[^{15}\text{N},^{31}\text{P}]$  coupling constants two titration series, starting at neutral pH and titrating to low and high pH conditions were measured. The sample for low pH titration was prepared by mixing 3.2 mg  $^{15}\text{N}_3$  L-histidine (isotec) with 2.9 mg phosphoramidate (PA; section: 2.6.1) in 200  $\mu\text{l}$   $\text{H}_2\text{O}$ . The pH was adjusted stepwise by adding 18.5 % HCl. For the titration to high pH 3.7 mg  $^{15}\text{N}_3$  L-histidine were mixed with 3.0 mg of PA and dissolved in 182.5  $\mu\text{l}$  of  $\text{H}_2\text{O}$  (180  $\mu\text{l}$   $\text{H}_2\text{O}$  and 2.5  $\mu\text{l}$  5 M NaOH) for initial pH adjustment. The pH was measured before and after each NMR experiment.

The NMR experiments were carried out at 303K using a 600 MHz NMR magnet equipped with an AvanceIII console and a QXI room temperature probe. The measurements were performed by accumulating 64 scans with 2048 complex points (center frequency 0 ppm, sweep width 20 ppm).  $^1\text{J}[^{15}\text{N},^{31}\text{P}]$  coupling constants were extracted with TOPSPIN 2.0 software (Bruker, Germany) and were non-linearly fitted with the sigmoidal function  $f(x) = a + \frac{b}{1+10^{-c(x-d)}}$  using the Igor Pro software package. In this equation  $a$  is the basis in y direction,  $b$  the height along the y axis (equals the difference between the lowest and the highest coupling constant),  $c$  a factor turning the graph and used as quality factor (should be 1 because of base 10) and  $d$  is the shift along the x-axis representing the inflection point.

### HNP-NMR

All HNP experiments were carried out with  $^{15}\text{N}$  uniformly labelled proteins. The experiments were performed at 303 K using a 600 MHz magnet equipped with a Bruker AvanceI console and a QCI cryo probe. The HNP experiments were carried out with 512 ( $^1\text{H}$ ), 13 ( $^{31}\text{P}$ ) and 15 ( $^{15}\text{N}$ ) complex points, unless indicated otherwise. Accumulated scans were ranging from 24 to 216 depending on the protein and its concentration. The processing was performed with NmrPipe (Table 2.3). Delays were set as follows:  $^1\text{H}$ ,  $^{15}\text{N}$ -transfer:  $\tau_a = 11$  ms and  $^{15}\text{N}$ ,  $^{31}\text{P}$ -transfer:  $\tau_a = 25$  ms.  $^1\text{H}$  carrier frequencies were set to 4.7 ppm for all samples whereas  $^{15}\text{N}$  carrier frequencies were set differently for each sample: Phosphohistidines: 210 ppm, HPr: 200 ppm, PRDI and PRDII: 205 ppm.

### 3 The new HNP-experiment

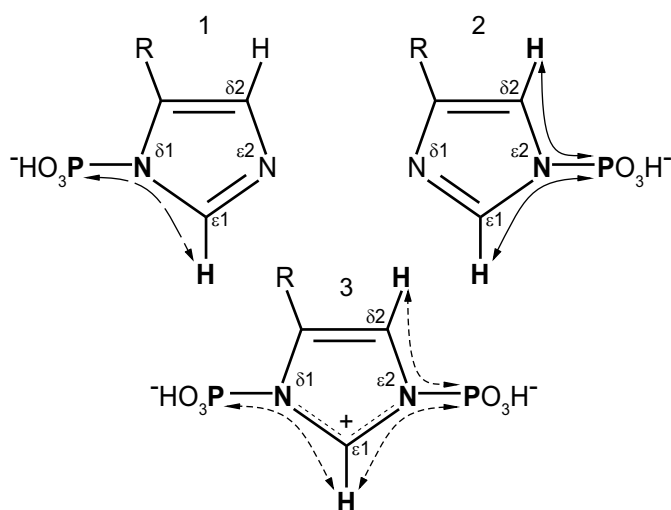


**Figure 3.1:** Illustration of phosphorylation states in the imidazole ring of histidine. 1:  $\delta 1$ -phosphorylation, 1-phosphohistidine; 2:  $\epsilon 2$ -phosphorylation, 3-phosphohistidine; 3:  $\delta 1, \epsilon 2$ -diphosphorylation, 1,3-diphosphohistidine. Arrows indicate possible magnetization transfer pathways used by NMR (HNP experiment) to identify all individual species. Long dashed line (1): a single  $^1\text{H}^{\epsilon 1}_{15}\text{N}^{\delta 1}_{31}\text{P}^{\delta 1}$  correlation; solid lines (2):  $^1\text{H}^{\epsilon 1}_{15}\text{N}^{\epsilon 2}_{31}\text{P}^{\epsilon 2}$  and  $^1\text{H}^{\delta 2}_{15}\text{N}^{\epsilon 2}_{31}\text{P}^{\epsilon 2}$  correlations; short dashed lines (3):  $^1\text{H}^{\epsilon 1}_{15}\text{N}^{\delta 1}_{31}\text{P}^{\delta 1}$ ,  $^1\text{H}^{\epsilon 1}_{15}\text{N}^{\epsilon 2}_{31}\text{P}^{\epsilon 2}$  and  $^1\text{H}^{\delta 2}_{15}\text{N}^{\epsilon 2}_{31}\text{P}^{\epsilon 2}$  correlations.  $^1\text{H}$ ,  $^{15}\text{N}$ , and  $^{31}\text{P}$  nuclei involved in the magnetization transfer are in bold. Magnetization is transferred through  $^2\text{J}[^1\text{H}, ^{15}\text{N}]$  and  $^1\text{J}[^{15}\text{N}, ^{31}\text{P}]$  scalar couplings. Identification of phosphorylation sites in the imidazole ring of histidine can be achieved by counting the number of cross peaks (which is the same as the number of arrows).

eratic chemical shift comparisons, a more reliable method is needed without to resort to chemical shift information. As shown in Figure 3.1 the correlation be-

As described in section 1.5, the goal of the thesis was to determine where PRDI and PRDII are phosphorylated in the regulation of the glucose uptake. As outlined in the mentioned section, the phosphorylation involves two regiochemistry problems: a) to find the correct histidine(s) that is (are) phosphorylated and b) to determine the regiochemistry of phosphorylation within the histidine(s). For the latter question, the HNP experiment was designed and is described in this chapter. Parts of this publication [Himmel *et al.*, 2010] are cited in the following paragraphs.

Since 1D  $^{31}\text{P}$  NMR spectra for the detection of histidine phosphorylation only allow for the distinction between certain phosphorylations based on er-

tween  $^1\text{H}$ ,  $^{15}\text{N}$  and  $^{31}\text{P}$  seems to be an obvious way to detect and resolve the regiochemistry either in 2D or 3D NMR experiments. Surprisingly, such experiments were not developed yet.

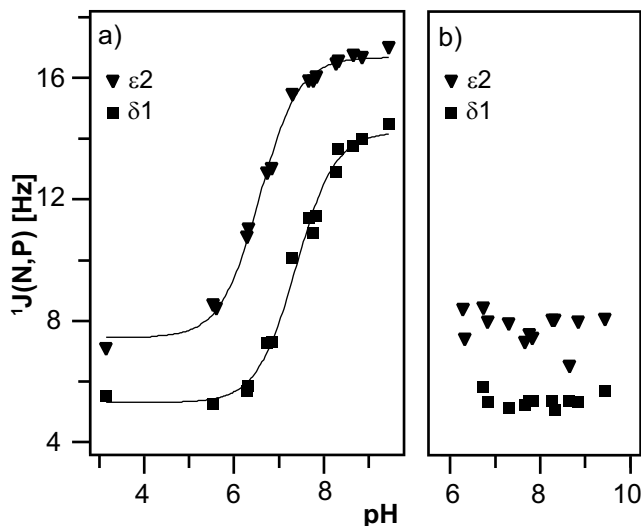


**Figure 3.2:** pH dependence for the  $^1J[^{15}\text{N}, ^{31}\text{P}]$  scalar coupling for a) 1 (■  $\delta 1$ -phosphorylation) and 2 (▼  $\epsilon 2$ -phosphorylation) and b) 3 (■  $\delta 1$ -phosphorylation and ▼  $\epsilon 2$ -phosphorylation). Numbering scheme is used according to Figure 3.1. The coupling constants were extracted from 1D  $^{31}\text{P}$  NMR experiments of a pH titration series and were fitted with a sigmoidal function shown as solid lines (section: 2.6.6). Inflection points of 1 and 2 were at pH 7.4 and 6.6, respectively, which reflect protonation of the non-phosphorylated nitrogen atom of histidine. Since 3 does not have a non-phosphorylated nitrogen atom no pH dependence is observed in (b). The Figure clearly shows that the coupling constants of 1 and 2 at low pH value are almost identical to the corresponding coupling constants of 3, due to the similarity of electron environment for the fully protonated imidazole ring. As a result of fast hydrolysis, signals of 3 could not be observed below pH 6.0.

can be transferred from  $^1\text{H}$  to  $^{31}\text{P}$  in phosphohistidines through scalar couplings between  $^1\text{H}$  and  $^{15}\text{N}$  ( $^2J[^1\text{H}, ^{15}\text{N}]$  and  $^3J[^1\text{H}, ^{15}\text{N}]$ ) and between  $^{15}\text{N}$  and  $^{31}\text{P}$  ( $^1J[^{15}\text{N}, ^{31}\text{P}]$ ) for all three possibilities of a phosphorylated histidine (Figure 3.1). One, two and three cross peaks between  $^1\text{H}$  and  $^{31}\text{P}$  can be seen in a spectrum for 1, 2, and 3, respectively, provided that the efficiency of the transfer through the  $^1J[^{15}\text{N}, ^{31}\text{P}]$  couplings is as independent as possible of the phosphorylation pattern.

Advantages of such an HNP experiment are obvious: i) HNP-NMR provides direct proof of histidine phosphorylation, ii) data can be interpreted based on the individual peak pattern independent of chemical shift information, iii) proteins can be measured in their folded states, iv) radioactively labelled  $^{32}\text{P}$  phosphorus can be avoided, v) HNP-NMR provides information about the regiochemistry of phosphorylation, thus providing information about the nitrogen site of the imidazole side chain. Therefore, HNP-NMR will provide essential contributions to investigate histidine phosphorylated proteins.

In Figure 3.1 individual magnetization transfer pathways are shown for all three species of phosphohistidines. Magnetization



Intensities of cross peaks depend on the size of couplings between  $^1\text{H}$  and  $^{15}\text{N}$  ( $^2J[^1\text{H},^{15}\text{N}]$  and  $^3J[^1\text{H},^{15}\text{N}]$ ). Since  $^3J[^1\text{H},^{15}\text{N}]$  (-2 Hz) is significantly smaller than  $^2J[^1\text{H},^{15}\text{N}]$  (-5 to -10 Hz) in histidine, the transfer through  $^3J[^1\text{H},^{15}\text{N}]$  is inefficient and thus cross peaks arising through  $^3J[^1\text{H},^{15}\text{N}]$  are smaller by a factor of 6 to 20 than those from the  $^2J[^1\text{H},^{15}\text{N}]$  couplings [Blomberg *et al.*, 1977, Pelton *et al.*, 1993]. Therefore, histidine phosphorylation and phosphorylation states, as shown in Figure 3.1, can be easily identified on the basis of individual peak patterns (HNP spectrum).

Beside proton-nitrogen couplings the  $^1J[^{15}\text{N},^{31}\text{P}]$  coupling needs to be known to set up an HNP experiment. However,  $^1J[^{15}\text{N},^{31}\text{P}]$  are not well documented in the literature for phosphohistidines. This might be due to the broad range of the  $^1J[^{15}\text{N},^{31}\text{P}]$  coupling constants that depend on the chemical structures of the compounds [Berger, Braun, Kalinowski; Wiley-Chichester, 1997, Wrackmeyer *et al.*, 2002, Marek *et al.*, 2007]. Therefore,  $^1J[^{15}\text{N},^{31}\text{P}]$  coupling constants were determined for all three phosphohistidines (1, 2, and 3 according to Figure 3.1) under which they were stable: from pH 3 to pH 10 for 1 and 2 and pH 6 to pH 9 for 3. The  $^1J[^{15}\text{N},^{31}\text{P}]$  coupling constants were extracted from 1D  $^{31}\text{P}$  pH titration series and summarized in Figure 3.2 (for further information see section: 2.6.6).

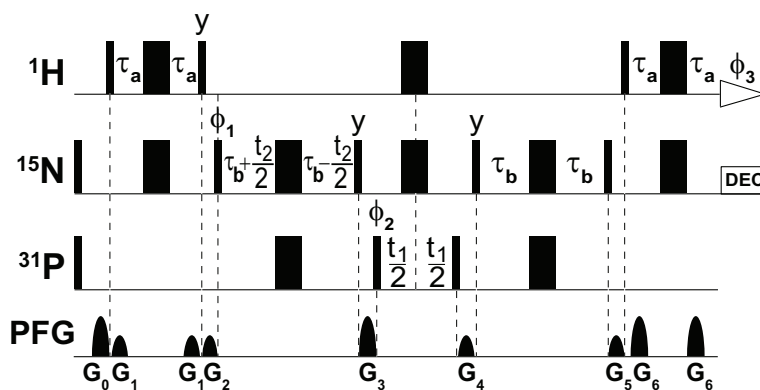


**Figure 3.3:** NMR pulse sequence of the HNP experiment for identification of phosphorylated histidines. Thin and thick bars represent  $90^\circ$  and  $180^\circ$  non-selective pulses, respectively. Default phases are x unless indicated otherwise. The phase cycle was set to  $\{\phi_1 = x, -x; \phi_2 = x, x, -x, -x; \phi_3 = -x, x, x, -x\}$ .  $^{15}\text{N}$  decoupling was achieved by the GARP pulse sequence with field strength of 1.3 kHz. Pulsed field gradients (PFG) indicate the magnetic field gradient strength applied along the z-axis:  $G_0$  and  $G_6$ : duration = 1 ms;  $G_{1-5}$  = 0.5 ms.  $G_0$ : amplitude =  $45 \text{ G cm}^{-1}$ ,  $G_1$  =  $11 \text{ G cm}^{-1}$ ,  $G_2$  =  $17 \text{ G cm}^{-1}$ ,  $G_3$  =  $36 \text{ G cm}^{-1}$ ,  $G_4$  =  $6 \text{ G cm}^{-1}$ ,  $G_5$  =  $15 \text{ G cm}^{-1}$ ,  $G_6$  =  $30 \text{ G cm}^{-1}$ . States-TPPI quadrature detection methods were applied for frequency discrimination in both indirect dimensions by altering phases  $\phi_1$  and  $\phi_2$ .

We find a strong dependence of the  $^1\text{J}[^{15}\text{N},^{31}\text{P}]$  couplings on the pH value for 1 and 2 varying between 5 and 17 Hz. Since the inflection point of the  $^1\text{J}[^{15}\text{N},^{31}\text{P}]$  couplings coincide with the pKa value of the respective non-phosphorylated nitrogen atom [Hultquist *et al.*, 1966, Gassner *et al.*, 1977] we conclude that the protonation state of this nitrogen atom strongly influences the size of the coupling constant. In agreement with this interpretation, for 3, which does not have a nitrogen atom that can be protonated, the  $^1\text{J}[^{15}\text{N},^{31}\text{P}]$  coupling constants are independent of pH value. Owing to the steepness of the titration curves, the difference in pKa values for 1 and 2 of only 0.8 units results in  $^1\text{J}[^{15}\text{N},^{31}\text{P}]$  couplings that differ by almost a factor of 2 at pH 6.3.

The strong dependence of  $^1\text{J}[^{15}\text{N},^{31}\text{P}]$  on the protonation state is not surprising, since similar effects were observed for  $^1\text{J}[^{13}\text{C},^{15}\text{N}]$  couplings in histidine [Blomberg *et al.*, 1977, Alei *et al.*, 1980, Schmidt *et al.*, 2008], for other amino acids [Severge *et al.*, 1976] and for  $^2\text{J}[^{31}\text{P},^{31}\text{P}]$  in guanosine nucleotides [Rösch *et al.*, 1980].

Similar to the  $^1\text{J}[^{15}\text{N},^{31}\text{P}]$  couplings for 1 and 2, pH-dependent sigmoidal curves were also observed for  $^{15}\text{N}$  chemical shifts (data not shown). It is noteworthy that the  $^1\text{J}[^{15}\text{N},^{31}\text{P}]$  values for 3 are almost identical to the ones for protonated 1 and 2. We conclude that the electron-withdrawing effect of the phosphate group is similar to that of a proton.

Based on the derived data about  $^1\text{J}[^{15}\text{N},^{31}\text{P}]$  coupling constants the HNP experiment was designed for magnetization transfer from  $^1\text{H}$  through  $^{15}\text{N}$  to  $^{31}\text{P}$  and back. The pulse sequence is shown in Figure 3.3.

The designed HNP-NMR experiment is a regular long-range  $^1\text{H},^{15}\text{N}$ -HSQC [Pelton *et al.*, 1993] combined with an additional  $^{15}\text{N},^{31}\text{P}$ -HSQC. The  $^1\text{H},^{15}\text{N}$ -HSQC is preferred over the HMBC since there are no homonuclear couplings of  $^1\text{H}$  that could reduce the transfer function in the HSQC. The dephasing and rephasing delay for the  $^1\text{J}[^{15}\text{N},^{31}\text{P}]$  is set to  $\tau_b=25$  ms based on an average coupling (10 Hz; Figure 3.2) of free phosphohistidines to achieve sufficient magnetization transfer for all phosphohistidine species.

To test the performance of the HNP experiment, we applied it to a mixture of 1, 2, and 3 which are readily obtained by phosphorylation of histidine by phosphoramidate (PA) [Hultquist *et al.*, 1966]. Two 2D projections of the 3D HNP experiment for phosphohistidines can be seen in Figure 3.4. In agreement with Figure 3.1, compound 1 gave one  $^1\text{H},^{31}\text{P}$  cross peak, compound 2 shows two  $^1\text{H},^{31}\text{P}$  cross peaks with identical  $^{31}\text{P}$  chemical shift, and compound 3 shows three  $^1\text{H},^{31}\text{P}$  cross peaks as three of the four corners of a rectangle. Additional minor peaks for

1 and 3 originate from non-zero  $^3J[{}^1\text{H}, {}^{15}\text{N}]$  couplings between  ${}^1\text{H}^{\delta 2}$  and  ${}^{15}\text{N}^{\delta 1}$  as described already before [Pelton *et al.*, 1993].

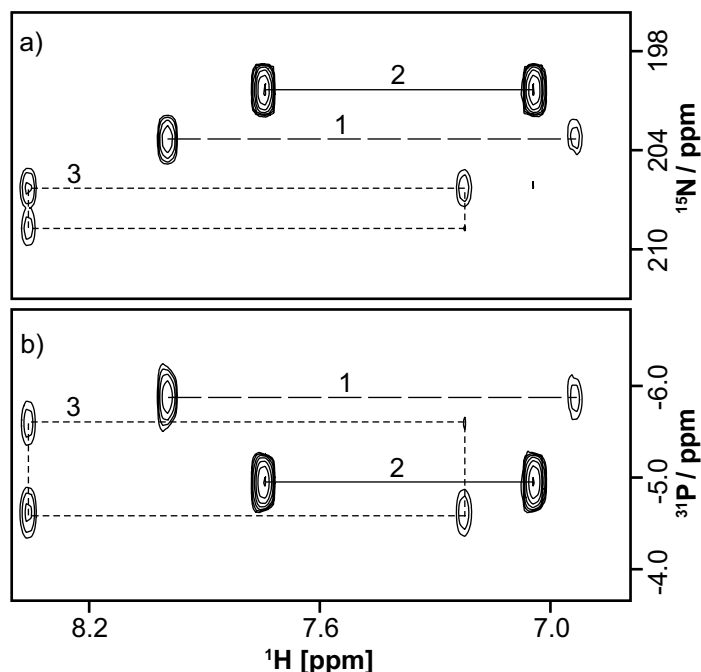


**Figure 3.4:** Contour plots of 2D projections from a 3D HNP spectrum of phosphorylated histidines at pH 7.5 and 303 K. a)  ${}^1\text{H}, {}^{15}\text{N}$  and b)  ${}^1\text{H}, {}^{31}\text{P}$  projections are shown. The spectrum was recorded with 4 scans in approximately 4 h and 17 ( ${}^{31}\text{P}$ ), 35 ( ${}^{15}\text{N}$ ), and 512 ( ${}^1\text{H}$ ) complex points with  $t_{1\text{max}}=8.7$  ms,  $t_{2\text{max}}=7.2$  ms, and  $t_{3\text{max}}=65.8$  ms. Identification of all three possible phosphorylation states in the imidazole ring of histidine is highlighted according to Figure 1: (1) one peak pattern (pattern 1) characteristic for 1, (2) two peak pattern (pattern 2) for 2, and (3) three peak pattern (pattern 3) for 3. The minor peaks in patterns 1 and 3 result from a small three-bond coupling  $^3J[{}^1\text{H}, {}^{15}\text{N}]$  between  ${}^1\text{H}^{\delta 2}$  and  ${}^{15}\text{N}^{\delta 1}$ .

Kalbitzer *et al.*, 1982]. The  ${}^1J[{}^{15}\text{N}, {}^{31}\text{P}]$  coupling constant was additionally measured for phosphorylated HPr by conventional long range 2D  ${}^1\text{H}, {}^{15}\text{N}$ -HSQC (data not shown). The determined value of 9.5 Hz at pH 7.4 agrees very well with the  ${}^1J[{}^{15}\text{N}, {}^{31}\text{P}]$  coupling constant for free 1-phosphohistidine obtained from the pH titration (Figure 3.2). However, further HNP experiments additionally revealed the presence of 3 in phospho-HPr. This result is discussed in chapter 6.

Since histidine phosphorylation is a fundamental step of phosphate transfer within the PTS [Meadow *et al.*, 1990] the histidine carrier protein (HPr) was the first protein tested by HNP-NMR to show the applicability of the pulse sequence. The phosphorylation of histidine 15 is well characterized [Anderson *et al.*, 1971, Schrecker *et al.*, 1975, Jones *et al.*, 1997] and can be efficiently achieved by enzymatic phosphorylation as described in section 2.6.6. Figure 3.5 shows the result of HPr phosphorylation detected by HNP-NMR.

A single one peak pattern can be nicely observed clearly indicating a  $\text{N}^{\delta 1}$  phosphorylation site corresponding to 1. This is in perfect agreement with the results already obtained for HPr [Anderson *et al.*, 1971, Schrecker *et al.*, 1975,

After successful application to HPr HNP-NMR was performed with the PRDI and PRDII domains of GlcT. These results are presented and discussed in sections 4.2 and 5.1.

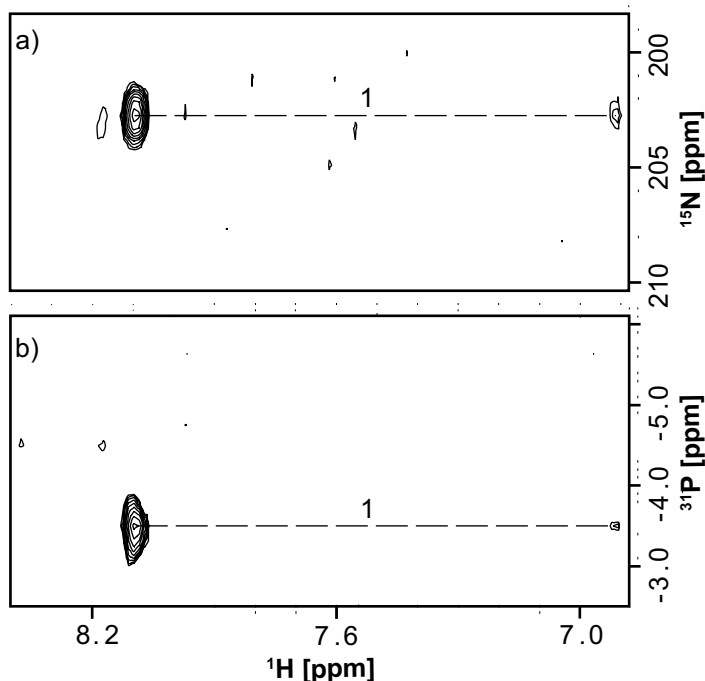


**Figure 3.5:** Contour plots of 2D projections from a 3D HNP experiment of phosphorylated HPr. In a) the  $^1\text{H}$ ,  $^{15}\text{N}$  and in b) the  $^1\text{H}$ ,  $^{31}\text{P}$  projections are shown. The experiment was measured at 303 K at pH 7.4. A one peak pattern points to a phosphorylated  $\delta 1$  site in HPr corresponding to 1.

One has to take into account that coupling constants for the HNP experiment also rely on values gained from reference compounds, such as phosphohistidines (1, 2 and 3). Further, the exact size of  $^1\text{J}[^{15}\text{N}, ^{31}\text{P}]$  couplings depends on two facts: i) the local pH conditions of the phosphohistidine and ii) the  $\text{pK}_a$  of the specific phosphohistidine. Both values might vary from protein to protein and can be affected by environmental conditions of the protein itself or the solvent. In addition,  $\text{pK}_a$  values can differ more than 1 pH unit before and after

phosphorylation of a histidine [Van Dijk *et al.*, 1990, Rajagopal *et al.*, 1994, Garrett *et al.*, 1998]. Hence, the precise knowledge of the exact  $\text{pK}_a$  value is mostly unknown especially for uncharacterized proteins. However, since all phosphorylation sites in the free phosphohistidine were easily identified from specific H,P correlation patterns (Figure 3.4),  $\tau_b = 25$  ms is a good starting point. In principle,  $\tau_b$  can also be adjusted so that all the phosphorylation states of a histidine can be determined based on the individual  $^1\text{J}[^{15}\text{N}, ^{31}\text{P}]$  coupling constants of the free phosphohistidine and the  $\text{pK}_a$  value of the specific phosphohistidine in a protein.

The sensitivity can be improved by a factor of  $\sqrt{2}$  by recording the experiment either as a 2D  $^1\text{H}$ ,  $^{15}\text{N}$  or  $^1\text{H}$ ,  $^{31}\text{P}$  correlation spectrum. However, if more than one histidine is phosphorylated in a protein, because of the narrow chemical shift

ranges of phosphohistidines (approx. 200 to 210 ppm for  $^{15}\text{N}$  and approx. 0 to -10 ppm for  $^{31}\text{P}$ ), ambiguities arising from possible overlap of  $^{15}\text{N}$  or  $^{31}\text{P}$  resonances are best avoided, by using the 3D version. For larger proteins with shorter proton and nitrogen  $T_2$  times the delays  $\tau_a$  and  $\tau_b$  can also be reduced.

### 3.1 Summary

The newly developed HNP-NMR experiment is a technique, which gives both the evidence of phosphohistidines and provides regiochemistry information of such phosphorylations. Histidine phosphorylation can be identified and characterized by its specific peak pattern in the spectrum.

We anticipate that the HNP experiment proposed herein will play a significant role in studying histidine phosphorylation which is important in prokaryotic systems. Furthermore, our HNP experiment may give insight into recent findings of phosphohistidines in eukaryotic proteins [Matthews, 1995, Steeg *et al.*, 2003, Srivastava *et al.*, 2006, Klumpp and Krieglstein, 2009, Xu *et al.*, 2010].

## 4 The PRDI of the antiterminator GlcT

As described in section 1.2 PRDI is the first regulatory domain of GlcT, which is controlled by histidine phosphorylation. In this chapter the analysis of PRDI phosphorylation is presented.

To determine the precise composition of the phosphorylation enzymes that phosphorylate PRDI, NMR spectra were recorded and compared to each other (section: 4.1). Furthermore, to study the regiochemistry of phosphohistidines in PRDI upon phosphorylation our newly developed HNP experiment was employed (Chapter 3) and the result is shown in section 4.2. The optimization of sample conditions for mass spectrometric experiments can be seen in section 4.3. These optimized conditions were used to determine the number of phosphate groups that were involved in the phosphorylation of PRDI (section: 4.4). In order to identify which histidine(s) was (were) phosphorylated in the protein sequence tandem mass spectrometry was applied (section: 4.5). The change in the aggregation state upon phosphorylation was verified by analytical gel filtration (section: 4.6).

The protein purification was performed as described in section 2.5.4 and the results are shown in section: 2.5.8. PRDI phosphorylation was carried out by mixing PRDI, Enzyme I (EI), HPr and a specific salt of phospho(enol)pyruvic acid (PEP). This basic mixture is called phosphorylation mix. For NMR experiments (section: 2.6.6) and analytical gel filtration (section: 2.6.2) phospho(enol)pyruvic acid trisodium salt was used to prepare this phosphorylation mix. This PEP contains no acidic protons and, hence, the phosphorylation mix did not affect the pH of those samples. PRDI phosphorylation, studied by mass spectrometry, was carried out according to section 2.6.3 using phospho(enol)pyruvic acid tri(cyclohexylammonium) salt.

## 4.1 Composition of the PRDI phosphorylation mix

To characterize the conditions, which were needed to obtain phosphorylated PRDI, NMR was used intensively. As reported, phosphorylation of PRDI is mediated by Enzyme II [Schmalisch *et al.*, 2003]. To study the role of Enzyme II upon PRDI phosphorylation the cytosolic AB-fragment of Enzyme II (EII) was added to the phosphorylation mix (for further details about Enzyme II see section: 1.2).  $^1\text{H}$ ,  $^{15}\text{N}$ -HSQC spectra of different sample compositions were measured and compared to each other in order to determine the best composition for the phosphorylation mix. According to this composition, which mainly depends on the concentration of HPr, different states of PRDI phosphorylation can be seen in Figure 4.1. In a) the spectrum of the pure PRDI is shown (the chemical shift list can be found in the appendix). In all the other figures (b to e) spectra are shown, where the samples contained an identical amount of PEP but different molar ratios of EI, HPr and EII compared to monomeric PRDI. In b) to d) of the same figure selected resonances are highlighted, which show the presence of a second set of signals. This indicated that non-phosphorylated but likewise phosphorylated PRDI was observed in those spectra. Upon reaching the final composition in the phosphorylation mix (PRDI : EI : HPr : EII : PEP = 1 : 1/70 : 1 : 1/10 : 100) one preferential set of signals was observed, which points out that under such conditions PRDI is almost fully phosphorylated. These experiments showed that a constant increase of HPr, finally reaching a 1:1 ratio compared to monomeric PRDI, was crucial to obtain PRDI phosphorylation whereas the EI and EII concentrations were significantly reduced. To exclude changes in the spectra that are not dependent on PRDI phosphorylation a spectrum of the phosphorylation mix without PEP was measured but no differences between the spectra of the pure PRDI and the PEP-free phosphorylation mix were observable (data not shown). Therefore, in the absence of PEP, PRDI is not affected by one of the other enzymes and changes in the spectra of Figure 4.1 can be attributed exclusively to the phosphorylation of PRDI.

As already mentioned, the concept of PRDI regulation is specifically achieved by Enzyme II-mediated phosphorylation [Schmalisch *et al.*, 2003]. The tendency that an increased HPr concentration, accompanied by a reduced concentration of EII-AB, increased the amount of phosphorylated PRDI prompted us to record a spectrum of the phosphorylation mix in the absence of EII. To our surprise identical peak shifts were observed upon phosphorylation pointing to a phosphorylated PRDI (data not shown). Hence, EII was not necessary for PRDI phosphorylation and further phosphorylation experiments of PRDI were carried out as follows:

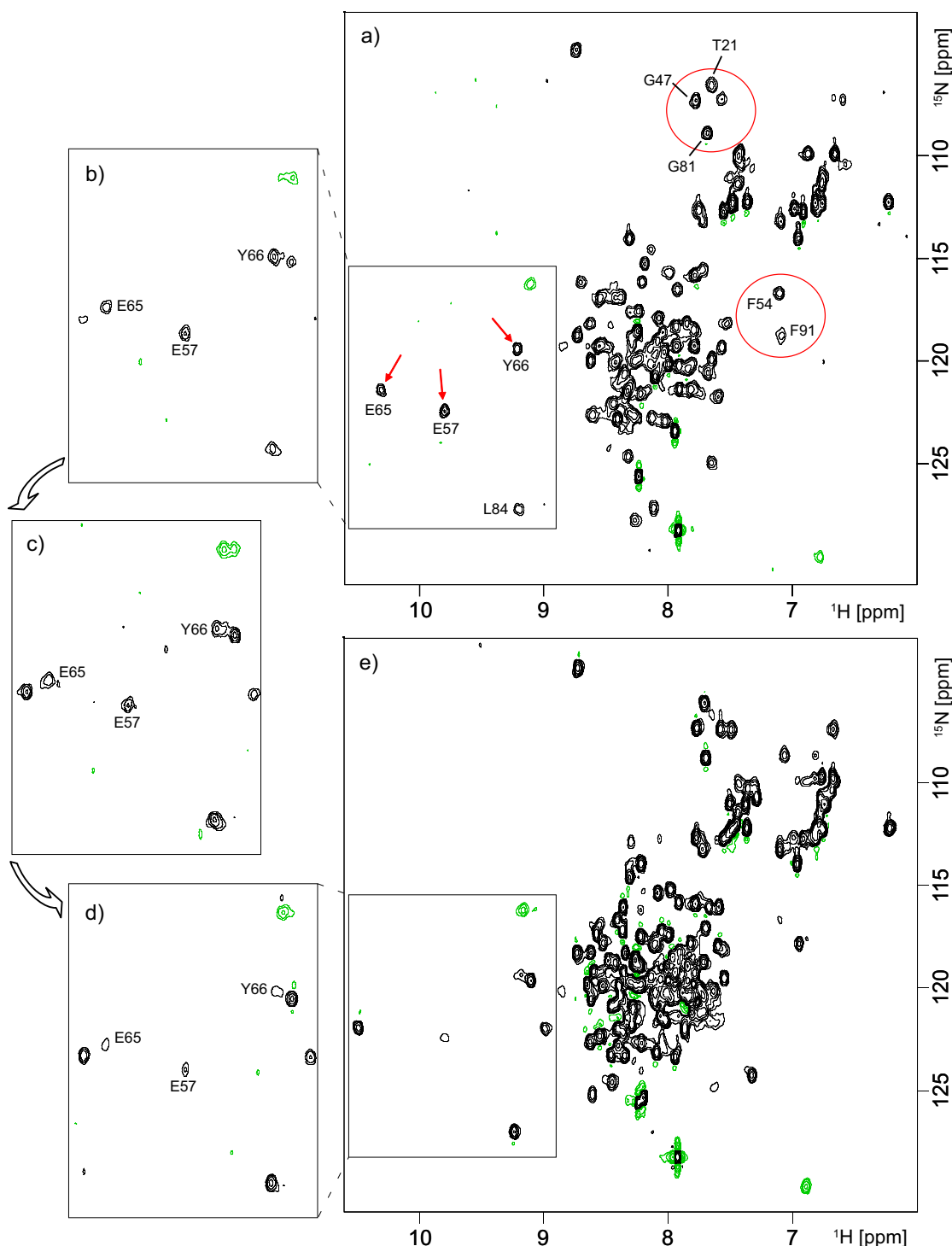


**Figure 4.1:**  $^1\text{H}$ ,  $^{15}\text{N}$ -HSQC spectra of PRDI measured at a  $^1\text{H}$  frequency of 700 MHz. Shown are the NH-signals of the amide backbone. In a) PRDI is shown before phosphorylation compared to e), which was recorded after phosphorylation. In b) to d) the partial phosphorylation is shown and can be followed by different peak intensities until the resonances of non-phosphorylated PRDI almost disappear. A selection of resonances showing significant changes upon phosphorylation are highlighted by red circles. (The chemical shift list of the non-phosphorylated PRDI can be found in the appendix.) The composition of the different phosphorylation mixtures are given in molar ratios compared to monomeric PRDI in the order PRDI : EI : HPr : EII : PEP a) pure PRDI, b) 1 : 1/5 : 1/7 : 1/5 : 100, c) 1 : 1/2 : 1/3 : 1/2 : 100, d) 1 : 1/2 : 2/3 : 1/2 : 100 and e) 1 : 1/70 : 1 : 1/10 : 100.



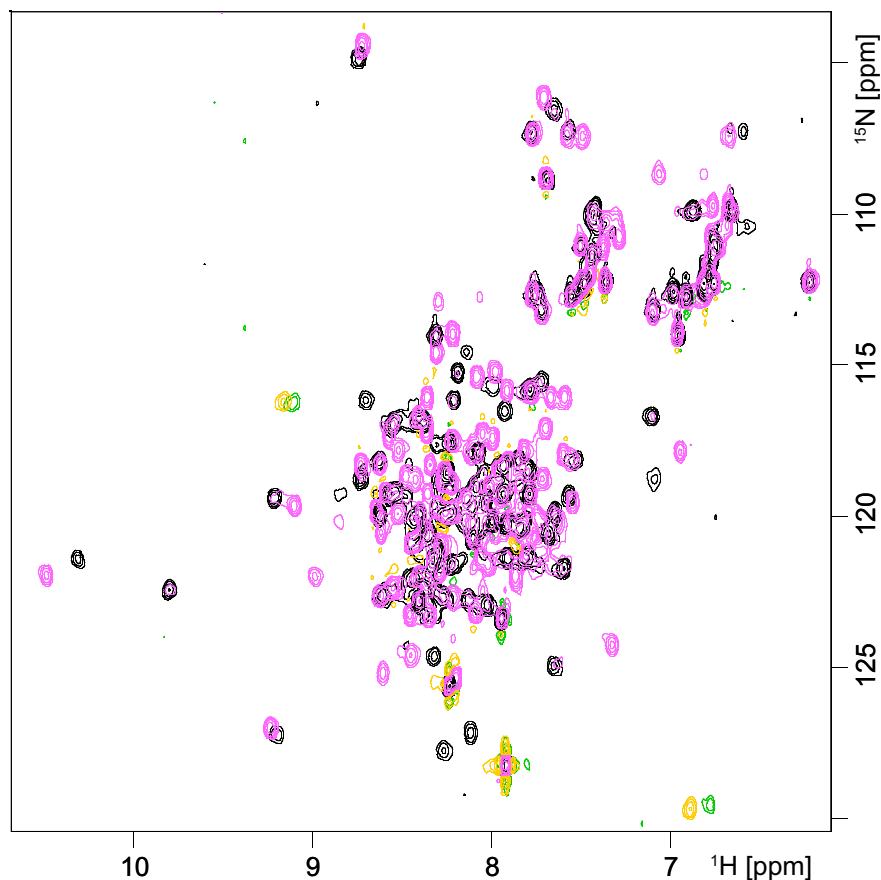


**Figure 4.2:** Superimposed  $^1\text{H},^{15}\text{N}$ -HSQC spectra of the PRDI-backbone before phosphorylation (positive and negative signals are shown in black and green, respectively) and after phosphorylation (positive and negative signals are in magenta and dark yellow, respectively). Both spectra were measured at 303 K at a  $^1\text{H}$  resonance frequency of 600 MHz.

$\text{PRDI} : \text{EI} : \text{HPr} : \text{PEP} = 1 : 1/30 : 1 : 100$ . These results emphasized that an equimolar ratio of HPr compared to monomeric PRDI is the minimal prerequisite to obtain almost fully phosphorylated PRDI.

In Figure 4.2 two superimposed  $^1\text{H},^{15}\text{N}$ -HSQC spectra of the phosphorylation mix in the absence and in the presence of PEP are shown. A multitude of resonance shifts can be observed and such dramatic changes between both HSQC spectra indicate massive structural rearrangements in the backbone of PRDI upon phosphorylation. In contrast to the non-phosphorylated PRDI, no chemical shift assignment is available for the phosphorylated PRDI.

## 4.2 Regiochemistry of PRDI phosphohistidines

The HNP spectrum of the PRDI phosphorylation mix was measured as described in section 2.6.6 and interpreted according to chapter 3.

Figure 4.3 shows a HNP spectrum of phosphorylated PRDI. In a) the  $^1\text{H}$ ,  $^{15}\text{N}$  and in b) the  $^1\text{H}$ ,  $^{31}\text{P}$  projections can be seen. The strongest resonances, which are approx. at 8.0 and 7.1 ppm showed an identical chemical shift of 202.5 and -4.8 ppm in their  $^{15}\text{N}$  and  $^{31}\text{P}$  dimensions, respectively (label 2). In both projections they form a clear two peak pattern, which can be attributed to the presence of 3-phosphohistidine.

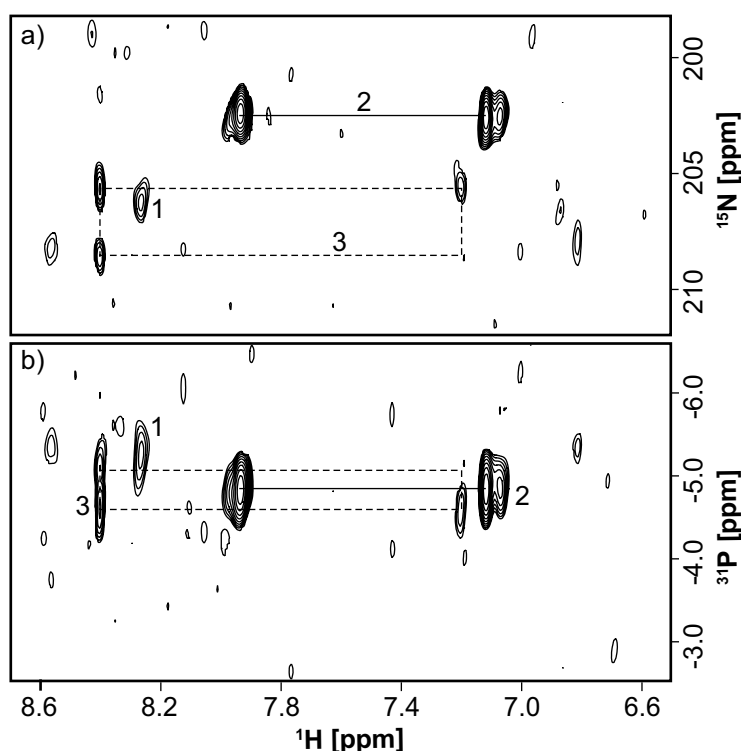


**Figure 4.3:** Contour plots of 2D projections from a 3D HNP spectrum of phosphorylated PRDI. In a)  $^1\text{H}$ ,  $^{15}\text{N}$  and in b)  $^1\text{H}$ ,  $^{31}\text{P}$  projections are shown, respectively. In both projections all three possible peak patterns can be observed, which are labelled with 1, 2 and 3. 13 ( $^{31}\text{P}$ ), 15 ( $^{15}\text{N}$ ), and 512 ( $^1\text{H}$ ) complex points with  $t_{1\text{max}}=6.7$  ms,  $t_{2\text{max}}=8.2$  ms, and  $t_{3\text{max}}=65.9$  ms, respectively, were recorded within 216 scans. The experiment was performed in 40 mM sodium phosphate buffer, 5 mM  $\text{MgCl}_2$ , 2 mM DTT and pH 7.3 at 303 K.

A second resonance of lower intensity, seen at 7.05 ppm, showed no chemical shift difference in both indirect dimensions compared to the resonances at 8.0 and 7.1 ppm, but possibly points to an additional overlapped two peak pattern. A further isolated resonance can be seen around 8.3 ppm (label 1), which represents a one peak pattern pointing to the presence of a 1-phosphohistidine in PRDI. Furthermore, two resonances can be seen at 8.4 ppm and one additional at 7.2 ppm forming a three peak pattern (label 3), which is characteristic for a 1,3-diphosphohistidine. On the basis of individual HNP correla-

tion patterns PRDI showed all the patterns that were observed for all three species of free phosphohistidines (Figure 3.4).

A very low noise level was chosen to identify all possible resonances in the spectrum. An additional two peak pattern of weak intensity is present around 8.6 and 6.8 ppm and could point to an additional formation of 3-phosphohistidine. However, the signal intensity is too low to reliably distinguish between spectral noise and true signals. However, the strong intensity of the other two peak pattern in the HNP spectrum of PRDI showed that 3-phosphohistidine is the dominant phosphohistidine species in this regulatory domain.

### 4.3 Sample optimization for mass spectrometry

Upon phosphorylation, HNP-NMR clearly confirmed the presence of phosphohistidines in PRDI of GlcT (section: 4.2). Mass spectrometry was used to study how many phosphate groups are involved in the phosphorylation reaction.

Electrospray ionization mass spectrometry (ESI-MS) was used for spectrometric experiments of PRDI. To identify protein phosphorylations the theoretical molecular weight of a protein needs to be known. A single phosphate group attached to a protein can be determined based on an increased molecular weight of 80 Da ( $\text{HPO}_3$ ) in the positive ion mode and 79 Da ( $\text{PO}_3$ ) in the negative ion mode [Besant and Attwood, 2009]. However, optimized sample conditions were needed to detect sensitive and labile phosphohistidines in proteins by mass spectrometry.

For successful ionization and signal detection, appropriate buffer conditions are crucial. Usually, protein buffers contain salt(s), buffer components or detergents in amounts, which cause severe problems for ESI-MS experiments. In these conditions, the signal intensity is significantly reduced and the formation of stable protein-ion adducts (e. g. with metal cations, such as sodium or potassium,  $[\text{M}^+ \text{-protein}]$ ) was often observed in mass spectra in combination with electrospray ionization [Kerwin *et al.*, 1994]. In a protein mixture each protein (and protein-ion adduct) shows a characteristic peak distribution according to its  $m/z$  ratio and contributes to a mass spectrum. As a result, the interpretation of such a mass spectrum becomes more complicated as different species are present in the sample. Hence, the purity of each enzyme and the use of an appropriate buffer, to minimize the formation of protein-ion adducts, is essential to obtain interpretable mass spectra of such a complex protein mixture. ESI-MS is a very sensitive ana-

lytical technique but the sensitivity deteriorates with the presence of non-volatile buffers and other additives, which should be avoided<sup>9</sup>. Hence, adjusted buffer conditions are inevitable in order to obtain optimal results. Buffer compounds such as ammonium acetate at neutral pH conditions were favourable to study PRDI phosphorylation.

Sample preparation as described in section 2.6.3 provided optimal conditions for mass spectrometric experiments. The use of phospho(enol)pyruvic acid tri(cyclohexylammonium) salt and liquid ammonia for the pH adjustment of the ammonium acetate buffer showed the best results that avoided the formation of protein-ion adducts. These conditions were of great advantage to measure the phosphorylation mix that contained not only the PRDI, but in addition all the other enzymes of the phosphorylation mix (Enzyme I and HPr).

The 50 fold excess of phospho(enol)pyruvic acid tri(cyclohexylammonium) salt in the phosphorylation mix did not disturb mass spectrometric experiments. Experiments, even carried out after 24 hours of phosphorylation, showed no negative effects during the measurement although histidine phosphorylated proteins are subjected to hydrolysis and the concentration of free phosphate increased over time in the sample.

The sample conditions, which were described in this section, were used to determine the amount of phosphate groups that were involved in PRDI phosphorylation (section: 4.4). Furthermore, these conditions were also applied to PRDII (section: 5.2).

## 4.4 Quantification of PRDI phosphorylation

In this section results are shown in order to determine the number of phosphate groups involved in PRDI phosphorylation. The quantity of histidine phosphorylation was already studied for homologous antiterminator proteins. It was shown that HPr-dependent *in vitro* phosphorylation of *Bacillus subtilis* LicT resulted in a one-, two and threefold phosphorylated LicT. Both conserved histidines in PRDII and one in PRDI were subjected to phosphorylation [Lindner *et al.*, 1999]. Further studies showed phosphorylation of the fourth histidine residue in PRDI of LicT by the PTS [Deutscher *et al.*, 1997, Tortosa *et al.*, 2001]. In contrast, a threefold and a single HPr-dependent phosphorylation was proposed for *Bacillus*

---

<sup>9</sup><http://www.astbury.leeds.ac.uk/facil/MStut/mstutorial.htm>

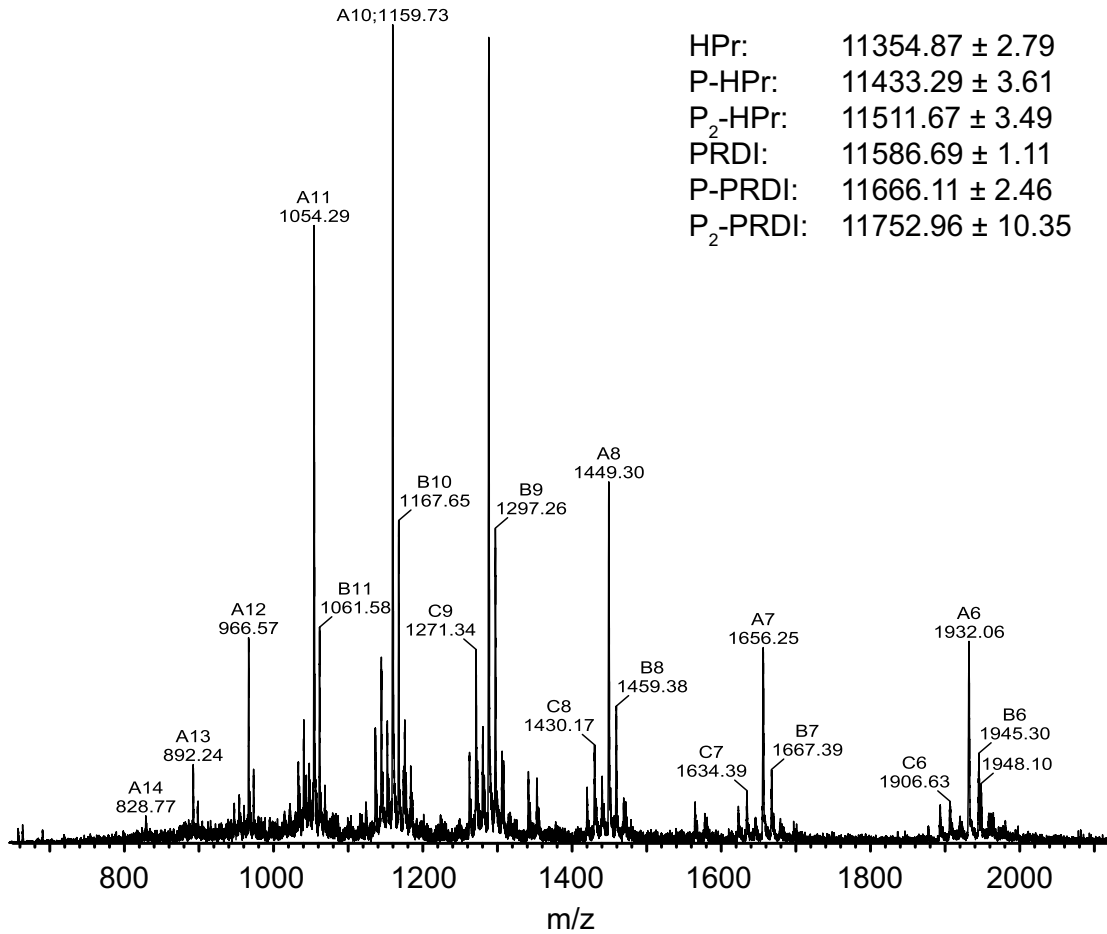


**Figure 4.4:** Mass spectrum of the PRDI phosphorylation mix measured in ammonium acetate buffer after approx. 27 hours of phosphorylation. Besides PRDI, HPr can be seen in the mass spectrum with its characteristic mass of  $11354.87 \pm 2.79$  Da (theoretical: 11353.6 Da) and PRDI, which was measured at  $11586.69 \pm 1.11$  Da (theoretical: 11586.1 Da). Phosphorylation was identified by a mass shift of 80 Da, which corresponded to a single phosphate group in both proteins: HPr at  $11433.29 \pm 3.61$  Da (theoretical: 11433.6 Da) and PRDI at  $11666.11 \pm 2.46$  Da (theoretical: 11666.1 Da). Additional masses indicated a second phosphate group, which is involved in PRDI and HPr phosphorylation. A further shift in mass by approx. 160 Da can be seen for HPr ( $11511.67 \pm 3.49$  Da; theoretical: 11513.6 Da) and PRDI ( $11752.96 \pm 10.35$  Da, theoretical: 11746.1 Da).

*subtilis* SacY [Tortosa *et al.*, 1997] and *Staphylococcus carnosus* GlcT [Knezevic *et al.*, 2000], respectively. Hence, no general rule about the number of phosphate groups that are involved in the phosphorylation of antiterminator proteins can be derived [van Tilbeurgh and Declerck, 2001]. Furthermore, no specific results were known so far for the regulatory domains of GlcT of *Bacillus subtilis*.

Figure 4.4 shows the mass spectrum of a sample that was measured after approx. 27 hours of phosphorylation. In the mass spectrum of the phosphorylation mix an increase of approx. 80 and 160 Da was observed for the molecular weights of PRDI as well as for HPr.

The mass of non-phosphorylated PRDI and HPr was found at  $11586.69 \pm 1.11$  Da (theoretical: 11586.1 Da) and  $11354.87 \pm 2.79$  Da (theoretical: 11353.6 Da), respectively. A molecular mass increased by 79.4 Da for PRDI and 78.4 Da for HPr resulted in molecular weights of  $11666.11 \pm 2.46$  Da (theoretical: 11666.1 Da) for PRDI and  $11433.29 \pm 3.61$  Da (theoretical: 11433.6 Da) for HPr. These mass differences corresponded well with a single phosphate group involved in the phosphorylation of both PRDI and HPr. Furthermore, additional masses were measured. The molecular weights of  $11752.96 \pm 10.35$  Da (theoretical: 11746.1 Da) and  $11511.67 \pm 3.49$  Da (theoretical: 11513.6 Da) differed by 166.3 Da and 156.8 Da compared to the non-phosphorylated species of PRDI and HPr, respectively. Such a difference in mass, which is approx. 160 Da, strongly indicated the presence of a second phosphate group in PRDI and HPr (for further details see chapter: 6).

Mass spectrometric analysis clearly showed that a single phosphate group is primarily involved in PRDI phosphorylation but a second phosphate group was also observed.

## 4.5 Histidine phosphorylation sites in PRDI

As shown in the introduction (section: 1.2) each regulatory domain individually comprises two conserved histidine residues [Greenberg *et al.*, 2002] which are proposed to be involved in histidine phosphorylation [van Tilbeurgh and Declerck, 2001]. Homology studies revealed that histidine residues 111 and 170 in PRDI are the potential targets of regulatory phosphorylation in PRDI of GlcT [Greenberg *et al.*, 2002]. Homologous antiterminators such as LicT were studied and phosphorylation sites were identified. It has been shown that LicT phosphorylation occurs at all four conserved histidines in both regulatory domains [Lindner *et al.*, 1999, Tortosa *et al.*, 2001]. As described in section 4.4 phosphorylation of PRDI in GlcT clearly involved a single phosphate group but the presence of a lower populated double phosphorylation was also suggested. This could indicate that both conserved histidines are phosphorylated (possibility A). However, HNP experiments of PRDI (section: 4.2) revealed the presence of 1,3-diphosphohistidine which leads to the possibility that only one histidine is phosphorylated but at both nitrogen

sites (possibility B; Figure 1.3). Mass spectrometric experiments, as shown in Figure 4.4 (section: 4.4), cannot distinguish between the possibilities A and B or exclude one of the two conserved histidines. To investigate the phosphorylation site(s) in PRDI tandem mass spectrometry was performed after tryptic proteolysis of phosphorylated PRDI (for further details see section: 2.6.3).

As described in sections 4.3 and 4.4 protein phosphorylation can be identified by an increased molecular weight of 80 Da, which corresponds to a single phosphate group. The identification of the phosphorylation sites was performed by tandem mass spectrometry, which was carried out by He-Hsuan Hsiao in the group of Dr. Henning Urlaub (Bioanalytical Mass Spectrometry) and the results are shown in Figure 4.5. After tryptic proteolysis the C-terminal peptide was found to have an increased molecular weight by approx. 80 Da. This peptide contains two histidines, the conserved His 170 and one additional histidine in close vicinity (His 172).

This C-terminal peptide of PRDI contains 37 amino acids and has a mass of 4005.5 Da. In Figure 4.5 a) the mass spectrum of the peptide is shown. This peptide was triple charged as seen by the isotopic distribution pattern. The difference between the peaks was approx. 0.33 thus, identifying the factor  $z$  in the  $m/z$  ratio with 3. 1362.01 Da multiplied by a factor of 3 resulted in a final mass of 4086.03 Da. Compared to the theoretical mass of the peptide, which is 4005.5 Da, a difference of 80.53 Da remains, which nicely corresponds to a single phosphate group (80 Da).

To further identify the phosphorylated amino acid and to distinguish between phosphoramidates and phosphoesters MS-MS (MS2) experiments were applied [Ross, 2007] in particular to the mass identified in a). Collision induced dissociation (CID) mostly carried out using inert gas (e.g. argon, helium or xenon) provides additional energy to destabilize chemical modifications, such as phosphorylations [Ross, 2007] (for further information see section: 2.6.3).

As seen in Figure 4.5 b) the MS-MS spectrum showed an additional triple charged peak of 1335.36 Da which is magnified in c). A back-calculation resulted in a mass of 4006.08 Da, which excellently corroborated with the theoretical mass of 4005.05 Da of the C-terminal peptide without the phosphate group. The difference between 1362.0 Da and 1335.4 Da in b) was 26.6 Da and, multiplied with 3, resulted in 79.8 Da. This difference in mass, of approx. 80 Da, was the experimental proof of a  $-\text{PO}_3$  group corresponding to a phosphoramidate ( $-\text{N}-\text{PO}_3$ ) in proteins.

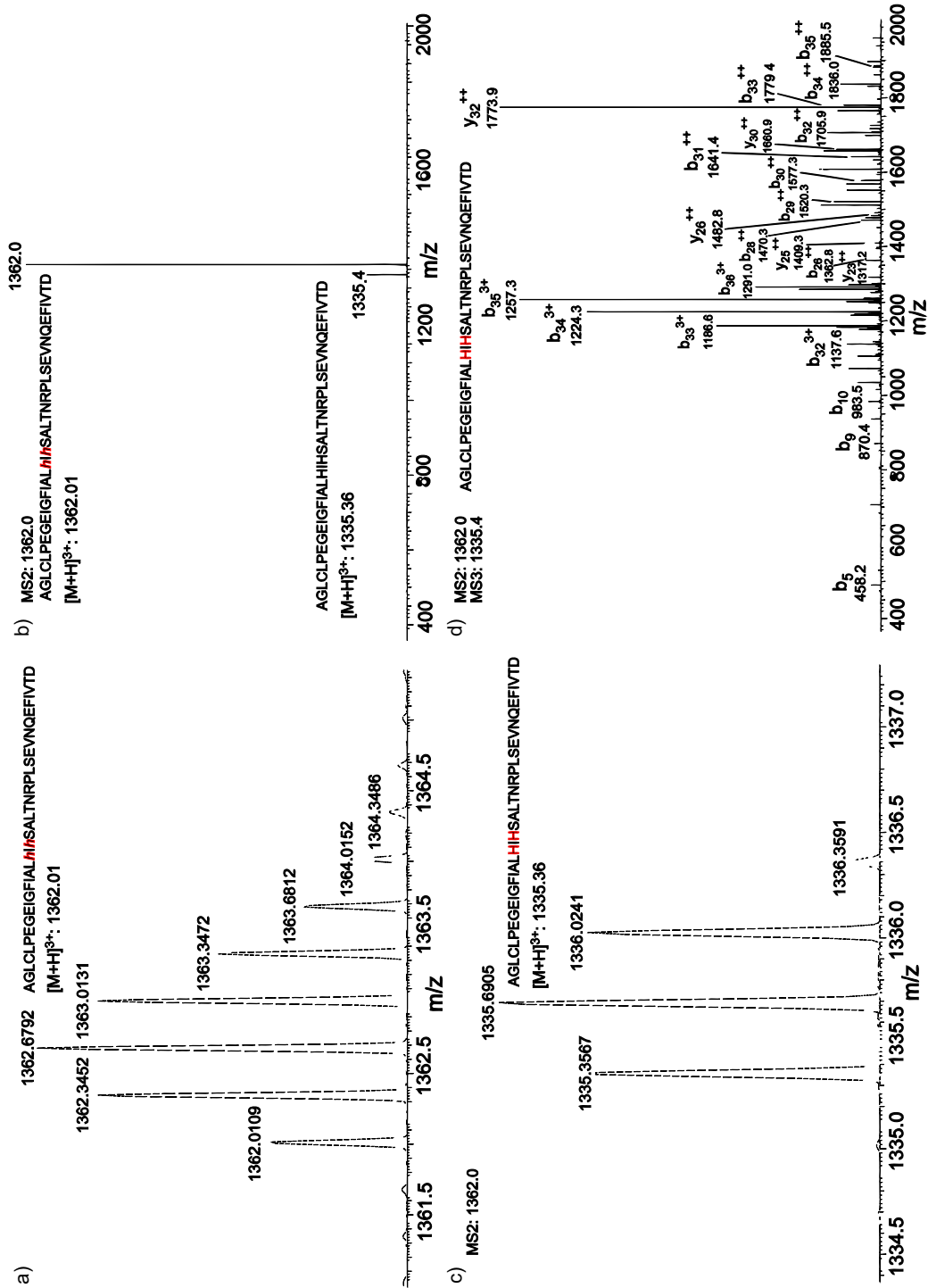


**Figure 4.5:** Results of tandem mass spectrometric experiments after tryptic proteolysis of PRDI, which confirms histidine phosphorylation in the C-terminal end of the domain. In a) the mass spectrum (MS) of the triple charged C-terminal peptide is shown. A calculated difference approx. of 80 Da indicates the phosphorylation of the peptide by a single phosphate group. Histidine phosphorylation is confirmed in b) by MS-MS (MS2) experiments, which is clearly indicated by a loss of 80 Da corresponding to a phosphoramidate bond. In c) the mass peak of 1335.4, which is shown in b), is magnified. The MS-MS-MS (MS3) experiment is shown in d) to verify the amino acid sequence of the peptide. Histidine residues are indicated in red (the first "H" in the sequence corresponds to His 170).



Phosphoesters in proteins ( $-O-PO_3$ ) would have resulted in a significant loss of 96 Da corresponding to a  $-O-PO_3$  group [Ross, 2007]. Thus, MS-MS experiments carried out with PRDI clearly showed histidine phosphorylation in the C-terminal peptide. However, possibly due to low chemical stability or low population no 1,3-diphosphohistidine was observed in this peptide.

In Figure 4.5 d) a MS-MS-MS (MS3) spectrum of the C-terminal peptide is shown. Upon increasing the collision energy (CID) fragments of the PRDI peptide

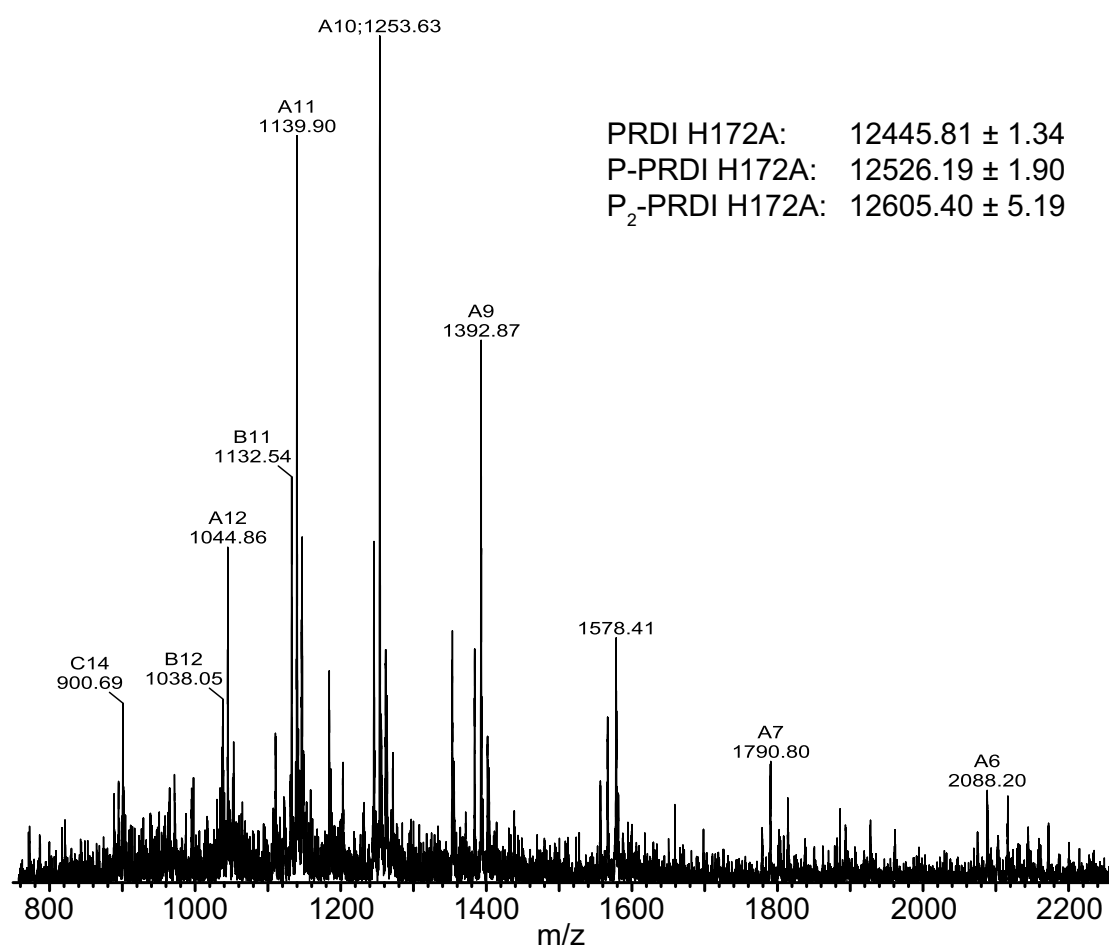


**Figure 4.6:** Phosphorylation of PRDI H172A shown by mass spectrometry. The non-phosphorylated PRDI H172A was measured with  $12445.81 \pm 1.34$  Da (theoretical mass: 12444.0 Da) and the single phosphorylated protein with  $12526.19 \pm 1.90$  Da (theoretical mass: 12524.0 Da). Besides a single phosphorylation an additional measured mass of  $12605.40 \pm 5.19$  Da indicates the presence of a second phosphate group attached to PRDI H172A (theoretical mass: 12604.0 Da)

were generated. This experiment was performed with the non-phosphorylated mass, shown in c), to validate the peptide sequence and to avoid matching to other peptides of identical masses. After fragmentation, y and b fragments with their specific charges are shown in Figure 4.5 d) and confirmed that the detected ions refer to the C-terminal peptide of PRDI. Further details about the analysis and interpretation of the MS3 spectrum are explained in section 2.6.3.

The tryptic proteolysis, which was performed after phosphorylation, resulted in peptides of defined length. These known lengths are needed to identify PRDI peptides later by mass spectrometry. Unfortunately, the C-terminal peptide, which is shown in Figure 4.5 and coincides with the location of the found phosphohistidine, contained not only the conserved histidine His 170 but one additional histidine His 172, which is considered not to be conserved [Greenberg *et al.*, 2002]. This histidine 172, which is part of a -His-Ile-His- motif, was mutated to alanine (-His-Ile-Ala-) in order to exclude phosphorylation of His 172 in the C-terminal end of PRDI. After phosphorylation of PRDI H172A mass spectrometric experiments without proteolysis were repeated as already shown in section 4.4.

In Figure 4.6 phosphorylation of PRDI H172A is shown. The non-phosphorylated protein has a theoretical molecular weight of 12444.0 Da and was measured at  $12445.18 \pm 1.34$  Da in the mass spectrum. A single phosphate group attached to PRDI H172A resulted in a theoretical mass of 12524.0 Da, which was clearly seen in the mass spectrum at  $12526.19 \pm 1.90$  Da. Besides the single phosphorylated PRDI H172A, an indication of a second phosphate group was observed. An additional mass, measured at  $12605.40 \pm 5.19$  Da, differed by 159.6 Da as compared to non-phosphorylated PRDI H172A. The theoretical mass of a double phosphorylated PRDI H172A (12604.0 Da) corresponded well to this finding. Furthermore, this is in good agreement with the result we obtained by mass spectrometry for the wild type PRDI (Figure 4.4). Hence, the phosphorylation of PRDI H172A excluded histidine 172 as phosphorylation site.

Since it was reported that mutation of one conserved histidine site prevents phosphorylation on both sites [Schmalisch *et al.*, 2003] PRDI H172A was the only mutant in order to exclude a phosphorylation site besides histidine 170 in the C-terminal peptide.

Thus, the combined results of ESI- and tandem mass spectrometry strongly suggest that PRDI is dominantly phosphorylated by a single phosphate group at His 170 in the C-terminal end of the protein.

## 4.6 Specificity of PRDI phosphorylation

As described in the introduction (section: 1.2), the regulation through histidine phosphorylation involves massive alterations in the aggregation state of PRDI. Upon phosphorylation PRDI causes the inactivation of GlcT by its monomerization which thereby interrupts RNA binding [Schmalisch *et al.*, 2003]. Such dramatic effects in the aggregation state can be observed by analytical gel filtration and are presented in this section.

As shown in section 4.4, PRDI and HPr are of similar molecular weights (12 to 9 kDa, respectively; Table 2.10) and phosphorylation of PRDI was performed according to section 2.6.2. The separation between both proteins during analytical gel filtration was improved by using a Superdex 75 (16/60) gel filtration column (120 ml separation volume) and His-tag free HPr. In addition, the gel filtration run was carried out at 4°C to minimize the hydrolysis of the phosphoprotein (for further experimental details see section: 2.6.2).

As shown in section 4.1, phosphorylation of PRDI led to significant changes in the  $^1\text{H}$ ,  $^{15}\text{N}$ -HSQC NMR spectra and, hence, in the protein conformation. In Figure 4.7 the gel filtration chromatograms of the PRDI phosphorylation mix in the absence and in the presence of PEP are shown. The phosphorylation mix without PEP can be seen in solid line whereas the dashed line shows phosphorylated PRDI. Prior to phosphorylation PRDI eluted at 76 ml and HPr at 87 ml. Upon phosphorylation PRDI was split into two peaks. The first peak (76 ml) refers to dimeric and non-phosphorylated PRDI whereas the second peak (81 ml) points to monomeric and phosphorylated PRDI. SDS-PAGE clearly confirmed that PRDI is present in both peaks (76 and 81 ml; fractions 40 - 48) whereas HPr is seen in the last peak (85 ml; fractions 49 - 51). Furthermore, upon phosphorylation, the retention volume of HPr was slightly reduced (from 87 to 85 ml). This minor difference is significant because it indicates the phosphorylation of HPr and can be used as an internal standard to validate successful HPr phosphorylation. This effect can be observed in all other gel filtration chromatograms in this work and was also observed by other authors [Knezevic *et al.*, 2000].

Interestingly, HPr and PRDI show swapped band positions on the SDS-PAGE gel in Figure 4.7 as compared to their molecular weights. Although HPr has the lowest molecular weight of the proteins in the phosphorylation mix its band appeared above PRDI, which is slightly larger. This inversion can be explained because it has been reported that HPr is not sensitive to higher temperatures. The first HPr samples were purified from heat treated crude extracts [Anderson *et al.*,

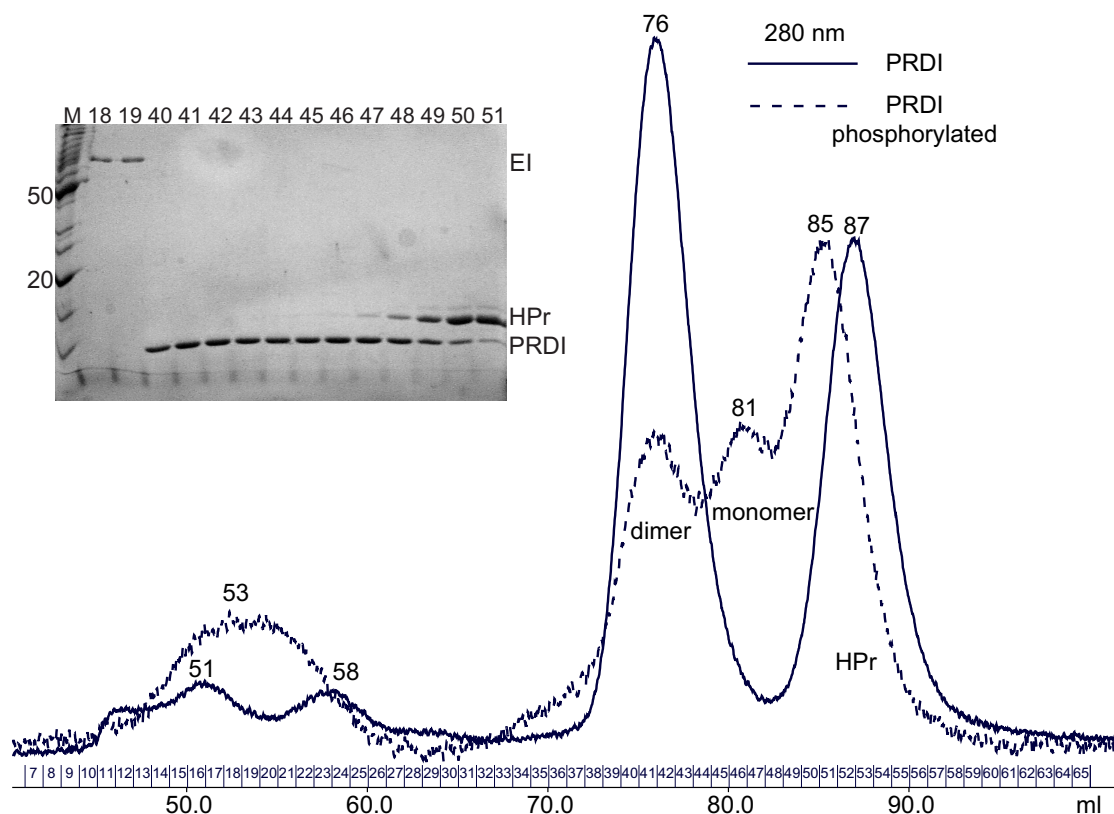


**Figure 4.7:** Superimposed analytical gel filtration chromatograms of PRDI before (solid line) and after (dashed line) phosphorylation performed in 200 mM NaCl, 50 mM Tris HCl, 5 mM MgCl<sub>2</sub>, 2 mM DTT, pH 7.4. The numbers on top of each peak represent the specific retention volumes of the peaks (in ml). The SDS-PAGE gel shows some selected fractions after phosphorylation was performed. M stands for the molecular weight marker and the numbers that are given for each lane correspond to the fraction numbers in the chromatogram of PRDI. No Enzyme II (EII) was used for phosphorylation.

1971]. Thus, HPr might be still partially folded although the sample was prepared for denaturing SDS-PAGE analysis. This could be reflected in unexpected band positions on the SDS gel.

Analytical gel filtration nicely confirmed the monomerization of PRDI upon phosphorylation, which was obtained in the absence of Enzyme II (EII). This was very surprising because the inactivating phosphorylation (leading to the monomeric form) of PRDI was supposed to be mediated by Enzyme II [Schmalisch *et al.*, 2003]. In order to confirm the result a GlcT fragment, which comprised the N-terminal RNA binding and the PRDI domain (RBD-PRDI) was phosphorylated and equally tested by analytical gel filtration (section:2.6.2). In two experiments phosphorylation was investigated in the i) absence and in the ii) presence of En-

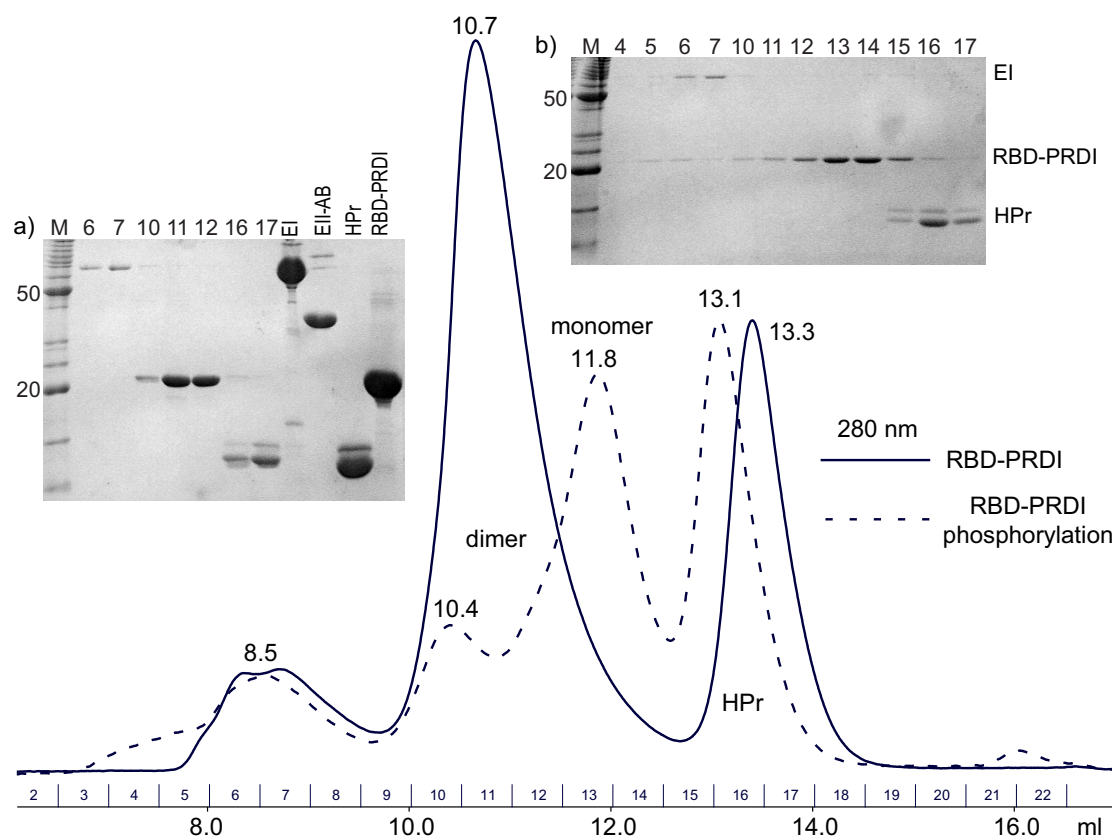


**Figure 4.8:** Two superimposed analytical gel filtration chromatograms of RBD-PRDI are shown before (solid line) and after (dashed line) phosphorylation (in the absence of Enzyme II). A clear monomerization can be seen for RBD-PRDI upon HPr-dependent phosphorylation. The numbers on top of each peak represent the specific retention volumes of the peaks (in ml). On the left side the SDS-PAGE gel, which is labelled with a) shows selected fractions before phosphorylation was carried out (solid line), on the right side (gel b) fractions can be seen after phosphorylation was performed (dashed line). M stands for the molecular weight marker and the numbers that are given for each lane correspond to the fraction numbers in the chromatograms, which are indicated at the x-axis. The gel labelled with a) also contains reference samples showing all PTS relevant enzymes. The analytical gel filtration was performed in 200 mM NaCl, 10 mM Tris HCl, 2 mM DTT, pH 8.0 and no Enzyme II (EII) was used for this experiment.

zyme II as shown in Figures 4.8 and 4.9, respectively. As seen in Figure 4.8 RBD-PRDI eluted at 10.7 ml prior to phosphorylation. Confirmed by SDS-PAGE analysis RBD-PRDI shifted to 11.8 ml upon phosphorylation. (On both gels HPr is present as split bands, because partly digested HPr was used and the phosphorylation mix also contained HPr with its His-tag.) In this sample no Enzyme II was present in the phosphorylation mix. The shift to a higher retention volume clearly indicated a similar effect as observed for the isolated PRDI (Figure 4.7) and can be interpreted as the monomerization of RBD-PRDI.

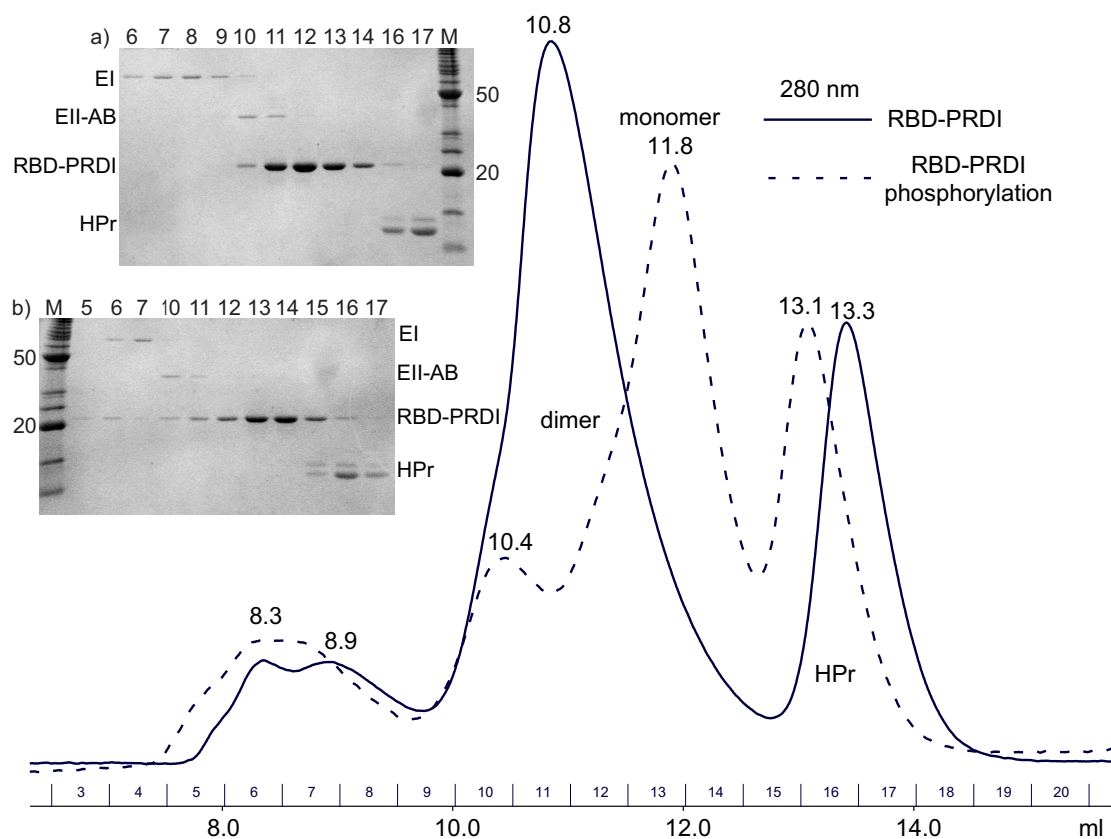


**Figure 4.9:** Two superimposed analytical gel filtration chromatograms of RBD-PRDI are shown before (solid line) and after (dashed line) phosphorylation. The phosphorylation mix contained catalytic amounts of Enzyme II (EII). The numbers on top of each peak represent the specific retention volumes of the peaks (in ml). No significant differences can be seen upon Enzyme II addition compared to the Enzyme II-free phosphorylation mix (Figure 4.8). The SDS-PAGE gel labelled with a) shows selected fractions before phosphorylation was carried out and selected fractions can be seen on the gel (labelled with b) after phosphorylation was performed. M stands for the molecular weight marker and the numbers that are given for each lane correspond to the fraction numbers in the chromatogram, which are indicated at the x-axis. The analytical gel filtration was performed in 200 mM NaCl, 10 mM Tris HCl, 2 mM DTT, pH 8.0.

The analytical gel filtration run with RBD-PRDI was repeated in the presence of catalytic amounts of Enzyme II (Figure 4.9). A molecular ratio of 1/13 compared to dimeric RBD-PRDI was used for the second gel filtration run. The RBD-PRDI eluted at 10.8 ml prior to phosphorylation, which is similar to the Enzyme II-free experiment (10.7 ml), and was equally shifted to 11.8 ml upon phosphorylation, corresponding to monomeric RBD-PRDI. These findings agree with the retention volumes that were reported for the non-phosphorylated RBD-PRDI of LicT [Déméné *et al.*, 2008]. The dimer and monomer of LicT RBD-PRDI were found approx. at 11.2 and 12.3 ml (Superdex 75, 10/300; GE Healthcare),

respectively. Our results showed that, upon phosphorylation, no significant difference in the aggregation state of RBD-PRDI can be observed irrespective of the absence or presence of Enzyme II. Hence, GlcT RBD-PRDI monomerization was efficiently mediated by HPr-dependent phosphorylation. This result confirms the monomerization of the isolated PRDI upon HPr-dependent phosphorylation. However, a significant difference of GlcT RBD-PRDI compared to RBD-PRDI of LicT is that non-phosphorylated LicT RBD-PRDI exists in a dimer / monomer equilibrium, always showing two concentration-dependent peaks upon gel filtration [Déméné *et al.*, 2008]. On the contrary, non-phosphorylated RBD-PRDI of GlcT showed a clear single peak upon analytical gel filtration, which can be attributed to the dimer. Furthermore, no tendency was observed that the dimeric GlcT RBD-PRDI converted into a monomer without phosphorylation.

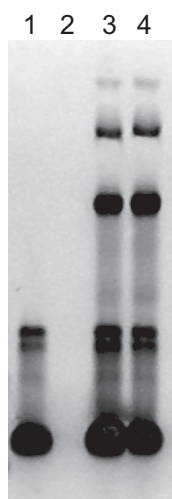


**Figure 4.10:** Ethidium bromide stained native gel of the RBD-PRDI-RAT complex. Lane 1 contains 2.6 nmol RAT RNA, whereas lane 2 contains only 0.1 nmol of RBD-PRDI. In the lanes 3 and 4 5.2 nmol RAT RNA were mixed with 0.38 and 0.57 nmol RBD-PRDI, respectively. A band shift can be seen in lanes 3 and 4 upon RNA binding. The complex formation was carried out in 200 mM NaCl, 50 mM Tris HCl, 2 mM DTT, pH 8.0 and incubation was performed for 60 minutes on ice.

In addition, the dimeric aggregation state of RBD-PRDI was confirmed by electrophoretic mobility shift assay (EMSA; Figure 4.10), which was performed according to section 2.6.5. A 33 nucleotide RAT RNA was prepared (section: 2.6.4) to form RAT-RBD-PRDI complexes (section: 2.6.5). The Ethidium bromide stained RNA can be seen in lane 1. Lane 2 contained the pure RBD-PRDI and as expected no Ethidium bromide staining was observed for the sole protein. As seen on the gel, upon addition of the RAT RNA a clear band shift can be observed in lanes 3 and 4. In the samples, which are shown in the lanes 3 and 4, the RNA was mixed with RBD-PRDI in molar ratios of 13:1 and 9:1, respectively, compared to dimeric RBD-PRDI, providing a 9 to 13 fold excess of RNA. An additional minor band can be seen for the pure RAT (lane 1), which has not been clearly attributed to a specific state of the RAT RNA. A similar effect can be observed upon complex formation (lanes 3 and 4), which could be possibly caused by an alternative secondary structure formation of the RNA.

It is suggested that only dimeric GlcT and, thus, dimeric RBD-PRDI is capable to bind its

RNA target [Schmalisch *et al.*, 2003] (Figure 1.1). Hence, one can conclude that GlcT RBD-PRDI is a dimer in solution.

## 4.7 Summary

PRDI is the first regulatory domain in GlcT, which is controlled by histidine phosphorylation (section: 1.2). Two conserved histidines (His 111 and His 170) are supposed to be the target of regulatory phosphorylation [Greenberg *et al.*, 2002, Schmalisch *et al.*, 2003]. HNP-NMR showed that the dominant phosphohistidine species in PRDI is 3-phosphohistidine (section: 4.2). Furthermore, PRDI is mainly regulated by a single phosphate group (section: 4.4), which is strongly suggested to be located at histidine 170 as shown by tandem mass spectrometry (section: 4.5). A second phosphate group was identified by mass spectrometry and can be attributed either to two onefold phosphorylated histidines or one twofold phosphohistidine (1,3-diphosphohistidine). A 1,3-diphosphohistidine was observed by HNP-NMR (section: 4.2) but its position in the protein sequence could not be established by NMR. Thus, the combined results of HNP-NMR and mass spectrometry revealed that the second phosphate group in PRDI forms a 1,3-diphosphohistidine most likely at histidine 170 (for further information see chapter: 6). Upon phosphorylation analytical gel filtration verified that dimeric PRDI forms monomers, a process which did not depend on the presence of Enzyme II in our experiments (section: 4.6).



## 5 The PRDII of the antiterminator GlcT

The PRDII is the second regulatory domain, which is regulated by histidine phosphorylation, and forms the C-terminal end of the antiterminator protein GlcT (Figure 1.1, section: 1.2).

In this chapter the application of the new HNP experiment (chapter: 3) is described in order to determine the regiochemistry of histidine phosphorylation in PRDII (section: 5.1). The number of phosphate groups, which are involved in PRDII phosphorylation was studied by mass spectrometry and is presented in section 5.2. Optimized sample conditions, which were also used for PRDI experiments, were necessary to apply mass spectrometry and were already described in section 4.3. To gain information about the phosphorylated histidine(s) in the protein sequence two PRDII single aspartate mutants (PRDII H218D and PRDII H279D; Table 2.10) were investigated by HNP-NMR and mass spectrometry (section: 5.3). Aspartate mutants were chosen because it was observed that those mutants are mimicking the phosphorylation of PRDII in the homologous antiterminator protein LicT [Tortosa *et al.*, 2001]. Finally, to study the aggregation state of PRDII upon phosphorylation, analytical gel filtration was used (section: 5.4).

Protein purification was performed as described in section 2.5.3 and the results are shown in section 2.5.9. Phosphorylation was carried out by mixing monomeric PRDII, Enzyme I (EI), HPr and phospho(enol)pyruvic acid (PEP). This mixture of the enzymes and PEP is again called phosphorylation mix in this chapter. Phosphorylation of PRDII was performed similar to PRDI (chapter: 4) according to sections 2.6.6 (NMR), 2.6.3 (mass spectrometry) and 2.6.2 (analytical gel filtration).

To avoid massive protein precipitation upon phosphorylation the experiments, which are described in this chapter, were performed with PRDII maintaining its His-Z fusion tag. Hence, PRDII refers to His-Z-PRDII in this work (for further information see section: 2.5.3).

## 5.1 Regiochemistry of PRDII phosphohistidines

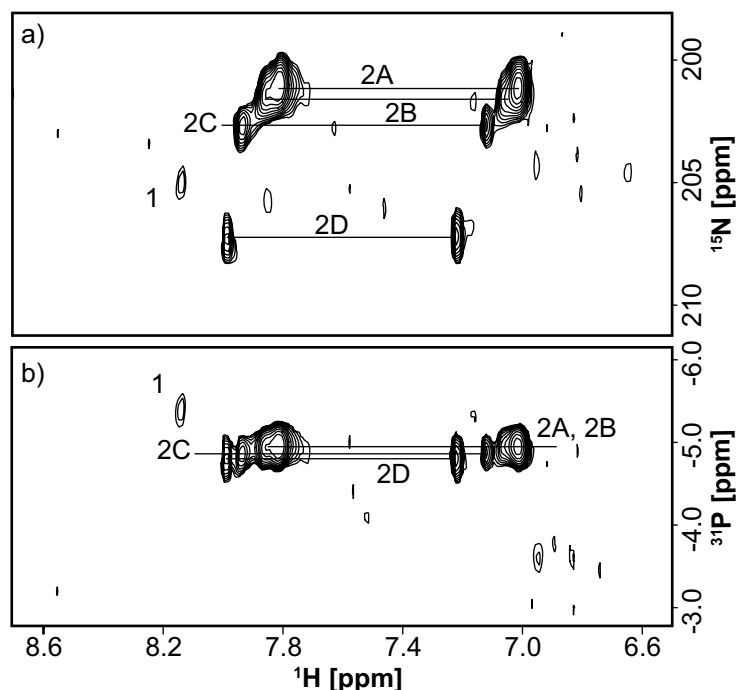


**Figure 5.1:** Contour plots of 2D projections of a 3D HNP spectrum of phosphorylated wild type PRDII showing the presence of phosphohistidines. In a) and b)  $^1\text{H}$ ,  $^{15}\text{N}$  and  $^1\text{H}$ ,  $^{31}\text{P}$  projections are shown, respectively. In both spectra four two peak patterns can be observed (labelled with 2A to 2D), which point out the presence of 3-phosphohistidines in PRDII. A one peak pattern (labelled with 1) indicates the presence of 1-phosphohistidine. 13 ( $^{31}\text{P}$ ), 15 ( $^{15}\text{N}$ ), and 512 ( $^1\text{H}$ ) complex points with  $t_{1\text{max}}=6.7$  ms,  $t_{2\text{max}}=8.2$  ms, and  $t_{3\text{max}}=66$  ms were recorded within 196 scans. The experiment was performed in 40 mM sodium phosphate buffer, 5 mM  $\text{MgCl}_2$ , 2 mM DTT and pH 7.4 at 303 K.

PRDII HNP-NMR experiments were carried out with the wild type protein and both single aspartate mutants (PRDII H218D and PRDII H279D) as described in section 2.6.6. In Figure 5.1 the HNP spectrum of the wild type PRDII is shown. In a) the  $^1\text{H}$ ,  $^{15}\text{N}$  and in b) the  $^1\text{H}$ ,  $^{31}\text{P}$  projections can be seen. Several peak patterns are present in both projections, which are labelled with 1 and 2A to 2D. Each pair of the latter resonances (2A to 2D) has their characteristic  $^{15}\text{N}$  chemical shift, ranging from 201 to 207 ppm. The same signals showed even less dispersion in the  $^1\text{H}$ ,  $^{31}\text{P}$  projection and their  $^{31}\text{P}$  chemical shifts are closely centered

around -4.9 ppm. The signals labelled with 2A to 2D can be clearly identified as four two peak patterns, clearly emphasizing the presence of 3-phosphohistidines in PRDII. A further single resonance at 8.1 ppm (label 1) possibly indicates a one peak pattern that represents 1-phosphohistidine.

As described in the introduction (section: 1.2) each regulatory domain (PRDs) comprises two conserved histidine residues [Greenberg *et al.*, 2002], which are attributed to their regulatory function [van Tilbeurgh and Declerck, 2001]. In

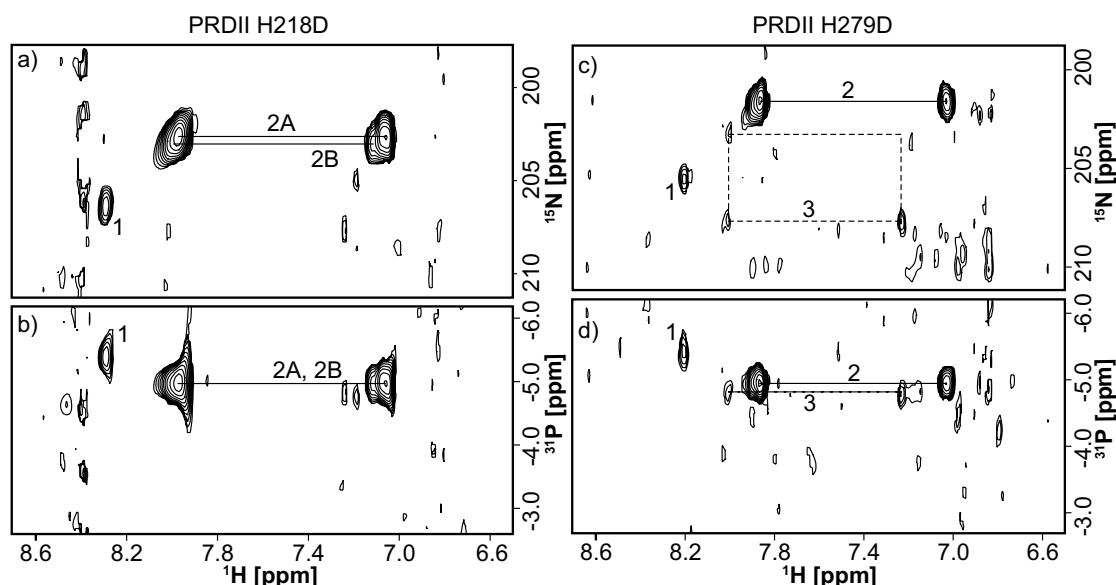


**Figure 5.2:** Contour plots of 2D projections of a 3D HNP spectrum of phosphorylated PRDII H218D (in a and b) and PRDII H279D (in c and d) to investigate histidine phosphorylation in both single aspartate mutants. In a) and c)  $^1\text{H}$ ,  $^{15}\text{N}$  and in b) and d)  $^1\text{H}$ ,  $^{31}\text{P}$  projections are shown, respectively. PRDII H218D (a and b) shows at least two two peak patterns in both projections (8.0 and 7.1 ppm; label 2A and 2B) together with a single one peak pattern (8.3 ppm, label 1). PRDII H279D (c and d) shows clearly one two peak pattern (7.9 and 7.0 ppm, label 2), a single one peak pattern (8.2 ppm, label 1) and possibly one three peak pattern (label 3), which is only seen in the  $^1\text{H}$ ,  $^{15}\text{N}$  projection. The clear two peak patterns, which can be seen in the spectra of both mutants, strongly indicate the presence of 3-phosphohistidines as the dominant phosphohistidine species in PRDII. 13 ( $^{31}\text{P}$ ), 15 ( $^{15}\text{N}$ ), and 512 ( $^1\text{H}$ ) complex points with  $t_{1\text{max}}=6.7$  ms,  $t_{2\text{max}}=8.2$  ms, and  $t_{3\text{max}}=66$  ms were recorded within 204 scans for H279D and 68 scans for H218D, respectively. The number of scans to measure PRDII H218D was reduced because the sample showed precipitation during three days of measurement time (reduced to one day). For both proteins the experiments were performed in 40 mM sodium phosphate buffer, 5 mM  $\text{MgCl}_2$ , 2 mM DTT and pH 7.4 at 303 K.

PRDII these histidines are His 218 and His 279 and they were individually mutated into aspartates. The HNP spectra of these two PRDII mutants were recorded to study the phosphorylation in the absence of one of those two conserved histidines. In Figure 5.2 the  $^1\text{H}$ ,  $^{15}\text{N}$  and  $^1\text{H}$ ,  $^{31}\text{P}$  projections of these spectra are shown for PRDII H218D (in a and b) as well as for PRDII H279D (in c and d).

Compared to the HNP spectrum of the wild type PRDII, where four two peak patterns were observed (Figure 5.1), two two peak patterns (labelled with 2A and 2B; not referring to 2A and 2B in Figure 5.1 of the wild type PRDII) were found in the spectrum of PRDII H218D (Figure 5.2 a and b). In the proton dimension, the chemical shifts of both two peak patterns are 8.0 and approx. 7.1 ppm and

the peaks have almost identical  $^{15}\text{N}$  and  $^{31}\text{P}$  chemical shifts, which are found at approx. 203 and -5 ppm, respectively. These two peak patterns clearly show that 3-phosphohistidine is the major phosphohistidine species in PRDII H218D. Compared to the HNP spectrum of the wild type PRDII a one peak pattern (labelled with 1) can be clearly seen at 8.3 ppm, pointing to a 1-phosphohistidine in PRDII H218D. Furthermore, this could also indicate the presence of a one peak pattern in the spectrum of the wild type PRDII, where a weak single resonance was observed approx. at 8.1 ppm.

The 2D projections of the HNP spectrum of PRDII H279D can be seen in Figure 5.2 c) and d). Upon phosphorylation a strong two peak pattern (labelled with 2) was observed in the spectrum at 7.9 and approx. 7.0 ppm in both projections. A chemical shift of 202 and -4.9 ppm can be noticed in the  $^{15}\text{N}$  and  $^{31}\text{P}$  dimensions, respectively. A three peak pattern (labelled with 3), which points to the presence of a 1,3-diphosphohistidine is very unlikely since i) the intensity is too weak to clearly distinguish between signal and spectral noise and ii) no resolved three peak pattern can be seen in the  $^1\text{H}, ^{31}\text{P}$  projection (Figure 5.2, d). Again, a single resonance was seen approx. at 8.2 ppm (label 1), which can be interpreted as a one peak pattern, indicating the presence of 1-phosphohistidine.

In the HNP spectra of both mutants as well as for the wild type protein a single one peak pattern of different intensities was observed, which indicated the presence of a 1-phosphohistidine in PRDII. However, based on the clear and strong two peak patterns that can be seen for the wild type PRDII as well as for both mutants 3-phosphohistidine is the major phosphohistidine in PRDII of GlcT. Furthermore, HNP-NMR revealed histidine phosphorylation for both single aspartate PRDII mutants.

As described in the outline of this chapter the phosphorylation of PRDII was carried out with the His(7x)-Z-PRDII. To exclude phosphorylation that potentially could originate from the fusion tag a mass spectrum of the phosphorylation mix, which contained a PRDII double aspartate mutant (PRDII H218D H279D), was measured. No phosphorylation was observed for this mutant and the results are further described in section 5.2. Thus, one can conclude that the histidines in the fusion protein as well as the hepta histidine tag are not involved in histidine phosphorylation.

## 5.2 Quantification of PRDII phosphorylation

As described in the beginning of this chapter PRDII contains its purification tag (His-Z-PRDII) to avoid protein precipitation upon phosphorylation. Hence, the molecular weight of PRDII is significantly increased by the additional His-Z fusion tag (His-Z-PRDII: 23.6 kDa; PRDI: approx. 11 to 13 kDa). In this section the results of the mass spectrometry studies are reported in order to identify the number of phosphate groups, which are involved in PRDII phosphorylation (for experimental details see section: 2.6.3).

In Figure 5.3 the mass spectrum of the PRDII wild type phosphorylation mix is shown. The measured mass of  $23582.42 \pm 10.47$  Da corresponds well with the theoretical molecular weight of non-phosphorylated PRDII (23581.8 Da). A mass, which was measured at  $23659.61 \pm 10.86$  Da showed a difference of 77.2 Da compared to the non-phosphorylated PRDII. This can be clearly interpreted as a single phosphate group, which is attached to PRDII (theoretical mass: 23661.8 Da). The low population of an additional mass at  $23753.41 \pm 13.36$  Da could indicate a second phosphate group that is involved in PRDII phosphorylation because it corresponds to a mass difference of 167.4 Da (approx. 2x 80 Da). The theoretical mass of a double phosphorylated PRDII is 23741.8 Da. A mass at  $23845.08 \pm 14.58$  Da, which differed by 262.7 and 185.5 Da as compared to the non-phosphorylated PRDII and single phosphorylated PRDII, respectively, could not yet be attributed to a protein in the phosphorylation mix.

As described in the introduction (section: 1.2) the domain specific phosphorylation of PRDs occurs at conserved histidine residues [van Tilbeurgh and Declerck, 2001], which are the histidines 218 and 279 in PRDII. Two single aspartate mutants (PRDII H218D and PRDII H279D), which were also used for HNP experiments (section: 5.1), were also measured by mass spectrometry. However, in contrast to the results of the HNP experiments the phosphorylation mix of PRDII H218D did not show a mass difference and hence, no evidence of a phosphorylation can be derived from this mutant (data not shown).

The mass spectrum of the PRDII H279D phosphorylation mix is shown in Figure 5.4. A mass of  $23562.91 \pm 14.80$  Da is in good agreement with the theoretical molecular weight of 23559.7 Da of the non-phosphorylated PRDII H279D. A mass, different by 79.5 Da, was measured at  $23642.38 \pm 17.02$  Da and strongly emphasized the attachment of a single phosphate group to PRDII H279D. The expected molecular weight of a single phosphorylated PRDII H279D is 23639.7 Da. Interestingly, the phosphorylated PRDII H279D was lowly populated as compared

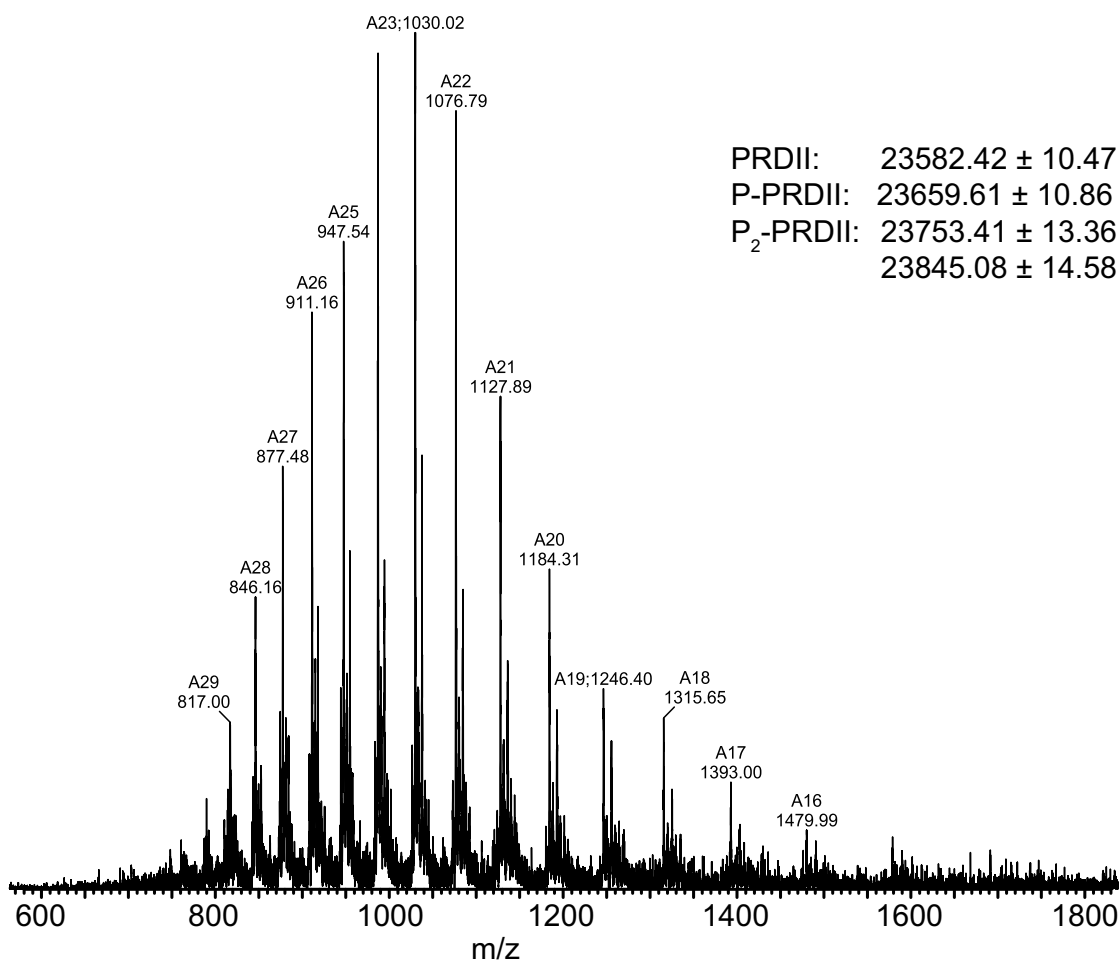


**Figure 5.3:** Mass spectrum of the PRDII wild type phosphorylation mix, which shows an increased molecular weight of PRDII upon phosphorylation. The theoretical molecular weight of PRDII is 23581.8 Da and was measured at  $23582.42 \pm 10.47$  Da. Phosphorylation is indicated by an increased mass of 80 Da compared to the non-phosphorylated PRDII. A measured mass at  $23659.61 \pm 10.86$  Da is increased by 77.2 Da, which corresponds to a single phosphate group attached to PRDII. The experiment was performed in 40 mM ammonium acetate, 2 mM DTT, pH 7.4.

to the non-phosphorylated protein whereas the mass spectrum of the wild type PRDII showed an almost fully phosphorylated protein (Figure 5.3). This clear difference indicates that the efficiency of phosphorylation is strongly decreased in PRDII H272D. An additional mass of  $23738.46 \pm 11.82$  Da, different by 175.6 Da as compared to the non-phosphorylated PRDII H272D, cannot yet be attributed to a protein and was already present in the mass spectrum of the non-phosphorylated PRDII H279D ( $23741.82 \pm 10.07$ ; data not shown).

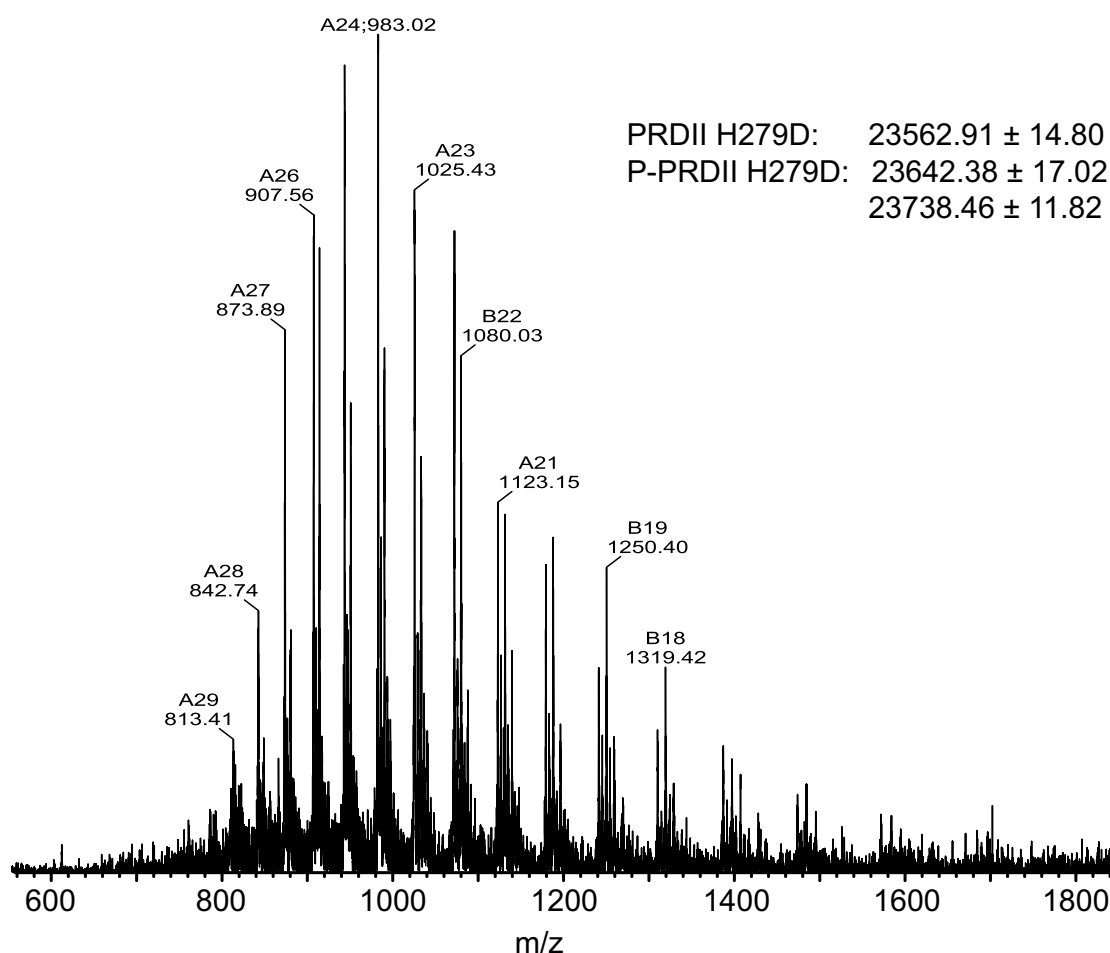


**Figure 5.4:** Mass spectrum of the PRDII H279D phosphorylation mix, which shows a minor phosphorylation effect. PRDII H279D was measured at  $23562.91 \pm 14.80$  Da, which is in good agreement with the theoretical molecular weight of 23559.7 Da. A lower population of a mass at  $23642.38 \pm 17.02$  Da, which is increased by 79.5 Da, indicates a single phosphate group attached to the protein (theoretical molecular weight: 23639.7 Da). The experiment was carried out in 40 mM ammonium acetate, 2 mM DTT, pH 7.4.

In section 5.1 it was shown that histidine phosphorylation was observed in the wild type PRDII as well as in both single aspartate PRDII mutants. A double aspartate mutant (PRDII H218D H279D) was prepared and tested by mass spectrometry to detect phosphorylation sites apart from the two conserved histidine residues (data not shown). No significant difference before ( $23537.24 \pm 13.35$  Da) and after ( $23537.69 \pm 12.89$  Da) phosphorylation was observed for the double mutant (theoretical molecular weight: 23537.7 Da), which strongly indicates that no other histidines than the two conserved ones (His 218 and His 279) are involved in the regulatory histidine phosphorylation of PRDII. As similarly observed for

the wild type PRDII as well as for PRDII H279D an additional mass, which is increased by 179.2 Da, was measured at  $23716.47 \pm 11.04$  Da in the spectrum of the non-phosphorylated PRDII H218D H279D. This mass, which was also present in the spectrum of the phosphorylation mix of PRDII H218D H279D ( $23718.82 \pm 11.56$  Da), is not yet attributed to a specific protein in the phosphorylation mix.

Hence, mass spectrometry clearly shows the presence of a single phosphate group attached to PRDII upon phosphorylation. Little indication was found for the wild type PRDII that a second phosphate group is involved in the phosphorylation reaction. PRDII H279D was equally phosphorylated by a single phosphate group but significantly lower in population as compared to the wild type PRDII. However, no phosphorylation was observed by mass spectrometry for PRDII H218D and the double aspartate mutant PRDII H218D H279D.

### 5.3 Histidine phosphorylation sites in PRDII

In this section the combined results obtained from HNP-NMR (section: 5.1) and mass spectrometry (section: 5.2) were used to identify the phosphorylation sites in PRDII of GlcT.

As shown in the introduction (section: 1.2) each regulatory domain of an antiterminator protein individually comprises two conserved histidine residues [Greenberg *et al.*, 2002] which are proposed to be involved in histidine phosphorylation [van Tilbeurgh and Declerck, 2001]. The homologous antiterminator protein LicT was studied and phosphorylation sites were identified. It has been shown that LicT phosphorylation occurs at both conserved histidines in PRDII [Lindner *et al.*, 1999, Tortosa *et al.*, 2001]. In GlcT, homology studies and previous experiments revealed that histidine residues 218 and 279 in PRDII are the potential targets of regulatory phosphorylation [Greenberg *et al.*, 2002, Schmalisch *et al.*, 2003].

The HNP-NMR spectra clearly confirmed histidine phosphorylation of the wild type PRDII as well as for both single aspartate mutants (section: 5.1). Mass spectrometric experiments performed with the phosphorylation mix of the PRDII double aspartate mutant (PRDII H218D H279D) confirmed that only these two conserved histidines are involved in the phosphorylation reaction (section: 5.2). This is in agreement with what has so far been suggested [van Tilbeurgh and Declerck, 2001, Schmalisch *et al.*, 2003], and confirms the concept of conserved histidines required for regulatory phosphorylation. The HNP-NMR spectra of both



single aspartate mutants clearly showed that both conserved histidines in PRDII can be individually phosphorylated (section: 5.1). The presence of phosphohistidines in these mutants showed that each conserved histidine can be phosphorylated independently from the other conserved one. Hence, one can conclude that those two histidines are involved in the phosphorylation reaction.

However, the primary result from mass spectrometry revealed that a single phosphate group is clearly involved in the phosphorylation of the wild type PRDII as well as of PRDII H279D (section: 5.2). A double phosphorylation of the wild type PRDII was indicated but in only minor population. Interestingly, the HNP spectrum of the wild type PRDII showed four individual two peak patterns (5.1), which - in principle - indicate four phosphorylated histidines. However, these four peak patterns exceed the number of potential phosphorylation sites in PRDII (two conserved histidines) by two. The NMR result also seems to contradict the mass spectrometric results, where a single phosphate group was clearly identified. Hence, the four individual two peak patterns in the HNP spectrum of the wild type PRDII could be explained by the presence of three different PRDII species: individual single phosphorylation of PRDII at i) histidine 218 and ii) histidine 279, which results in two two peak patterns in the spectrum and iii) the simultaneous phosphorylation of PRDII at histidine 218 and 279, which additionally contributes two two peak patterns. This would be in agreement with a twofold phosphorylated PRDII, which was indicated by mass spectrometry in lower population (section: 5.2). The second two peak pattern, which was observed for the H218D mutant, might be the result of local conformational changes of the phosphohistidine (see also chapter: 6).

## 5.4 Specificity of PRDII phosphorylation

The regulatory HPr-dependent phosphorylation of PRDII domains in various antiterminator proteins stimulates the activity of the full length protein by forming stable dimers in order to modulate the binding activity of the N-terminal RBD (RNA-binding domain). Whereas this activating phosphorylation is mandatory for PRDII domains of other antiterminator proteins, such as SacT and LicT, HPr is not required to stimulate the activity of GlcT because constitutive activity of GlcT was observed in mutants affecting HPr or Enzyme II [Schmalisch *et al.*, 2003]. A similar effect was observed for the homologous antiterminator protein SacY [Bachem and Stülke, 1998]. It was also shown that HPr (phosphorylated by EI) is able to efficiently phosphorylate PRDII of GlcT in order to reach its full

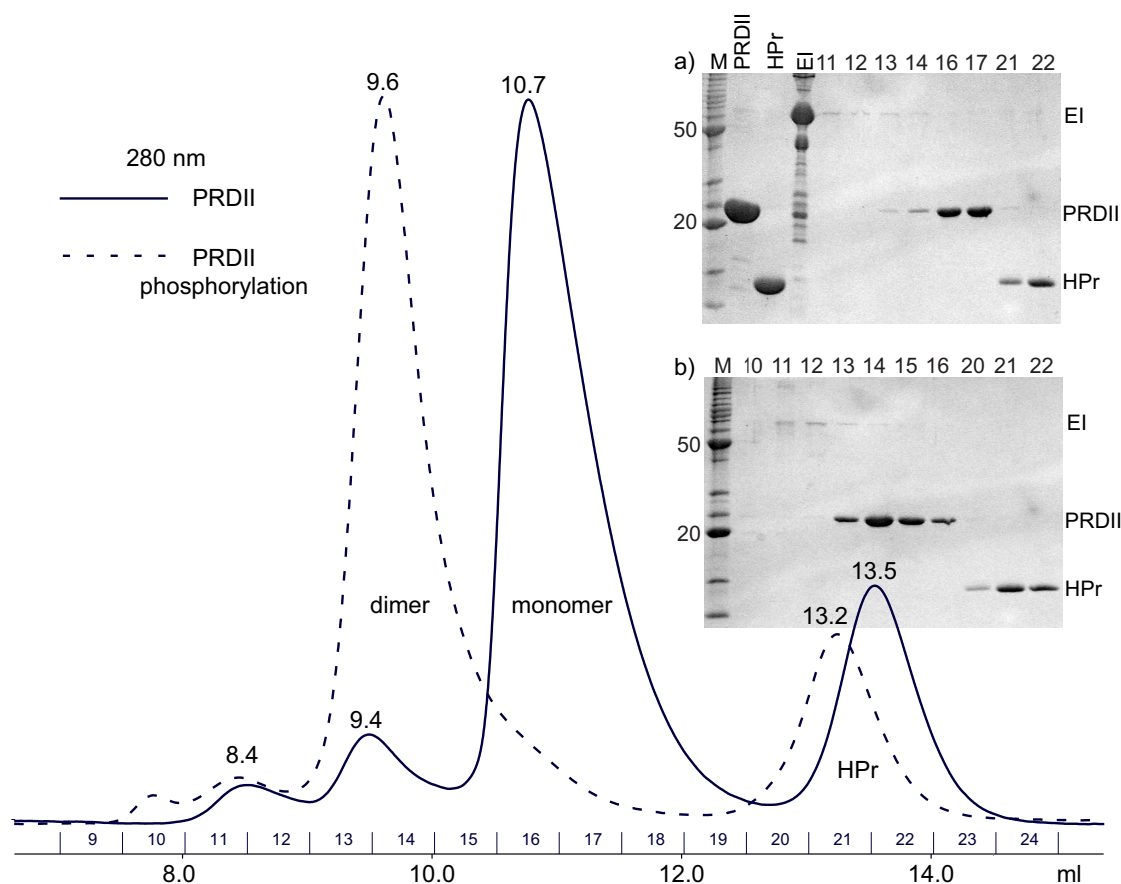


**Figure 5.5:** Superimposed analytical gel filtration chromatograms showing the aggregation state of monomeric PRDII before (solid line) and after (dashed line) phosphorylation. A clear shift to a lower retention volume can be observed upon phosphorylation, which indicates the dimerization of PRDII. The proteins were detected by their 280 nm UV absorption and the numbers on top of each peak represent the specific retention volumes of the peaks (in ml). Two SDS-PAGE gels show selected fractions before (a) and after (b) phosphorylation. M stands for the molecular weight marker and the numbers that are given for each lane correspond to the fraction numbers in the chromatogram, which are indicated at the x-axis. The gel filtration run was performed in 200 mM NaCl, 50 mM Tris HCl, 5 mM MgCl<sub>2</sub>, 2 mM DTT, pH 7.4.

activity [Schmalisch *et al.*, 2003]. Such findings are in agreement with the results, which were found for the isolated PRDII domain of GlcT in this study. Protein purification of PRDII revealed three peaks after preparative gel filtration, which can be attributed to the monomer, dimer and a higher aggregate (Figure 2.5). All three peaks were subjected to phosphorylation and reloaded onto the gel filtration column according to section 2.6.2. As described in the introduction, phosphorylation of monomeric PRDII leads to the dimer (section: 1.2), which is shown in this section by analytical gel filtration.

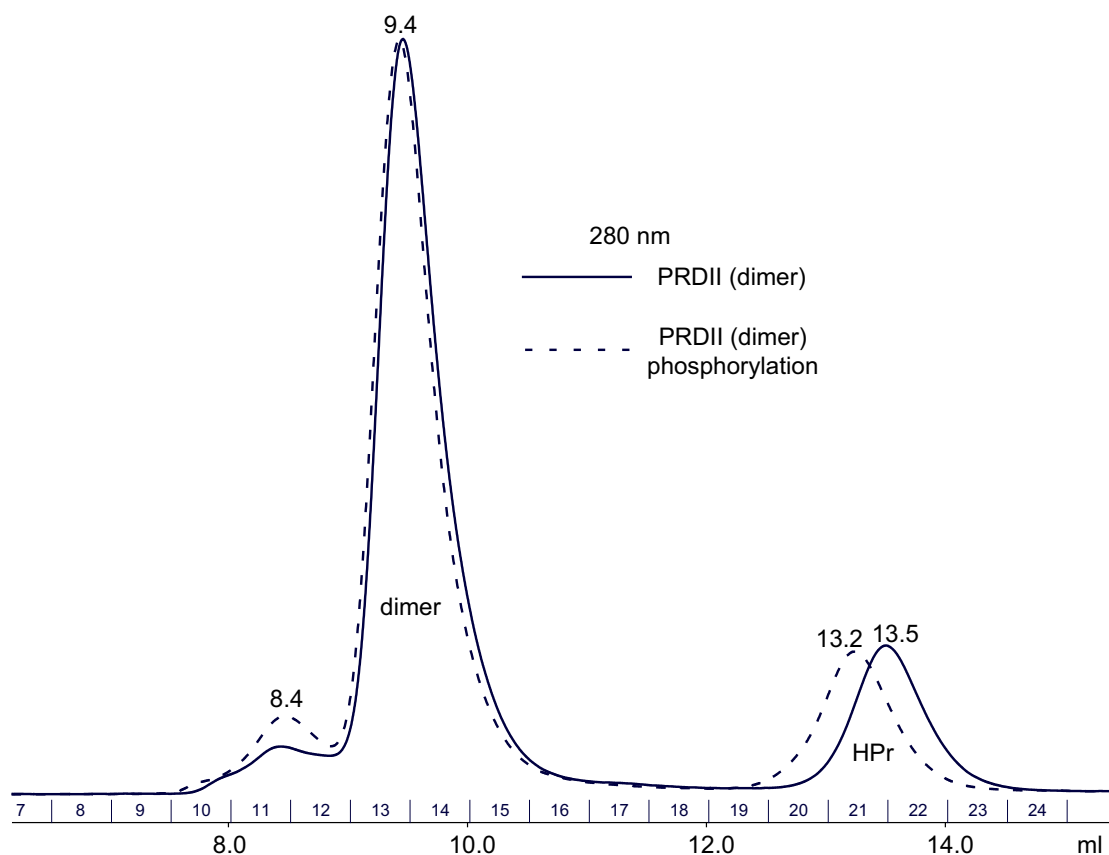


**Figure 5.6:** Superimposed analytical gel filtration chromatograms of the phosphorylation mix of dimeric PRDII, which was performed in the absence (solid line) and in the presence (dashed line) of PEP. No significant difference can be observed upon phosphorylation. The numbers on top of each peak correspond to their retention volumes (in ml). The gel filtration was performed in 200 mM NaCl, 50 mM Tris HCl, 5 mM  $\text{MgCl}_2$ , 2 mM DTT, pH 7.4.

In Figure 5.5 the superimposed analytical gel filtration chromatograms of the monomeric wild type PRDII phosphorylation mix can be seen in the absence (solid line) and in the presence (dashed line) of PEP. Prior to phosphorylation the chromatogram (solid line) showed the elution of PRDII at 10.7 ml and of HPr at 13.5 ml. Both proteins were confirmed by SDS-PAGE analysis. The chromatogram of the phosphorylated PRDII (dashed line) significantly highlights the shift of PRDII to a lower retention volume at 9.6 ml, which indicated a change in the aggregation state of PRDII upon phosphorylation. Interestingly, the retention volume of the constitutively dimeric PRDII (9.4 ml; Figure 5.6) was almost identical with the PRDII dimer upon phosphorylation (9.6 ml). This clearly showed that due to phosphorylation, the monomeric PRDII was converted into a dimer (Figure 5.5), whereas phosphorylation of the constitutive dimer did not show any shift and re-

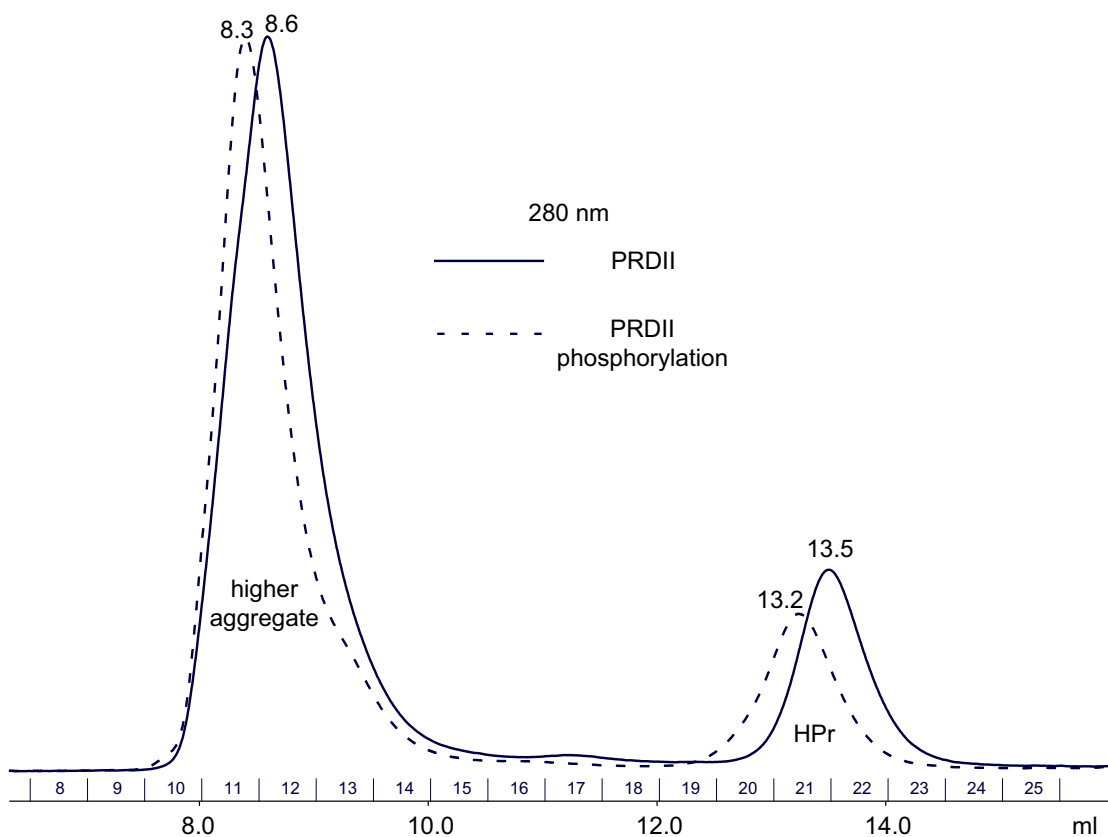


**Figure 5.7:** Superimposed analytical gel filtration chromatograms of the phosphorylation mix, which contained the higher aggregate of PRDII. The experiments were carried out in the absence (solid line) and in the presence (dashed line) of PEP. No significant difference can be observed upon phosphorylation. The numbers on top of each peak correspond to their retention volumes (in ml). The gel filtration was performed in 200 mM NaCl, 50 mM Tris HCl, 5 mM MgCl<sub>2</sub>, 2 mM DTT, pH 7.4.

mained unaltered at 9.4 ml (Figure 5.6). The existence of dimeric PRDII (after preparative gel filtration; Figure 2.5) in the absence of the phosphorylation enzymes (Figure 5.6) confirmed the concept of constitutive GlcT activity [Schmalisch *et al.*, 2003]. However, the full activity (dimerization) might be achieved through the additional phosphorylation of monomeric PRDII.

Analytical gel filtration was also performed with the higher aggregate of PRDII, which was reinjected onto the gel filtration column (Figure 5.7). No significant differences in the retention volumes were observed in the chromatograms before (8.6 ml, solid line) and after (8.3 ml, dashed line) phosphorylation. This aggregation state of PRDII was not further investigated in this study, but most likely represents a biologically inactive form, or a "dead end folding state". A similar effect

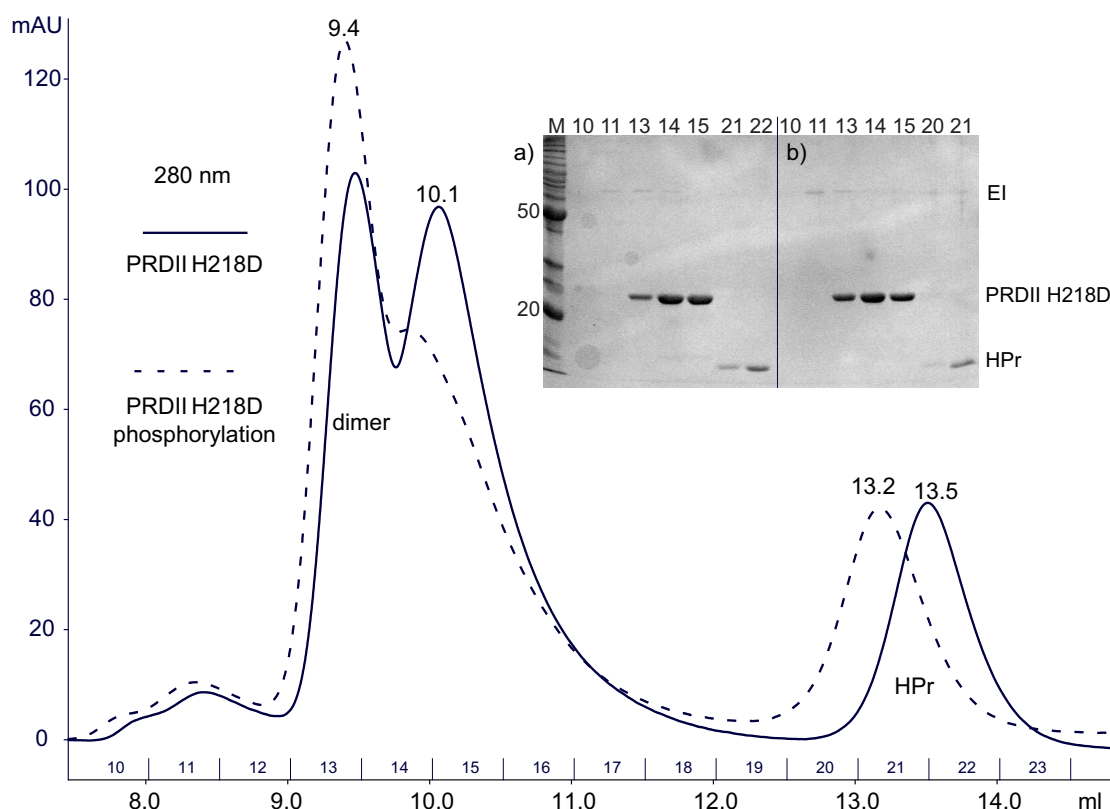


**Figure 5.8:** Superimposed analytical gel filtration chromatograms, which show the aggregation states of PRDII H218D before (solid line) and after (dashed line) phosphorylation. Upon phosphorylation an increased amount of PRDII H218D can be seen at lower retention volume (9.4 ml), which corresponds to the dimer. The numbers on top of each peak represent the specific retention volumes of the peaks (in ml). The SDS-PAGE gel shows in a) selected fractions before and in b) after phosphorylation was carried out. M stands for the molecular weight marker and the numbers that are given for each lane correspond to the fraction numbers in the chromatogram, which are indicated at the x-axis. Analytical gel filtration was performed in 200 mM NaCl, 50 mM Tris HCl, 2 mM DTT, pH 7.4.

was observed for RBD-PRDI of LicT [Déméné *et al.*, 2008]. It was reported that upon reaching a protein concentration of 15 mg/ml they noticed the presence of minor peaks in the gel filtration chromatogram corresponding to higher molecular weight aggregates, which were not further characterized in their study.

As shown in sections 5.1 and 5.2 single aspartate mutants of PRDII were investigated and histidine phosphorylation was observed by HNP-NMR. The aggregation state of both PRDII mutants (PRDII H218D and PRDII H279D) upon phosphorylation was analysed by analytical gel filtration. In the Figures 5.8 and 5.9 the results are shown for PRDII H218D and PRDII H279D, respectively. As

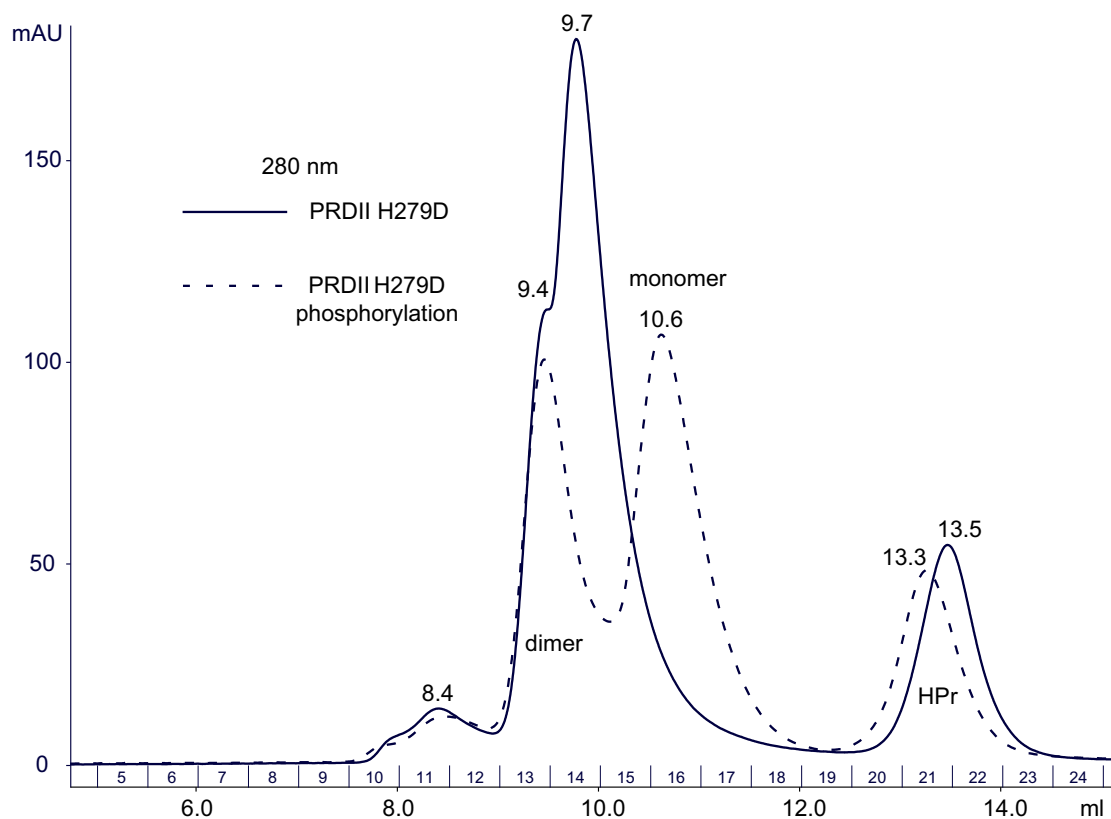


**Figure 5.9:** Superimposed analytical gel filtration chromatograms, which show the aggregation states of PRDII H279D before (solid line) and after (dashed line) phosphorylation. The numbers on top of each peak represent the specific retention volumes of the peaks (in ml). Upon phosphorylation a clear shift to a larger retention volume can be observed. This retention volume is in good agreement with the aggregation state of monomeric wild type PRDII. The gel filtration run was carried out in 200 mM NaCl, 50 mM Tris HCl, 2 mM DTT, pH 7.4.

described at the beginning of this chapter aspartate mutants were chosen because they successfully mimicked histidine phosphorylation in the PRDII domain of the homologous antiterminator protein LicT [Tortosa *et al.*, 2001, Declerck *et al.*, 2001]. Since, non-phosphorylated dimeric wild type PRDII eluted at 9.4 ml both mutants showed the tendency to form dimers, which were equally found at approx. 9.4 ml. Upon phosphorylation of PRDII H218D an increase of dimeric PRDII at 9.4 ml was observed (dashed line; Figure 5.8) compared to a significantly decreased PRDII species at 10.1 ml. The presence of PRDII H218D was confirmed by SDS-PAGE analysis.

Upon phosphorylation of PRDII H279D, a different effect was observed as shown in Figure 5.9. PRDII H279D eluted at 9.4 and 9.7 ml prior to phosphorylation.

Upon phosphorylation a significant shift to a larger retention volume (10.6 ml) was observed, which agrees with the retention volume of the monomeric wild type PRDII (10.7 ml). This change in the aggregation state was unexpected since HPr-dependent PRDII phosphorylation is expected to lead to the dimer or the stabilizing dimeric aggregation state. A possible explanation could be the repulsive interaction of the phosphorylated histidine 218 and the negatively charged aspartate at residue 279. Ionic interactions were identified to be the driving force of protein dimerization in the homologous antiterminator protein LicT [Ben-Zeev *et al.*, 2005]. It was reported that phosphorylation in PRDI (His 100 and His 159) results in strong electrostatic repulsion, which leads to a monomerization whereas phosphorylation in PRDII (His 207 and His 269) improves the geometric-electrostatic complementarity and hence, contributes to the stabilization of the dimer. Thus, the artificially introduced H279D mutation in PRDII of GlcT could negatively interact with the phosphate group at histidine 218, leading to unexpected PRDII monomers.

## 5.5 Summary

PRDII is the C-terminal end and the second regulatory domain of GlcT, which is controlled by histidine phosphorylation (section: 1.2). The dominant phosphohistidine species in PRDII is 3-phosphohistidine, which was identified by HNP-NMR (section: 5.1). The clear presence of a single phosphate group, which is involved in the phosphorylation reaction, was found by mass spectrometry (section: 5.2) and our results suggest that both conserved histidines are individually subjected to phosphorylation (section: 5.3). However, a second phosphate group is possibly involved in the phosphorylation of the wild type PRDII, since such an indication was found by mass spectrometry (section: 5.2). This result is further discussed in chapter 7. Analytical gel filtration confirmed that, upon HPr-dependent phosphorylation, monomeric PRDII is converted into a dimer (section: 5.4).

## 6 1,3-diphosphohistidines in proteins

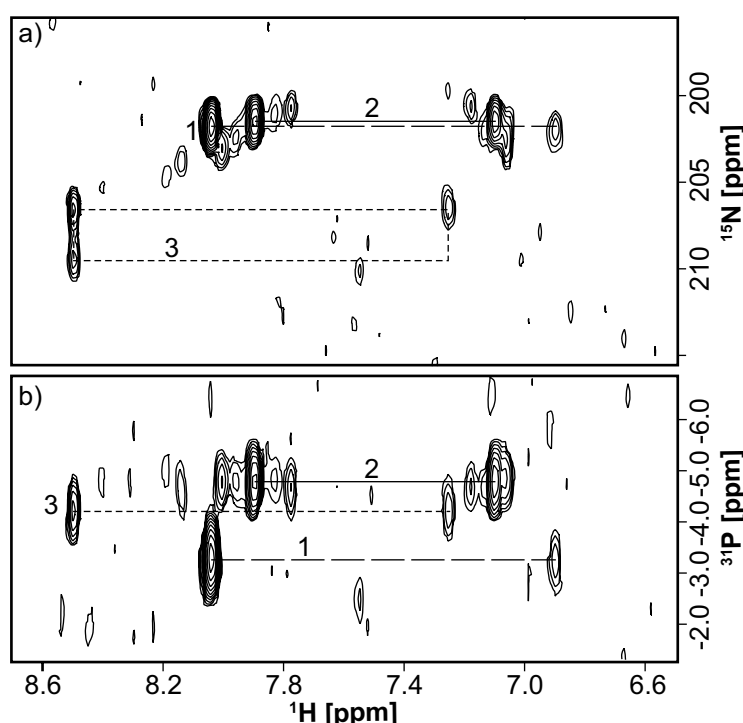


**Figure 6.1:** The HNP experiments of an approx. 6 mM HPr sample after 12 hours of phosphorylation are shown. In a) and b) the  $^1\text{H}$ ,  $^{15}\text{N}$  and  $^1\text{H}$ ,  $^{31}\text{P}$  projections are shown, respectively. 32 ( $^{31}\text{P}$ ), 32 ( $^{15}\text{N}$ ), and 512 ( $^1\text{H}$ ) complex points with  $t_{1\text{max}}=6.6$  ms,  $t_{2\text{max}}=6.6$  ms, and  $t_{3\text{max}}=66$  ms were recorded within 4 scans. A clear one peak and three peak pattern can be seen as well as a strong and some minor two peak patterns. HPr of *Bacillus subtilis* contains a single histidine residue (His 15).

In the last years it has been found that in histidine phosphorylated proteins either 1-phosphohistidine or 3-phosphohistidine is present. For example in the PTS, 1-phosphohistidine is known to occur in HPr [Kalbitzer *et al.*, 1982] whereas 3-phosphohistidine was found in Enzyme I and some isoforms of Enzyme II [Weigel *et al.*, 1982, Alpert *et al.*, 1985, Postma *et al.*, 1993] (the latter one for a thorough review). Interestingly, so far no report has been published about 1,3-diphosphohistidine phosphorylation in proteins [Besant and Attwood, 2009].

As shown by HNP-NMR, for PRDI 1,3-diphosphohistidine was clearly identified by a three peak pat-



tern in the HNP spectrum (section: 4.2). To study this phenomenon the phosphorylation of HPr was further investigated. In Figure 6.1 the 2D  $^1\text{H}$ ,  $^{15}\text{N}$ - (a) and  $^1\text{H}$ ,  $^{31}\text{P}$ -projections (b) of a HNP spectrum of HPr are presented. A 6 mM HPr sample was phosphorylated for approx. 12 hours. In both projections multiple peak patterns can be observed, which are labelled with 1, 2 and 3. The characteristic one peak pattern (label 1) can be observed at 8.05 ppm and has a  $^{31}\text{P}$  chemical shift which is close to -3.3 ppm. This resonance agrees well with what was already found for HPr by HNP-NMR (Figure 3.5, Chapter: 3). However, additional peak patterns (labels 2 and 3) were present in this spectrum. A significant two peak pattern (7.9 and 7.1 ppm) can be seen at -4.8 ppm in the  $^1\text{H}$ ,  $^{31}\text{P}$  projection, which is accompanied by additional two peak patterns of lower intensity. A three peak pattern (labelled with 3) is clearly present and can be seen at 8.5 and 7.25 ppm, respectively, but is better resolved in the  $^1\text{H}$ ,  $^{15}\text{N}$  projection (Figure 6.1 a). Besides PRDI, this clear three peak pattern emphasized the presence of 1,3-diphosphohistidine in HPr.

The HPr protein of *Bacillus subtilis* comprises only a single histidine residue (His 15) and its phosphorylation is well described [Schrecker *et al.*, 1975, Gassner *et al.*, 1977, Deutscher *et al.*, 2006]. Hence, all peak patterns that were observed in the HNP spectrum of HPr (Figure 6.1) can be attributed to the phosphorylation of histidine 15. During the 12 hours of phosphorylation  $^1\text{H}$ ,  $^{15}\text{N}$ -HSQC spectra were measured to observe the constancy of the phosphorylation reaction (data not shown). Small differences in those spectra could indicate local structural changes, which could explain that different two peak patterns were observed for HPr. On the other hand, the presence of a one peak pattern and the additional three peak pattern indicates that different phosphohistidine species were formed during phosphorylation. In the  $^1\text{H}$ ,  $^{15}\text{N}$ -HSQC spectra some additional minor resonances appeared over time, which could be interpreted as additional sets of signals. They possibly indicate the presence of HPr in different phosphorylation states such as 3-phosphohistidine-HPr and 1,3-diphosphohistidine-HPr although such effects were not observed for PRDI (chapter: 4).

The HNP experiments of HPr and PRDI clearly showed the presence of 1,3-diphosphohistidine in phosphoproteins. This is in very good agreement with the mass spectrometric results obtained for PRDI and HPr (section: 4.4). For both proteins an increase of the molecular weight by approx. 160 Da was observed (Figure 4.4), which clearly indicated that two phosphate groups were individually involved in the phosphorylation reaction of HPr and PRDI.

## 7 Discussion and comparison between PRDI and PRDII

In this chapter the results of PRDI and PRDII are discussed and compared to each other. A detailed overview of our results is shown in Table 7.1 and references are given to the sections where those details were presented.

The results we obtained from the HNP-NMR experiments of PRDI, PRDII and HPr clearly proved the presence of phosphorylated histidines. The intense two peak patterns in the spectra of PRDI and PRDII identified 3-phosphohistidine as the dominant phosphohistidine species (sections: 4.2 and 5.1) whereas in HPr the presence of 1-phosphohistidine was confirmed (chapter: 3). In the HNP spectra of PRDI and HPr additional three peak patterns were found (section: 4.2 and chapter: 6), which indicated the existence of 1,3-diphosphohistidines. So far, 1,3-diphosphohistidines have not been observed in phosphoproteins [Besant and Attwood, 2009]. Hence, we show for the first time that 1,3-diphosphohistidine exists in phosphoproteins. However, the exact significance or biological relevance of a 1,3-diphosphohistidine in proteins is not yet known.

Several attempts were made to identify the phosphorylation sites in antiterminator proteins and a summary of these results can be found in the literature [van Tilbeurgh and Declerck, 2001] (for a brief review). It is generally accepted that the four conserved histidines in the two PRDs are the targets of regulatory phosphorylation to modulate the nucleic acid binding activity of the RBD (RNA binding domain) [van Tilbeurgh and Declerck, 2001]. However, no general rule can be established for antiterminator proteins, in predicting which or how many of the conserved histidines can be phosphorylated in each PRD. Examples have been shown where all four (LicT) [Deutscher *et al.*, 1997, Bachem and Stülke, 1998, Lindner *et al.*, 1999, Tortosa *et al.*, 2001] or three histidines (SacY; one in PRDI and two in PRDII) [Tortosa *et al.*, 1997] were phosphorylated by HPr.

Characteristic	PRDI	Section	PRDII	Section
conserved histidines	111, 170	1.2	218, 279	1.2
wild type phosphorylation	yes	4.2	yes	5.1
number of phosphate groups indication of a second phosphate	mainly 1 yes	4.4	mainly 1 yes	5.2
dominant phosphohistidine species presence of 1,3-diphosphohistidine	3-phosphohistidine yes	4.2	3-phosphohistidine no	5.1
identified phosphorylation site(s)	170	4.5	218, 279	5.3
phosphorylation of single aspartate mutants	no	–	yes	5.1
aggregation state before phosphorylation	dimer	4.6	monomer and dimer monomer to dimer (dimer unchanged)	5.4
aggregation state after phosphorylation	monomer			
HPr-dependent phosphorylation	yes	4.2	yes	5.4

**Table 7.1:** Summary of relevant results and comparison between PRDI and PRDII.

Matters were complicated further by the fact that the activity of some antiterminator proteins, such as GlcT and SacY is irrespective of the presence or absence of HPr, whereas HPr-dependent phosphorylation of PRDII is mandatory for LicT and SacT activity [Crutz *et al.*, 1990, Arnaud *et al.*, 1992, Le Coq *et al.*, 1995, Stülke *et al.*, 1997]. For GlcT of *Bacillus subtilis* the first conserved histidine (His 111) in the PRDI protein sequence was proposed to be the target of regulatory phosphorylation [Bachem and Stülke, 1998]. In this study reporter gene assays were used to investigate the Enzyme II-dependent PRDI phosphorylation of GlcT. Similar results were obtained for SacY [Tortosa *et al.*, 1997, Tortosa *et al.*, 2001] and LicT [Tortosa *et al.*, 2001] where the first conserved histidine in both PRDIs is the target of regulatory phosphorylation. Hence, it was concluded that the activity is regulated by Enzyme II-controlled or -mediated phosphorylation of the first conserved histidine residue in the PRDI of antiterminator proteins [Deutscher *et al.*, 2006]. In contrast, mutagenesis studies with the PRDI of LacT in *Lactobacillus casei* suggested that both conserved histidines contribute equally to the regulatory activity [Gosalbes *et al.*, 2002] which emphasizes the difficulty to establish a general rule for the determination of the phosphorylation sites. However, the tandem mass analysis in this work strongly suggests that HPr-dependent phosphorylation (no Enzyme II-dependence) of PRDI in GlcT of *Bacillus subtilis* occurs at histidine 170, the second conserved histidine in PRDI (section: 4.5). In addition, mass spectrometry showed the presence of a single and double phosphorylated PRDI. This double phosphorylation is in agreement with the result of our HNP spectrum of PRDI, which showed the existence of a 1,3-diphosphohistidine whereas the single phosphate group can be attributed primarily to 3-, but also to 1-phosphohistidine which was also found by HNP-NMR (section: 4.2). Mutational studies of PRDI (PRDI H111D, PRDI H170D) showed that no phosphorylation was observed for PRDI H111D and no protein expression was seen for PRDI H170D (data not shown). The result for PRDI H111D is in agreement with the finding that the mutation of one potential phosphorylation site prevents phosphorylation of the whole PRDI in GlcT [Schmalisch *et al.*, 2003]. On the basis of this result, it can be concluded that the Enzyme II-free phosphorylation of PRDI leads to all three possible phosphorylation states of histidine 170 but primarily to 3-phosphohistidine (Figure 1.3). In contrast, histidine 172, which is the second C-terminal histidine in PRDI, is not involved in histidine phosphorylation.

Interestingly in our studies, the PRDI of *Bacillus subtilis* GlcT was significantly phosphorylated by HPr in the absence of Enzyme II. Similar findings have been reported for homologous antiterminator proteins, such as for SacY, where HPr-dependent phosphorylation was not only observed for both conserved histidines in PRDII, but also for the first conserved histidine in PRDI [Tortosa *et al.*, 1997]. In contrast, phosphorylation in PRDI of *Bacillus subtilis* GlcT has been shown to occur through Enzyme II [Schmalisch *et al.*, 2003] and this Enzyme II-dependence was also proposed for other antiterminator proteins, such as LicT and SacY [Tortosa *et al.*, 2001] (for a review see [Deutscher *et al.*, 2006]). However, in our

experiments the phosphorylation of PRDI in the absence of Enzyme II, which has not been shown before, led to the monomerization of PRDI (section: 4.6). The monomeric aggregation state was proposed to similarly exist upon Enzyme II-dependent phosphorylation of GlcT [Schmalisch *et al.*, 2003]. Hence, one can conclude that the phosphorylation of PRDI, which is independent of Enzyme II, is biologically relevant. Furthermore, analytical gel filtration runs, which were performed with RBD-PRDI, confirmed the same HPr-dependent monomerization upon phosphorylation (section: 4.6). Thus, the N-terminal RBD obviously did not counteract the regulatory phosphorylation of PRDI through HPr.

The highly efficient HPr-dependent phosphorylation of PRDII (independent of Enzyme II; Figure 1.2) has already been described [Schmalisch *et al.*, 2003]. However, it was not yet clear whether HPr phosphorylates the first, the second, or both conserved histidines in PRDII [Schmalisch *et al.*, 2003]. The HNP spectra of the two PRDII single aspartate mutants (PRDII H218D and PRDII H279D) clearly showed individual phosphorylation of both conserved histidines at their N<sup>ε</sup>2 nitrogen atoms (section: 5.1). Additional phosphorylation sites besides them were excluded by mass spectrometric results of the double aspartate mutant (PRDII H218D H279D). Furthermore, mass spectrometry revealed that a primary single phosphate group is involved in PRDII phosphorylation but our results also suggest a second phosphate group in a minor population. Thus, it can be concluded that both conserved histidines in PRDII (His 218, His 279) are mono-phosphorylated by HPr in different quantities at their N<sup>ε</sup>2 nitrogen atoms.

Previously, three general scenarios for PRD phosphorylation were suggested [Schmalisch *et al.*, 2003]: i) The two conserved histidine residues in each PRD may be both phosphorylated individually; ii) there might be an intra-PRD phosphate transfer and iii) one of the two conserved histidines in each of the PRDs might be phosphorylated, whereas the other one would be required for the phosphorylation reaction. Phosphorylation of PRDI could be attributed to model iii), since mutation of H111D led to the loss of phosphorylation and a single phosphate group was clearly found by mass spectrometry upon PRDI phosphorylation. Phosphorylation of PRDII fits in some cases to model i) but also to model ii). Our HNP results suggest that both conserved histidines can be individually phosphorylated (model i). However, mass spectrometry clearly showed that PRDII is primarily phosphorylated by a single phosphate group. Hence, one can conclude that one of the conserved histidine residues might be the final preferential phosphate acceptor in PRDII and an intra-PRDII phosphate transfer might be possibly involved in PRDII phosphorylation (model ii). However, at that moment we cannot assign one of the two conserved histidines to that specific function.

Our results, obtained by analytical gel filtration, showed that PRDII constitutively forms monomers and dimers (section: 2.5.9). Since the GlcT dimer is considered as the active form, which binds to the nucleic acid ( [Schmalisch *et al.*,

2003]; section: 1.2) the tendency of both PRDI and PRDII to constitutively form dimers without phosphorylation could possibly explain why GlcT is active irrespective of the presence or absence of HPr [Bachem and Stülke, 1998]. However, our results clearly showed the efficient phosphorylation of monomeric PRDII leading to the dimerization of PRDII. This possibly explains why the GlcT activity is enhanced upon HPr-dependent phosphorylation [Schmalisch *et al.*, 2003].

Our results about the HPr-dependent PRDI and PRDII phosphorylation of *Bacillus subtilis* GlcT allow us to contribute to the question of phosphorylation specificity. The two PRDs of GlcT are similar to each other in their protein sequence and share 34 % identical amino acids [Schmalisch *et al.*, 2003]. It was proposed that the PRDs are specialized in the choice of their phosphorylation partner and that some specific determinants in the PRDs determine whether they are targets for HPr- (PRDII) or Enzyme II- (PRDI) dependent phosphorylation [Schmalisch *et al.*, 2003]. Those determinants are yet unknown. However, our results show that HPr can individually phosphorylate both regulatory domains, which indicates that HPr cannot distinguish between the two isolated PRDs of GlcT. Hence, the arrangement of the two regulatory domains in the full length GlcT could affect the specificity of domain phosphorylation in a way that PRDI, as an individual domain, is accessible for HPr but less approachable in full length GlcT [Schmalisch *et al.*, 2003] (personal communication with Prof. Stülke).

Interestingly, the same phosphorylation cascade (Enzyme I, HPr and the target domain) led to opposite aggregation states of the PRDs. Whereas HPr-dependent PRDI phosphorylation resulted in a monomer, PRDII formed a dimer upon phosphorylation. As shown in sections 2.6.3 and 2.6.6, phosphorylation of PRDII was efficiently achieved using a molar ratio of 1 : 1/8 of monomeric PRDII to HPr, respectively. On the contrary, PRDI phosphorylation strongly depends on a minimal 1 : 1 molar ratio between monomeric PRDI and HPr (section: 4.1). This difference in the molar ratios indicated a reduced specificity of HPr-dependent PRDI phosphorylation, since this phosphorylation is attributed to the carbohydrate specific Enzyme II (PRDI is a minor substrate) [Bachem and Stülke, 1998, Schmalisch *et al.*, 2003].

An additional and interesting side effect is that HPr phosphorylation, which depends on Enzyme I (Figure 1.1), was successfully carried out in the absence of magnesium ions. The auto-phosphorylation of Enzyme I requires  $Mg^{2+}$  ions for its activity, but divalent ions such as  $Mn^{2+}$  and  $Co^{2+}$  can, in an appropriate concentration range, substitute for  $Mg^{2+}$  [Weigel *et al.*, 1982, Alpert *et al.*, 1985]. However, sample preparation for mass spectrometric experiments was performed in ammonium acetate buffer even throughout preparative gel filtration of the enzymes and target proteins (section: 2.6.3). Efficient phosphorylation was also observed although no  $Mg^{2+}$  salts or other divalent cations were used or added to the buffer.

## 7.1 Conclusion

The newly developed HNP-NMR experiment will be a great tool to characterize the regiochemistry of phosphohistidines in other proteins. The combined results of this newly developed HNP-NMR experiment, mass spectrometry and analytical gel filtration revealed new insight in the regulatory histidine phosphorylation of PRDI and PRDII of the *Bacillus subtilis* antiterminator protein GlcT. We successfully

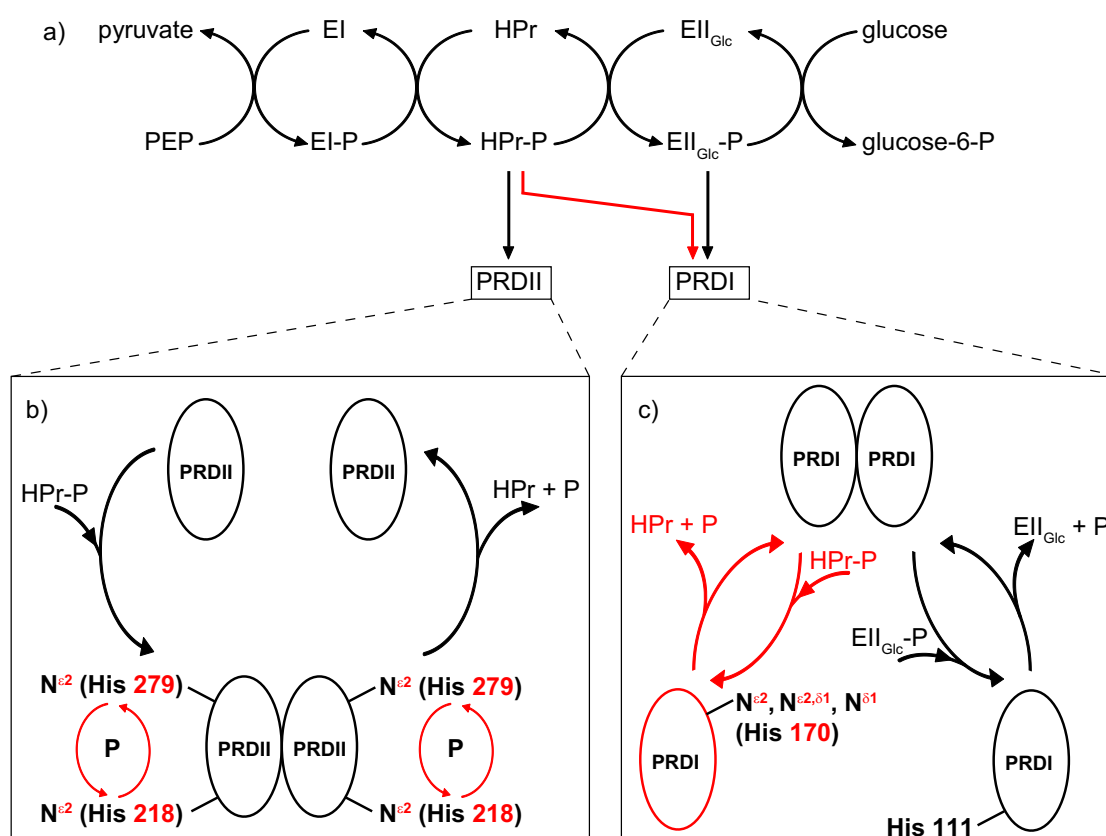


**Figure 7.1:** Phosphorylation pathways in the PTS. In black: state of knowledge before start of the PhD, **red: insights from this PhD thesis**. In a) the phosphate transfer from PEP to glucose via Enzyme I, HPr and Enzyme II is shown. The regulatory phosphate transfer to the PRDs of *Bacillus subtilis* GlcT is shown by additional arrows and further explained in b) and c). Experimental results and interpretations of this thesis are highlighted in red and compared to the published literature. In b) and c) the individual phosphorylation effects of PRDI and PRDII are emphasized. In b) the HPr-dependent phosphorylation of PRDII is illustrated which leads to a dimer. Both conserved histidines (His 218 and His 279) can be individually phosphorylated at their N<sup>ε2</sup> imidazole nitrogen atoms. An intramolecular phosphate transfer is possibly involved between both histidine residues. In c) the regulatory phosphorylation pathways of PRDI are shown. In red the newly found Enzyme II-free phosphorylation pathway is highlighted which leads to a monomer. Phosphorylation occurs at histidine 170 and includes N<sup>δ1</sup>, N<sup>ε2</sup>-double phosphorylation of the imidazole ring. In black the well known Enzyme II-dependent phosphorylation of PRDI is shown which phosphorylates the first conserved histidine in PRDI. Both phosphorylation pathways result in a PRDI monomer.

confirmed HPr-dependent histidine phosphorylation in both regulatory domains of GlcT and conclude that HPr plays a similar role in the phosphorylation of GlcT as for homologous antiterminator proteins. The results of this thesis are summarized and visualized in Figure 7.1.





## 8 References

- A. Alei (Jr.), L. O. Morgan, W. E. Wageman, T. W. Whaley, pH Dependence of  $^{15}\text{N}$  NMR Shifts and Coupling Constants in Aqueous Imidazole and 1-Methylimidazole. Comments on Estimation of Tautomeric Equilibrium Constants for Aqueous Histidine, *JACS* 102, 9, 2881-2887 (1980)
- C.-A. Alpert, R. Frank, K. Stüber, J. Deutscher, W. Hengstenberg, Phosphoenolpyruvate-Dependent Protein Kinase Enzyme I of *Streptococcus faecalis*: Purification and Properties of the Enzyme and Characterization of Its Active Center, *Biochemistry* 24, 959-964 (1985)
- O. Amster-Choder, A. Wright, Modulation of the Dimerization of a Transcriptional Antiterminator Protein by Phosphorylation, *Science* 257, 1395-1398 (1992)
- O. Amster-Choder, A. Wright, BglG, the Response Regulator of the *Escherichia coli* *bgl* Operon, Is Phosphorylated on a Histidine Residue, *J. of Bacteriology* 179, 17, 5621-5624 (1997)
- B. Anderson, N. Weigel, W. Kundig, S. Roseman, Sugar Transport: III. Purification And Properties Of A Phosphocarrier Protein (HPR) Of The Phosphoenolpyruvate-Dependent Phosphotransferase System Of *Escherichia Coli*, *J. Biol. Chem.* 246, 22, 7023-7033 (1971)
- L. Andersson, J. Porath, Isolation of Phosphoproteins by Immobilized Metal ( $\text{Fe}^{3+}$ ) Affinity Chromatography, *Analytical Biochemistry* 154, 250-254 (1986)
- M. Arnaud, P. Vary, M. Zagorec, A. Klier, M. Debarbouille, P. Postma, G. Rapoport, Regulation of the *sacPA* Operon of *Bacillus subtilis*: Identification of Phosphotransferase System Components Involved in SacT Activity, *J. of Bacteriology* 174, 10, 3161-3170 (1992)
- P. V. Attwood, M. J. Piggott, X. L. Zu, P. G. Besant, Focus on phosphohistidines, *Amino Acids* 32, 145-156 (2007)
- S. Bachem, J. Stülke, Regulation of the *Bacillus subtilis* GlcT Antiterminator Protein by Components of the Phosphotransferase System, *J. of Bacteriology* 180, 20, 5319-5326 (1998)

- E. Ben-Zeev, L. Fux, O. Amster-Choder, M. Eisenstein, Experimental and Computational Characterization of the Dimerization of the PTS-regulation Domains of BglG from *Escherichia coli*, *J. Mol. Biol.* 347, 693-706 (2005)
- S. Berger, S. Braun, H.-O. Kalinowski, NMR Spectroscopy of the Non-Metallic Elements, *Wiley-Chichester* (1997)
- G. Bertani, Studies on lysogenesis I. The mode of phage liberation by lysogenic *Escherichia coli*, *J. of Bacteriology* 62, 293-300 (1951)
- G. Bertani, Lysogeny at Mid-Twentieth Century: P1, P2, and Other Experimental Systems, *J. of Bacteriology* 186, 595-600 (2004)
- P. G. Besant, L. Byrne, G. Thomas, P. V. Attwood, A Chromatographic Method for the Preparative Separation of Phosphohistidines, *Analytical Biochemistry* 258, 372-375 (1998)
- P. G. Besant, M. V. Lasker, C. D. Bui, C. W. Turck, Phosphohistidine Analysis Using Reversed-Phase Thin-Layer Chromatography, *Analytical Biochemistry* 282, 149-153 (2000)
- P. G. Besant, P. V. Attwood, Detection and analysis of protein histidine phosphorylation, *Mol. Cell. Biochem.* 329, 93-106 (2009)
- F. Blomberg, W. Maurer, H. Rüterjans, Nuclear Magnetic Resonance Investigation of  $^{15}\text{N}$ -Labeled Histidine in Aqueous Solution, *JACS* 99, 25, 8149-8159 (1977)
- J. L. Bock, B. Sheard,  $^{31}\text{P}$  NMR Of Alkaline Phosphatase, *Biochemical And Biophysical Research Communications* 66, 1, 24-30 (1975)
- M. Brauer, B. D. Sykes, Phosphorus-31 Nuclear Magnetic Resonance Studies of Phosphorylated Proteins, *Methods in Enzymology* 107, 36-81 (1984)
- J. R. Brody, S. E. Kern, History and principles of conductive media for standard DNA electrophoresis, *Analytical Biochemistry* 333, 1-13 (2004)
- D. R. Buckler, A. M. Stock, Synthesis of [ $^{32}\text{P}$ ]Phosphoramidate for Use as a Low Molecular Weight Phosphordonor Reagent, *Analytical Biochemistry* 283, 222-227 (2000)
- J. Cavanagh, W. J. Fairbrother, A. G. Palmer III, M. Rance, N. J. Skelton, Protein NMR Spectroscopy, 2nd Ed., Elsevier Academic Press, (2007)

- C. Chen, Q.-L. Huang, S.-H. Jiang, X. Pan, Z.-C. Hua, Immobilized protein ZZ, an affinity tool for immunoglobulin isolation and immunological experimentation, *Biotechnol. Appl. Biochem.* 45, 87-92 (2006)
- P. Cohen, The regulation of protein function by multisite phosphorylation - a 25 year update, *Trends In Biochemical Science* 25, 12, 596-601 (2000)
- A.-M. Crutz, M. Steinmetz, S. Aymerich, R. Richter, D. Le Coq, Induction of Levansucrase in *Bacillus subtilis*: an Antitermination Mechanism Negatively Controlled by the Phosphotransferase System, *J. of Bacteriology* 172, 2, 1043-1050 (1990)
- N. Declerck, F. Vincent, F. Hoh, S. Aymerich, H. van Tilbeurgh, RNA Recognition by Transcriptional Antiterminators of the BglG/SacY Family: Functional and Structural Comparison of the CAT Domain from SacY and LicT, *J. Mol. Biol.* 294, 389-402 (1999)
- N. Declerck, H. Dutartre, V. Receveur, V. Dubois, C. Royer, S. Aymerich, H. van Tilbeurgh, Dimer Stabilization upon Activation of the Transcriptional Antiterminator LicT, *J. Mol. Biol.* 314, 671-681 (2001)
- F. Delaglio, S. Grzesiek, G. W. Vuister, G. Zhu, J. Pfeifer, A. Bax, NMRPipe: A multidimensional spectral processing system based on UNIX pipes, *J. Biomolecular NMR* 6, 3, 277-293 (1995)
- J. Deutscher, C. Fischer, V. Charrier, A. Galinier, C. Lindner, E. Darbon, V. Dossonnet, Regulation of Carbon Metabolism in Gram-Positive Bacteria by Protein Phosphorylation, *Folia Microbiol.* 42, 3, 171-178 (1997)
- J. Deutscher, C. Francke, P. Postma, How Phosphotransferase System-Related Protein Phosphorylation Regulates Carbohydrate Metabolism in Bacteria, *Microbiology and Molecular Biology Reviews* 70, 4 939-1031 (2006)
- G. Dooijewaard, F. F. Roossien, G. T. Robillard, *Escherichia coli* Phosphoenolpyruvate Dependent Phosphotransferase System. NMR Studies of the Conformation of HPr and P-HPr and the Mechanism of Energy Coupling, *Biochemistry* 18, 14, 2996-3001 (1979)
- T. Ducat, N. Declerck, M. Kochoyan, H. Déméné, Letter to the Editor:  $^1\text{H}$ ,  $^{15}\text{N}$  and  $^{13}\text{C}$  Backbone resonance assignments of the 40 kDa LicT-CAT-PRD1 protein, *J. Biomolecular NMR* 23, 325-326 (2002)
- T. Ducat, N. Declerck, T. Gostan, M. Kochoyan, H. Déméné, Rapid determination of protein solubility and stability conditions for NMR studies using incomplete factorial design, *J. Biomolecular NMR* 34, 137-151 (2006)

- H. Déméné, T. Ducat, K. De Guillen, C. Birck, S. Aymerich, M. Kochoyan, N. Declerck, Structural Mechanism of Signal Transduction between the RNA-binding Domain and the Phosphotransferase System Regulation Domain of the LicT Antiterminator, *J. Biol. Chem.* 283, 45, 30838-30849 (2008)
- J. V. Frangioni, B. G. Neel, Solubilization and Purification of Enzymatically Active Glutathione S-Transferase (pGEX) Fusion Proteins, *Analytical Biochemistry* 210, 179-187 (1993)
- J. M. Fujitaki, G. Fung, E. Y. Oh, R. Smith, Characterization of chemical and enzymatic acid-labile phosphorylation of histone H4 using phosphorus-31 nuclear magnetic resonance, *Biochemistry* 20, 3658-3664 (1981)
- M. M. Garner, A. Revzin, A gel electrophoresis method for quantifying the binding of proteins to specific DNA regions: application to components of the *Escherichia coli* lactose operon regulatory system, *Nucleic Acids Research* 9, 13, 3047-3060 (1981)
- D. S. Garrett, Y. J. Seok, A. Peterkofsky, G. M. Clore, A. M. Gronenborn, Tautomeric state and pK(a) of the phosphorylated active site histidine in the N-terminal domain of enzyme I of the *Escherichia coli* phosphoenolpyruvate:sugar phosphotransferase system, *Protein Science* 7, 789-793 (1998)
- M. Gassner, D. Stehlik, O. Schrecker, W. Hengstenberg, W. Maurer, H. Rüterjans, The Phosphoenolpyruvate-Dependent Phosphotransferase System of *Staphylococcus aureus*, *Eur. J. Biochem* 75, 287-296 (1977)
- S. C. Gill, P. H. Hippel, Calculation of Protein Extinction Coefficients from Amino Acid Sequence Data, *Analytical Biochemistry* 182, 319-326 (1989)
- M. J. Gosalbes, C. D. Esteban, G. Pérez-Martínez, *In vivo* effect of mutations in the antiterminator LacT in *Lactobacillus casei*, *Micobiology* 148, 695-702 (2002)
- M. Graille, C.-Z. Zhou, V. Receveur-Bréchet, B. Collinet, N. Declerck, H. van Tilbeurgh, Activation of the LicT Transcriptional Antiterminator Involves a Domain Swing/Lock Mechanism Provoking Massive Structural Changes, *J. Biol. Chem.* 280, 15, 14780-14789 (2005)
- D. B. Greenberg, J. Stülke, M. H. Saier Jr., Domain analysis of transcriptional regulators bearing PTS regulatory domains, *Research in Microbiology* 153, 519-526 (2002)
- J. Grodberg, J. J. Dunn, *ompT* Encodes the *Escherichia coli* Outer Membrane Protease That Cleaves T7 RNA Polymerase during Purification, *J. of Bacteriology* 170, 3, 1245-1253 (1988)

- S. Himmel, S. Wolff, S. Becker, D. Lee, C. Griesinger, Detection and Identification of Protein-Phosphorylation Sites in Histidines through HNP Correlation Patterns, *Angew. Chem. Int. Ed.* 49, 47, 8971-8974 (2010)
- S. Himmel, S. Wolff, S. Becker, D. Lee, C. Griesinger, Nachweis und Identifizierung von Protein-Phosphorylierungen in Histidinen mithilfe von HNP-Korrelationen, *Angew. Chem.* 122, 47, 9155-9158 (2010)
- A. P. Hitchens, M. C. Leikind, The Introduction of Agar-Agar into Bacteriology, *J. of Bacteriology* 37, 485-493 (1939)
- D. E. Hultquist, R. W. Moyer, P. D. Boyer, The Preparation and Characterization of 1-Phosphohistidine and 3-Phosphohistidine, *Biochemistry* 5, 322-331 (1966)
- D. E. Hultquist, The Preparation and Characterization of Phosphorylated Derivatives of Histidine, *Biochimica et Biophysica Acta* 153, 329-340 (1968)
- T. L. James, Phosphorus-31 NMR as a Probe for Phosphoproteins, *Crit. Rev. Biochem.* 18, 1-30
- R. S. Johnson, K. Biemann, Computer Program (SEQPEP) to Aid in the Interpretation of High-energy Collision Tandem Mass Spectra of Peptides, *Biomedical and Environmental Mass Spectrometry* 18, 945-957 (1989)
- B. E. Jones, P. Rajagopal, R. E. Klevit, Phosphorylation on histidine is accompanied by localized structural changes in the phosphocarrier protein, HPr from *Bacillus subtilis*, *Protein Science* 6, 2107-2119 (1997)
- H. R. Kalbitzer, W. Hengstenberg, P. Rösch, P. Muss, P. Bernsmann, R. Engelmann, M. Dörschug, J. Deutscher, HPr Proteins of Different Microorganisms Studied by Hydrogen-1 High-Resolution Nuclear Magnetic Resonance: Similarities of Structures and Mechanisms, *Biochemistry* 21, 2879-2885 (1982)
- S. M. Kelly, T. J. Jess, N. C. Price, How to study proteins by circular dichroism, *Biochimica et Biophysica Acta* 1751, 119-139 (2005)
- J. L. Kerwin, A. R. Tuininga, L. H. Ericsson, Identification of molecular species of glycerophospholipids and sphingomyelin using electrospray mass spectrometry, *Journal of Lipid research* 35, 1102-1114 (1994)
- S. Klumpp, J. Krieglstein, Phosphorylation and dephosphorylation of histidine residues in proteins, *Eur. J. Biochem* 269, 1067-1071 (2002)

- S. Klumpp, J. Krieglstein, Reversible Phosphorylation of Histidine Residues in Proteins from Vertebrates, *Science Signalling* 2, 61, pe13 (2009)
- I. Knezevic, S. Bachem, A. Sickmann, H. E. Meyer, J. Stülke, W. Hengstenberg, Regulation of the glucose-specific phosphotransferase system (PTS) of *Staphylococcus carnosus* by the antiterminator protein GlcT, *Microbiology* 146, 2333-2342 (2000)
- U. K. Laemmli, Cleavage of Structural Proteins during the Assembly of the Head of Bacteriophage T4, *Nature* 227, 680-685 (1970)
- D. Le Coq, C. Lindner, S. Krüger, M. Steinmetz, J. Stülke, New  $\beta$ -Glucoside (*bgl*) Genes in *Bacillus subtilis*: the *bglP* Gene Product Has Both Transport and Regulatory Functions Similar to Those of BglF, Its *Escherichia coli* Homolog, *J. of Bacteriology* 177, 6, 1527-1535 (1995)
- A. Lecroisey, I. Lascu, A. Bominaar, M. Véron, M. Delepierre, Phosphorylation Mechanism of Nucleoside Diphosphate Kinase:  $^{31}\text{P}$ -Nuclear Magnetic Resonance Studies, *Biochemistry* 34, 12445-12450 (1995)
- C. LiCalsi, T. S. Crocenzi, E. Freire, S. Roseman, Sugar Transport by the Bacterial Phosphotransferase System. Structural and thermodynamic domains of enzyme I of *Salmonella typhimurium*, *J. Biol. Chem.* 266, 29, 19519-19527 (1991)
- C. Lindner, A. Galinier, M. Hecker, J. Deutscher, Regulation of the activity of the *Bacillus subtilis* antiterminator LicT by multiple PEP-dependent, enzyme I- and HPr-catalysed phosphorylation, *Molecular Microbiology* 31, 3, 995-1006 (1999)
- F. Lottspeich, H. Zorbas, Bioanalytik, *Spektrum Akademischer Verlag* (1998)
- B. Macek, I. Mijakovic, J. V. Olsent, F. Gnadt, C. Kumar, P. R. Jensen, M. Mann, The Serine/Threonine/Tyrosine Phosphoproteome of the Model Bacterium *Bacillus subtilis*, *Molecular & Cellular Proteomics* 6, 4, 697-707 (2007)
- R. Marek, A. Lycka, E. Kolehmainen, E. Sievänen, J. Tousek,  $^{15}\text{N}$  NMR Spectroscopy in Structural Analysis: An Update (2001-2005), 11, 1154-1205 (2007)
- J. Marmur, P. Doty, Determination of the Base Composition of Deoxyribonucleic Acid from its Thermal Denaturation Temperature, *J. Mol. Biol.* 5, 109-118 (1962)

- H. R. Matthews, Protein Kinases And Phosphatases That Act On Histidine, Lysine, Or Arginine, Residues In Eukaryotic Proteins: A Possible Regulator Of The Mitogen-Activated Protein Kinase Cascade, *PHARMACOLOGY & THERAPEUTICS* 67, 3, 323-350 (1995)
- N. D. Meadow, D. K. Fox, S. Roseman, The Bacterial Phosphoenol-Pyruvate: Glucose Phosphotransferase System, *Annu. Rev. Biochem.* 59, 497-542 (1990)
- M. Niepmann, Discontinuous native protein gel electrophoresis: pro and cons, *Expert. Rev. Proteomics* 4, 3, 355-361 (2007)
- I. A. Papayannopoulos, The Interpretation of Collision-Induced Dissociation Tandem Mass Spectra of Peptides, *Mass Spectrometry Reviews* 14, 49-73 (1995)
- J. S. Parkinson, Signal Transduction Schemes of Bacteria, *Cell* 73, 857-871 (1993)
- J. G. Pelton, D. A. Torchia, N. D. Meadow, S. Roseman, Tautomeric states of the active-site histidines of phosphorylated and unphosphorylated III<sup>Glc</sup>, a signal-transducing protein from *Escherichia coli*, using two-dimensional heteronuclear NMR techniques, *Protein Science* 2, 543-558 (1993)
- P. W. Postma, J. W. Lengeler, G. R. Jacobson, Phosphoenolpyruvate:Carbohydrate Phosphotransferase Systems of Bacteria, *Microbiology and Molecular Biology Reviews* 57, 3, 543-594 (1993)
- J. Puttick, E. N. Baker, L. T. J. Delbaere, Histidine phosphorylation in biological systems, *Biochimica et Biophysica Acta* 1784, 100-105 (2008)
- P. Rösch, H. R. Kalbitzer, R. S. Goody, <sup>31</sup>P NMR Spectra Of Thiophosphate Analogues Of Guanosine Nucleotides-pH dependence of chemical shifts and coupling constants, *FEBS Letters* 121, 2, 211-214 (1980)
- P. Rösch, NMR-Studies Of Phosphoryl Transferring Enzymes, *Progress in NMR Spectroscopy* 18, 123-169 (1986)
- P. Rajagopal, E. B. Waygood, R. E. Klevit, Structural Consequences of Histidine Phosphorylation: NMR Characterization of the Phosphohistidine Form of Histidine-Containing Protein from *Bacillus subtilis* and *Escherichia coli*, *Biochemistry* 33, 15271-15282 (1994)
- V. L. Robinson, A. M. Stock, High energy exchange: proteins that make or break phosphoramidate bonds, *Structure* 7, R47-R53 (1999)



- A. R. S. Ross, Identification of Histidine Phosphorylations in Proteins Using Mass Spectrometry and Affinity-Based Techniques, *Methods in Enzymology* 423, 549-572 (2007)
- R. K. Saiki, D. H. Gelfand, S. Stoffel, S. J. Scharf, R. Higuchi, G. T. Horn, K. B. Mullis, H. A. Erlich, Primer-Directed Enzymatic Amplification of DNA with a Thermostable DNA Polymerase, *Science* 239, 487-491 (1988)
- O. Schilling, I. Langbein, M. Müller, M. H. Schmalisch, J. Stülke, A protein-dependent riboswitch controlling *ptsGHI* operon expression in *Bacillus subtilis*: RNA structure rather than sequence provides interaction specificity, *Nucleic Acids Research* 32, 9 2853-2864 (2004)
- M. H. Schmalisch, S. Bachem, J. Stülke, Control of the *Bacillus subtilis* Antiterminator Protein GlcT by Phosphorylation, *J. Biol. Chem.* 278, 51, 51108-51115 (2003)
- H. Schmidt, S. Himmel, K. F. A. Walter, V. Klaukien, M. Funk, D. Lee, Transverse relaxation-optimized HCN experiment for tautomeric states of histidine sidechains, *J. Korean Magnetic Resonance Society* 12, 89-95 (2008)
- O. Schrecker, R. Stein, W. Hengstberg, M. Gassner, D. Stehlik, The Staphylococcal PEP Dependent Phosphotransferase System, Proton Magnetic Resonance (PMR) Studies on the Phosphoryl Carrier Protein HPr: Evidence for a Phosphohistidine Residue in the Intact Phospho-HPr Molecule, *FEBS Letters* 51, 309-312 (1975)
- C. D. Schwieters, J.-Y. Suh, A. Grishaev, R. Ghirlando, Y. Takayama, G. M. Clore, Solution Structure of the 128 kDa Enzyme I Dimer from *Escherichia coli* and Its 146 kDa Complex with HPr Using Residual Dipolar Couplings and Small- and Wide-Angle X-ray Scattering, *JACS* 132, 37, 13026-13045 (2010)
- R. K. Scopes, Measurement of Protein by Spectrophotometry at 205 nm, *Analytical Biochemistry* 59, 277-282 (1974)
- A. Severage, F. Jüttner, E. Breitmaier, G. Jung, pH-Abhängigkeit der  $^{13}\text{C}$ - $^{15}\text{N}$ -Kopplungskonstanten  $^{15}\text{N}$ -hochmarkierter Aminosäuren, gewonnen aus Algenmassenkulturen, *Biochimica et Biophysica Acta* 437, 289-300 (1976)
- S. Srivastava, Z. Li, K. Ko, P. Choudhury, M. Albaqumi, A. K. Johnson, Y. Yan, J. M. Backer, D. Unutmaz, W. A. Coetzee, E. Y. Skolnik, Histidine Phosphorylation of the Potassium Channel KCa3.1 by Nucleoside Diphosphate Kinase B Is Required for Activation of KCa3.1 and CD4 T Cells, *Molecular Cell* 24, 665-675, (2006)

- J. Stülke, I. Martin-Verstraete, M. Zagorec, M. Rose, A. Klier, G. Rapoport, Induction of the *Bacillus subtilis ptsGHI* operon by glucose is controlled by a novel antiterminator, GlcT, *Molecular Microbiology* 25, 65-78 (1997)
- P. S. Steeg, D. Palmieri, T. Ouatas, M. Salerno, Histidine kinases and histidine phosphorylated proteins in mammalian cell biology, signal transduction and cancer, *Cancer Letters* 190, 1-12 (2003)
- M. G. Surette, M. Levit, Y. Liu, G. Lukat, E. G. Ninfa, A. Ninfa, J. B. Stock, Dimerization Is Required for the Activity of the Protein Histidine Kinase CheA That Mediates Signal Transduction in Bacterial Chemotaxis, *J. Biol. Chem.* 271, 2, 939-945 (1996)
- P. Thomason, R. Kay, Eukaryotic signal transduction via histidine-aspartate phosphorelay, *J. of Cell Science* 113, 3141-3150 (2000)
- P. Tortosa, S. Aymerich, C. Lindner, M. H. Saier (Jr.), J. Reizer, D. Le Coq, Multiple Phosphorylation of SacY, a *Bacillus subtilis* Transcriptional Antiterminator Negatively Controlled by the Phosphotransferase System, *J. Biol. Chem.* 272, 27, 17230-17237 (1997)
- P. Tortosa, N. Declerck, H. Dutartre, C. Lindner, J. Deutscher, D. Le Coq, Sites of positive and negative regulation in the *Bacillus subtilis* antiterminators LicT and SacY, *Molecular Microbiology* 41, 6, 1381-1393 (2001)
- A. A. Van Dijk, L. C. M. De Lange, W. W. Bachovchin, G. T. Robillard, Effect of Phosphorylation on Hydrogen-Bonding Interactions of the Active Site Histidine of the Phosphocarrier Protein HPr of the Phosphoenolpyruvate-Dependent Phosphotransferase System Determined by <sup>15</sup>N NMR Spectroscopy, *Biochemistry* 29, 8164-8171 (1990)
- H. van Tilbeurgh, D. Le Coq, N. Declerck, Crystal structure of an activated form of the PTS regulation domain from the LicT transcriptional antiterminator, *The EMBO Journal* 20, 14, 3789-3799 (2001)
- H. van Tilbeurgh, N. Declerck, Structural insights into the regulation of bacterial signalling proteins containing PRDs, *Current Opinion in Structural Biology* 11, 685-693 (2001)
- H. J. Vogel, W. A. Bridger, A Phosphorus 31 Nuclear Magnetic Resonance Study of the Intermediates of the *Escherichia coli* Succinyl Coenzyme A Synthetase Reaction, *J. Biol. Chem.* 257, 9, 4834-4842 (1982)
- H. J. Vogel, Phosphorus-31 Nuclear Magnetic Resonance of Phosphoproteins, *Methods in Enzymology* 177, 263-282 (1989)

- E. B. Waygood, E. Erickson, O. A. L. El-Kabbani, L. T. J. Delbaere, Characterization of Phosphorylated Histidine-Containing Protein (HPr) of the Bacterial Phosphoenolpyruvate: Sugar Phosphotransferase System, *Biochemistry* 24, 6938-6945 (1985)
- N. Weigel, E. B. Waygood, M. A. Kukuruzinska, A. Nakazawa, S. Roseman, Sugar Transport by the Bacterial Phosphotransferase System, Isolation and Characterization of Enzyme I from *Salmonella typhimurium*, *J. Biol. Chem.* 257, 23, 14461-14469 (1982)
- B. Wrackmeyer, C. Köhler, W. Milius, J. M. Grevy, Z. García-Hernández, R. Contreras, Aminophosphanes with Bulky Amino Groups: Molecular Structure, Coupling Constants  $^1J(^{31}\text{P}, ^{15}\text{N})$  and  $^2J(^{31}\text{P}, ^{29}\text{Si})$ , and Isotope-Induced Chemical Shifts  $^1\delta^{14/15}\text{N}(^{31}\text{P})$ , *Heteroatom Chemistry* 13, 7, 667-676 (2002)
- A. Xu, J. Hao, Z. Zhang, T. Tian, S. Jiang, J. Hao, C. Liu, L. Huang, X. Xiao, D. He, 14-kDa phosphohistidine phosphatase and its role in human lung cancer cell migration and invasion, *Lung cancer* 67, 48-56 (2010)
- H. Zhou, F. W. Dahlquist, Phosphotransfer Sites of the Chemotaxis-Specific Protein Kinase CheA as Revealed by NMR, *Biochemistry* 36, 699-710 (1997)
- X.-L. Zu, P. G. Besant, A. Imhof, P. V. Attwood, Mass spectrometric analysis of protein histidine phosphorylation, *Amino Acids* 32, 347-357 (2007)

## 9 Appendix

### Tobacco Etch Virus (TEV) protease

A pMALC-TEV plasmid, coding for the MBP fusion protein of the TEV protease with a TEV cleavage site between MBP and TEV, was transformed into BL21 Codon Plus for protein overexpression. For this purpose, 1 ml of LB medium, containing ampiciline ( $50 \mu\text{g ml}^{-1}$ ) and chloramphenicol ( $50 \mu\text{g ml}^{-1}$ ), was inoculated and cells were grown for 6 hours at  $37^\circ\text{C}$ .  $50 \mu\text{l}$  of this culture were used to inoculate 20 ml of LB medium for overnight growth. At the next morning the grown cells were diluted 1:80 compared to 750 ml of LB medium to start the final cultivation. After the bacterial growth ( $37^\circ\text{C}$ ) reached the  $\text{OD}_{600}$  of 0.3 the culture was cooled down to  $17^\circ\text{C}$ . Upon reaching an  $\text{OD}_{600}$  of 0.6 to 0.7 the protein overexpression was induced by adding IPTG to a final concentration of 0.4 mM. The overexpression took place overnight at  $17^\circ\text{C}$  and the harvested cells were stored at  $-80^\circ\text{C}$ .

The frozen cells were resuspended on ice in 40 ml lysis buffer (Table 9.1) and sonication was performed 8x 20 sec (approx. 90 % of the maximum power) to break the cells. Afterwards, the cell debris was centrifuged at  $4^\circ\text{C}$  for 45 minutes at 25,000 rcf. The supernatant was incubated for 45 minutes at  $4^\circ\text{C}$  with 3 ml of equilibrated Ni-NTA agarose. 10 ml single use plastic columns (PIERCE) were used to collect the loaded resin, which was washed with 50 ml of the lysis buffer followed by another 60 ml of the wash buffer. The elution was done stepwise (10x 2 ml) with elution buffer I and II. The protein content of each fraction was checked by SDS-PAGE analysis. The elution buffer III was only applied if there was still protein attached to the resin. After elution, the pooled fractions were dialysed overnight at  $4^\circ\text{C}$  against the dialysis buffer. VIVA spin concentrators (MWCO: 10,000; Sartorius) were used to concentrate the dialysed protein up to  $2 \text{ mg ml}^{-1}$ . After concentrating the protein, glycerol was added to dilute the TEV protease down to a final concentration of  $1 \text{ mg ml}^{-1}$  and was stored at  $-80^\circ\text{C}$ .

Name	Chemicals	Amount	Remarks
lysis buffer	Tris HCl	20 mM	pH 8.0
	NaCl	100 mM	
	Imidazole	5 mM	
	2-mercaptoethanol	10 mM	
	PMSF	0.5 mM (final)	
wash buffer	Tris HCl	20 mM	pH 8.0
	NaCl	100 mM	
	Imidazole	20 mM	
	PMSF	0.5 mM (final)	
	2-mercaptoethanol	10 mM	
elution buffer I	Tris HCl	20 mM	pH 8.0
	NaCl	100 mM	
	Imidazole	100 mM	
	2-mercaptoethanol	10 mM	
	PMSF	0.5 mM (final)	
elution buffer II	Tris HCl	20 mM	pH 8.0
	NaCl	100 mM	
	Imidazole	300 mM	
	2-mercaptoethanol	10 mM	
	PMSF	0.5 mM (final)	
elution buffer III	Tris HCl	20 mM	pH 8.0
	NaCl	100 mM	
	Imidazole	500 mM	
	2-mercaptoethanol	10 mM	
	PMSF	0.5 mM (final)	
dialysis buffer	Tris HCl	100 mM	pH 7.5
	EDTA	1 mM	
	DTT	5 mM	

**Table 9.1:** List of buffers, which were used for the purification of the TEV protease. PMSF needs to be added freshly.

## Chemical shift (cs) list of PRDI

Res. Nr.	Res. label	At. name	cs [ppm]	Res. Nr.	Res. label	At. name	cs [ppm]
2	SER	CA	58.312	6	LEU	CD1	24.004
2	SER	CB	63.250	6	LEU	CD2	23.780
2	SER	HA	4.432	6	LEU	H	7.916
2	SER	HB2	3.841	6	LEU	HA	4.086
2	SER	HB3	3.841	6	LEU	HB2	1.708
3	ASP	CA	54.489	6	LEU	HB3	1.604
3	ASP	CB	40.558	6	LEU	HG	1.610
3	ASP	H	8.579	6	LEU	HD1	0.867
3	ASP	HA	4.527	6	LEU	HD2	0.824
3	ASP	HB2	2.595	6	LEU	N	120.094
3	ASP	HB3	2.686	7	VAL	CA	65.136
3	ASP	N	122.181	7	VAL	CB	31.590
4	GLU	CA	57.843	7	VAL	CG1	20.627
4	GLU	CB	29.251	7	VAL	CG2	21.722
4	GLU	CG	36.121	7	VAL	H	7.847
4	GLU	H	8.440	7	VAL	HA	3.686
4	GLU	HA	4.106	7	VAL	HB	2.060
4	GLU	HB2	1.971	7	VAL	HB	2.060
4	GLU	HB3	2.040	7	VAL	HG1	0.899
4	GLU	HG2	2.260	7	VAL	HG2	0.960
4	GLU	HG3	2.260	7	VAL	N	120.899
4	GLU	N	121.719	8	ASP	CA	56.402
5	LYS	CA	57.110	8	ASP	CB	40.354
5	LYS	CB	31.995	8	ASP	H	7.805
5	LYS	CG	24.543	8	ASP	HA	4.477
5	LYS	CD	28.541	8	ASP	HB2	2.682
5	LYS	CE	41.550	8	ASP	HB3	2.759
5	LYS	H	8.236	8	ASP	N	121.091
5	LYS	HA	4.253	9	ILE	CA	63.647
5	LYS	HB2	1.847	9	ILE	CB	38.011
5	LYS	HB3	1.847	9	ILE	CG1	28.914
5	LYS	HG2	1.479	9	ILE	CG2	17.679
5	LYS	HG3	1.436	9	ILE	CD1	13.918
5	LYS	HD2	1.686	9	ILE	H	8.043
5	LYS	HD3	1.686	9	ILE	HA	3.874
5	LYS	HE2	2.962	9	ILE	HB	1.849
5	LYS	HE3	2.962	9	ILE	HG12	1.732
5	LYS	N	120.349	9	ILE	HG13	0.999
6	LEU	CA	56.511	9	ILE	HG2	0.801
6	LEU	CB	41.168	9	ILE	HD1	0.758
6	LEU	CG	26.911	9	ILE	N	118.895

Res. Nr.	Res. label	At. name	cs [ppm]	Res. Nr.	Res. label	At. name	cs [ppm]
10	SER	CA	62.305	14	ILE	N	121.284
10	SER	CB	58.003	15	TYR	CA	60.912
10	SER	H	8.301	15	TYR	CB	37.288
10	SER	HA	3.875	15	TYR	CD1	133.006
10	SER	N	115.841	15	TYR	CE1	117.604
11	ASN	CA	55.927	15	TYR	H	8.193
11	ASN	CB	37.380	15	TYR	HA	4.214
11	ASN	H	8.209	15	TYR	HB2	3.176
11	ASN	HA	4.362	15	TYR	HB3	3.176
11	ASN	HB2	2.733	15	TYR	HD1	7.210
11	ASN	HB3	2.930	15	TYR	HE1	6.815
11	ASN	HD21	7.782	15	TYR	N	121.335
11	ASN	HD22	6.808	16	HIS	CA	60.398
11	ASN	N	119.773	16	HIS	CB	31.601
11	ASN	ND2	112.769	16	HIS	CD2	114.675
12	ASP	CA	57.234	16	HIS	CE1	139.292
12	ASP	CB	39.911	16	HIS	H	8.018
12	ASP	H	7.987	16	HIS	HA	4.236
12	ASP	HA	4.472	16	HIS	HB2	3.080
12	ASP	HB2	2.647	16	HIS	HB3	3.309
12	ASP	HB3	2.864	16	HIS	HD2	6.473
12	ASP	N	121.264	16	HIS	HE1	7.741
13	VAL	CA	65.981	16	HIS	N	119.539
13	VAL	CB	31.203	17	ILE	CA	66.055
13	VAL	CG1	22.510	17	ILE	CB	37.867
13	VAL	CG2	22.330	17	ILE	CG1	29.011
13	VAL	H	8.328	17	ILE	CG2	16.953
13	VAL	HA	3.776	17	ILE	CD1	13.948
13	VAL	HB	2.309	17	ILE	H	8.379
13	VAL	HG1	1.033	17	ILE	HA	3.245
13	VAL	HG2	0.920	17	ILE	HB	1.806
13	VAL	N	120.423	17	ILE	HG12	1.986
14	ILE	CA	64.436	17	ILE	HG13	0.677
14	ILE	CB	36.387	17	ILE	HG2	0.810
14	ILE	CG1	29.258	17	ILE	HD1	0.736
14	ILE	CG2	17.171	17	ILE	N	116.896
14	ILE	CD1	12.347	18	SER	CA	61.351
14	ILE	H	8.303	18	SER	CB	62.532
14	ILE	HA	3.439	18	SER	H	8.484
14	ILE	HB	1.754	18	SER	HA	4.143
14	ILE	HG12	0.919	18	SER	HB2	3.892
14	ILE	HG13	1.361	18	SER	HB3	3.953
14	ILE	HG2	0.497	18	SER	N	116.686
14	ILE	HD1	0.521	19	ASN	CA	55.492

Res. Nr.	Res. label	At. name	cs [ppm]	Res. Nr.	Res. label	At. name	cs [ppm]
19	ASN	CB	38.329	23	HIS	H	8.092
19	ASN	H	8.187	23	HIS	HA	4.584
19	ASN	HA	4.287	23	HIS	HB2	3.020
19	ASN	HB2	2.549	23	HIS	HB3	2.788
19	ASN	HB3	2.549	23	HIS	HD2	6.894
19	ASN	HD21	7.359	23	HIS	HE1	7.816
19	ASN	HD22	6.224	23	HIS	N	117.604
19	ASN	N	119.329	24	SER	CA	58.227
19	ASN	ND2	112.245	24	SER	CB	62.910
20	ARG	CA	56.399	24	SER	HA	4.313
20	ARG	CB	30.423	24	SER	HB2	3.791
20	ARG	CG	28.072	24	SER	HB3	3.753
20	ARG	CD	40.899	25	LEU	CA	53.597
20	ARG	H	8.268	25	LEU	CB	41.299
20	ARG	HA	4.093	25	LEU	CG	26.531
20	ARG	HB2	1.596	25	LEU	CD1	25.491
20	ARG	HB3	1.659	25	LEU	CD2	22.888
20	ARG	HG2	1.132	25	LEU	H	8.883
20	ARG	HG3	0.726	25	LEU	HA	4.358
20	ARG	HD2	3.088	25	LEU	HB2	1.182
20	ARG	HD3	3.117	25	LEU	HB3	1.898
20	ARG	N	117.589	25	LEU	HG	1.692
21	THR	CA	61.238	25	LEU	HD1	0.744
21	THR	CB	70.301	25	LEU	HD2	0.700
21	THR	CG2	21.608	25	LEU	N	124.256
21	THR	H	7.635	26	ASN	CA	52.411
21	THR	HA	4.306	26	ASN	CB	38.740
21	THR	HB	4.250	26	ASN	H	7.979
21	THR	HG2	1.149	26	ASN	HA	4.534
21	THR	N	106.445	26	ASN	HB2	3.001
22	ASN	CA	53.979	26	ASN	HB3	3.001
22	ASN	CB	37.411	26	ASN	HD21	7.710
22	ASN	H	7.905	26	ASN	HD22	7.114
22	ASN	HA	4.357	26	ASN	N	119.072
22	ASN	HB2	2.715	26	ASN	ND2	113.413
22	ASN	HB3	3.060	27	GLU	CA	59.224
22	ASN	HD21	7.498	27	GLU	CB	29.260
22	ASN	HD22	6.724	27	GLU	CG	35.591
22	ASN	N	119.322	27	GLU	H	8.866
22	ASN	ND2	112.303	27	GLU	HA	3.857
23	HIS	CA	55.713	27	GLU	HB2	1.913
23	HIS	CB	31.876	27	GLU	HB3	1.913
23	HIS	CD2	119.609	27	GLU	HG2	2.076
23	HIS	CE1	137.718	27	GLU	HG3	2.076



Res. Nr.	Res. label	At. name	cs [ppm]	Res. Nr.	Res. label	At. name	cs [ppm]
27	GLU	N	119.529	31	ILE	HG12	1.722
28	HIS	CA	58.399	31	ILE	HG13	1.154
28	HIS	CB	29.628	31	ILE	HG2	0.890
28	HIS	CD2	119.440	31	ILE	HD1	0.844
28	HIS	CE1	138.628	31	ILE	N	120.210
28	HIS	H	8.097	32	ALA	CA	54.968
28	HIS	HA	4.406	32	ALA	CB	17.690
28	HIS	HB2	3.190	32	ALA	H	7.704
28	HIS	HB3	3.190	32	ALA	HA	4.273
28	HIS	HD2	6.947	32	ALA	HB	1.410
28	HIS	HE1	7.763	32	ALA	N	121.512
28	HIS	N	117.902	33	LEU	CA	57.481
29	ILE	CA	62.800	33	LEU	CB	41.638
29	ILE	CB	37.074	33	LEU	CG	26.908
29	ILE	CG1	28.265	33	LEU	CD1	25.228
29	ILE	CG2	18.403	33	LEU	CD2	22.566
29	ILE	CD1	12.865	33	LEU	H	8.462
29	ILE	H	7.800	33	LEU	HA	3.850
29	ILE	HA	3.691	33	LEU	HB2	1.753
29	ILE	HB	1.843	33	LEU	HB3	1.182
29	ILE	HG12	1.502	33	LEU	HG	1.462
29	ILE	HG13	0.982	33	LEU	HD1	0.541
29	ILE	HG2	0.841	33	LEU	HD2	0.286
29	ILE	HD1	0.799	33	LEU	N	118.457
29	ILE	N	120.418	34	THR	CA	67.734
30	HIS	CA	59.672	34	THR	CB	67.237
30	HIS	CB	30.901	34	THR	CG2	21.166
30	HIS	CD2	117.772	34	THR	H	8.024
30	HIS	CE1	137.935	34	THR	HA	4.334
30	HIS	H	8.091	34	THR	HB	3.672
30	HIS	HA	3.996	34	THR	HG2	1.162
30	HIS	HB2	3.184	34	THR	N	116.253
30	HIS	HB3	3.184	35	ASP	CA	56.899
30	HIS	HD2	6.670	35	ASP	CB	39.646
30	HIS	HE1	7.584	35	ASP	H	8.511
30	HIS	N	119.968	35	ASP	HA	4.244
31	ILE	CA	64.190	35	ASP	HB2	2.850
31	ILE	CB	37.972	35	ASP	HB3	2.850
31	ILE	CG1	28.761	35	ASP	N	122.613
31	ILE	CG2	17.009	36	HIS	CE1	136.755
31	ILE	CD1	12.883	36	HIS	HE1	7.169
31	ILE	H	8.086	37	ILE	CA	65.220
31	ILE	HA	3.716	37	ILE	CB	37.398
31	ILE	HB	1.849	37	ILE	CG1	29.033

Res. Nr.	Res. label	At. name	cs [ppm]	Res. Nr.	Res. label	At. name	cs [ppm]
37	ILE	CG2	17.072	41	ILE	HD1	0.697
37	ILE	CD1	12.995	41	ILE	N	119.075
37	ILE	H	8.281	42	LYS	CA	59.468
37	ILE	HA	3.332	42	LYS	CB	32.314
37	ILE	HB	1.905	42	LYS	CG	24.990
37	ILE	HG12	1.721	42	LYS	CD	29.009
37	ILE	HG13	0.907	42	LYS	CE	41.529
37	ILE	HG2	0.757	42	LYS	H	8.001
37	ILE	HD1	0.662	42	LYS	HA	3.996
37	ILE	N	119.328	42	LYS	HB2	1.900
38	ALA	CA	55.221	42	LYS	HB3	1.954
38	ALA	CB	17.698	42	LYS	HG2	1.471
38	ALA	H	8.164	42	LYS	HG3	1.381
38	ALA	HA	3.867	42	LYS	HD2	1.655
38	ALA	HB	1.412	42	LYS	HD3	1.655
38	ALA	N	121.062	42	LYS	HE2	2.820
39	PHE	CA	59.149	42	LYS	HE3	2.923
39	PHE	CB	38.074	42	LYS	N	121.262
39	PHE	CD1	130.435	43	ARG	CA	59.684
39	PHE	CZ	128.817	43	ARG	CB	29.863
39	PHE	H	8.106	43	ARG	CG	28.067
39	PHE	HA	4.332	43	ARG	CD	43.827
39	PHE	HB2	2.772	43	ARG	H	8.269
39	PHE	HB3	2.863	43	ARG	HA	4.046
39	PHE	HD1	6.994	43	ARG	HB2	1.862
39	PHE	HZ	7.060	43	ARG	HB3	1.862
39	PHE	N	118.527	43	ARG	HG2	1.504
40	ALA	CA	54.835	43	ARG	HG3	1.504
40	ALA	CB	16.990	43	ARG	HD2	2.839
40	ALA	H	8.328	43	ARG	HD3	2.839
40	ALA	HA	3.709	43	ARG	N	117.758
40	ALA	HB	1.285	44	GLN	CA	58.461
40	ALA	N	123.271	44	GLN	CB	26.907
41	ILE	CA	65.590	44	GLN	CG	33.670
41	ILE	CB	37.885	44	GLN	H	7.514
41	ILE	CG1	29.506	44	GLN	HA	4.126
41	ILE	CG2	16.262	44	GLN	HB2	2.101
41	ILE	CD1	13.908	44	GLN	HB3	2.287
41	ILE	H	8.257	44	GLN	HG2	2.420
41	ILE	HA	3.482	44	GLN	HG3	2.361
41	ILE	HB	1.816	44	GLN	HE21	7.419
41	ILE	HG12	1.847	44	GLN	HE22	6.702
41	ILE	HG13	0.805	44	GLN	N	119.220
41	ILE	HG2	0.789	44	GLN	NE2	110.796

Res. Nr.	Res. label	At. name	cs [ppm]	Res. Nr.	Res. label	At. name	cs [ppm]
45	GLN	CA	58.036	49	ASP	HB2	2.369
45	GLN	CB	28.096	49	ASP	HB3	2.480
45	GLN	CG	33.993	49	ASP	N	127.622
45	GLN	H	8.356	50	MET	CA	54.059
45	GLN	HA	3.969	50	MET	CB	32.374
45	GLN	HB2	2.043	50	MET	CG	32.544
45	GLN	HB3	2.311	50	MET	CE	17.085
45	GLN	HG2	2.376	50	MET	H	8.276
45	GLN	HG3	2.566	50	MET	HA	4.146
45	GLN	HE21	7.402	50	MET	HB2	1.467
45	GLN	HE22	6.734	50	MET	HB3	1.424
45	GLN	N	119.970	50	MET	HG2	2.305
45	GLN	NE2	111.453	50	MET	HG3	2.090
46	GLN	CA	55.399	50	MET	HE	1.532
46	GLN	CB	28.762	50	MET	N	124.788
46	GLN	CG	33.647	51	LYS	CA	56.191
46	GLN	H	7.779	51	LYS	CB	32.351
46	GLN	HA	4.202	51	LYS	CG	25.001
46	GLN	HB2	2.167	51	LYS	CD	28.442
46	GLN	HB3	2.071	51	LYS	CE	41.751
46	GLN	HG2	2.423	51	LYS	H	8.183
46	GLN	HG3	2.372	51	LYS	HA	4.031
46	GLN	HE21	7.399	51	LYS	HB2	1.662
46	GLN	HE22	6.560	51	LYS	HB3	1.754
46	GLN	N	115.830	51	LYS	HG2	1.379
46	GLN	NE2	110.377	51	LYS	HG3	1.379
47	GLY	CA	45.569	51	LYS	HD2	1.566
47	GLY	H	7.758	51	LYS	HD3	1.636
47	GLY	HA2	3.796	51	LYS	HE2	2.927
47	GLY	HA3	3.984	51	LYS	HE3	2.927
47	GLY	N	107.510	51	LYS	N	127.364
48	PHE	CA	55.925	52	ASN	CA	48.013
48	PHE	CB	39.990	52	ASN	CB	39.927
48	PHE	CD1	131.347	52	ASN	H	8.763
48	PHE	H	7.960	52	ASN	HA	5.083
48	PHE	HA	4.675	52	ASN	HB2	2.175
48	PHE	HB2	2.912	52	ASN	HB3	2.979
48	PHE	HB3	2.782	52	ASN	HD21	6.979
48	PHE	HD1	6.950	52	ASN	HD22	6.194
48	PHE	N	120.567	52	ASN	N	116.500
49	ASP	CA	52.602	52	ASN	ND2	106.633
49	ASP	CB	41.257	53	PRO	CA	62.527
49	ASP	H	8.204	53	PRO	CB	31.294
49	ASP	HA	4.472	53	PRO	CG	25.146

Res. Nr.	Res. label	At. name	cs [ppm]	Res. Nr.	Res. label	At. name	cs [ppm]
53	PRO	CD	50.314	56	MET	HE	1.964
53	PRO	HA	4.324	56	MET	N	118.737
53	PRO	HB2	1.872	57	GLU	CA	60.315
53	PRO	HB3	0.856	57	GLU	CB	28.821
53	PRO	HG2	0.466	57	GLU	CG	36.968
53	PRO	HG3	1.646	57	GLU	H	9.848
53	PRO	HD2	3.350	57	GLU	HA	3.851
53	PRO	HD3	3.629	57	GLU	HB2	1.782
54	PHE	CA	54.873	57	GLU	HB3	1.875
54	PHE	CB	37.807	57	GLU	HG2	2.197
54	PHE	CD1	130.957	57	GLU	HG3	2.498
54	PHE	CE1	131.070	57	GLU	N	122.392
54	PHE	CZ	128.523	58	THR	CA	67.547
54	PHE	H	7.091	58	THR	CB	67.735
54	PHE	HA	5.320	58	THR	CG2	21.468
54	PHE	HB2	2.114	58	THR	H	8.188
54	PHE	HB3	2.164	58	THR	HA	4.561
54	PHE	HD1	6.803	58	THR	HB	3.955
54	PHE	HE1	7.216	58	THR	HG2	1.609
54	PHE	HZ	6.774	58	THR	N	116.182
54	PHE	N	116.719	59	GLN	CA	58.996
55	LEU	CA	59.359	59	GLN	CB	26.507
55	LEU	CB	41.332	59	GLN	CG	33.394
55	LEU	CG	26.350	59	GLN	H	7.574
55	LEU	CD1	25.133	59	GLN	HA	3.185
55	LEU	CD2	23.809	59	GLN	HB2	1.585
55	LEU	H	7.734	59	GLN	HB3	0.528
55	LEU	HA	3.810	59	GLN	HG2	1.697
55	LEU	HB2	1.736	59	GLN	HG3	1.697
55	LEU	HB3	1.643	59	GLN	HE21	6.930
55	LEU	HG	1.724	59	GLN	HE22	6.633
55	LEU	HD1	0.940	59	GLN	N	121.950
55	LEU	HD2	0.944	59	GLN	NE2	109.936
55	LEU	N	124.900	60	SER	CA	60.281
56	MET	CA	58.024	60	SER	CB	62.774
56	MET	CB	31.134	60	SER	H	7.421
56	MET	CG	32.017	60	SER	HA	4.001
56	MET	CE	16.957	60	SER	HB2	3.790
56	MET	H	8.723	60	SER	HB3	3.757
56	MET	HA	4.007	60	SER	N	109.925
56	MET	HB2	1.946	61	LEU	CA	56.607
56	MET	HB3	1.840	61	LEU	CB	42.937
56	MET	HG2	2.565	61	LEU	CG	26.306
56	MET	HG3	2.407	61	LEU	CD1	24.498

Res. Nr.	Res. label	At. name	cs [ppm]	Res. Nr.	Res. label	At. name	cs [ppm]
61	LEU	CD2	22.900	65	GLU	H	10.248
61	LEU	H	7.604	65	GLU	HA	3.709
61	LEU	HA	3.837	65	GLU	HB2	1.994
61	LEU	HB2	1.196	65	GLU	HB3	2.291
61	LEU	HB3	0.303	65	GLU	HG2	2.117
61	LEU	HG	1.243	65	GLU	HG3	2.348
61	LEU	HD1	0.621	65	GLU	N	121.276
61	LEU	HD2	0.522	66	TYR	CA	62.317
61	LEU	N	120.588	66	TYR	CB	39.175
62	TYR	CA	53.121	66	TYR	CD1	132.379
62	TYR	CB	37.735	66	TYR	CE1	117.831
62	TYR	CD1	132.050	66	TYR	H	9.187
62	TYR	CE1	116.831	66	TYR	HA	3.783
62	TYR	H	7.766	66	TYR	HB2	2.923
62	TYR	HA	5.120	66	TYR	HB3	3.181
62	TYR	HB2	2.866	66	TYR	HD1	6.736
62	TYR	HB3	3.385	66	TYR	HE1	6.556
62	TYR	HD1	6.830	66	TYR	N	119.335
62	TYR	HE1	6.051	67	GLN	CA	58.255
62	TYR	N	115.602	67	GLN	CB	26.916
63	PRO	CA	65.820	67	GLN	CG	32.455
63	PRO	CB	31.119	67	GLN	H	7.800
63	PRO	CG	27.500	67	GLN	HA	4.062
63	PRO	CD	49.567	67	GLN	HB2	2.224
63	PRO	HA	4.476	67	GLN	HB3	2.343
63	PRO	HB2	1.977	67	GLN	HG2	2.540
63	PRO	HB3	2.403	67	GLN	HG3	2.332
63	PRO	HG2	2.094	67	GLN	HE21	8.348
63	PRO	HG3	2.094	67	GLN	HE22	6.946
63	PRO	HD2	3.240	67	GLN	N	118.054
63	PRO	HD3	3.709	67	GLN	NE2	114.255
64	GLU	CA	59.444	68	ILE	CA	64.907
64	GLU	CB	28.816	68	ILE	CB	38.003
64	GLU	CG	36.078	68	ILE	CG1	28.787
64	GLU	H	8.619	68	ILE	CG2	18.630
64	GLU	HA	4.221	68	ILE	CD1	14.389
64	GLU	HB2	2.069	68	ILE	H	8.043
64	GLU	HB3	1.970	68	ILE	HA	3.654
64	GLU	HG2	2.302	68	ILE	HB	1.727
64	GLU	HG3	2.302	68	ILE	HG12	2.006
64	GLU	N	119.951	68	ILE	HG13	0.686
65	GLU	CA	61.747	68	ILE	HG2	0.807
65	GLU	CB	27.818	68	ILE	HD1	0.697
65	GLU	CG	38.704	68	ILE	N	118.665

Res. Nr.	Res. label	At. name	cs [ppm]	Res. Nr.	Res. label	At. name	cs [ppm]
69	ALA	CA	55.030	73	ILE	CG1	28.576
69	ALA	CB	20.063	73	ILE	CG2	17.456
69	ALA	H	8.465	73	ILE	CD1	10.710
69	ALA	HA	3.649	73	ILE	H	8.334
69	ALA	HB	1.410	73	ILE	HA	3.657
69	ALA	N	122.163	73	ILE	HB	2.043
70	LYS	CA	59.813	73	ILE	HG12	1.534
70	LYS	CB	31.684	73	ILE	HG13	1.152
70	LYS	CG	24.794	73	ILE	HG2	0.796
70	LYS	CD	29.027	73	ILE	HD1	0.580
70	LYS	CE	41.744	73	ILE	N	121.869
70	LYS	H	8.372	74	ASP	CA	57.349
70	LYS	HA	3.583	74	ASP	CB	39.414
70	LYS	HB2	2.055	74	ASP	H	8.324
70	LYS	HB3	2.055	74	ASP	HA	4.410
70	LYS	HG2	1.381	74	ASP	HB2	2.582
70	LYS	HG3	1.470	74	ASP	HB3	2.745
70	LYS	HD2	1.668	74	ASP	N	120.536
70	LYS	HD3	1.734	75	MET	CA	58.916
70	LYS	HE2	3.027	75	MET	CB	33.073
70	LYS	HE3	3.027	75	MET	CG	31.295
70	LYS	N	120.187	75	MET	CE	15.793
71	GLU	CA	58.367	75	MET	H	7.917
71	GLU	CB	28.796	75	MET	HA	4.106
71	GLU	CG	35.395	75	MET	HB2	2.189
71	GLU	H	7.841	75	MET	HB3	2.010
71	GLU	HA	3.998	75	MET	HG2	2.514
71	GLU	HB2	2.681	75	MET	HG3	2.335
71	GLU	HB3	1.888	75	MET	HE	1.694
71	GLU	HG2	2.782	75	MET	N	120.196
71	GLU	HG3	2.417	76	ILE	CA	65.734
71	GLU	N	118.651	76	ILE	CB	37.889
72	VAL	CA	66.077	76	ILE	CG1	28.799
72	VAL	CB	30.895	76	ILE	CG2	17.494
72	VAL	CG1	21.964	76	ILE	CD1	14.269
72	VAL	CG2	23.357	76	ILE	H	8.375
72	VAL	H	8.496	76	ILE	HA	3.368
72	VAL	HA	3.593	76	ILE	HB	1.814
72	VAL	HB	2.468	76	ILE	HG12	1.873
72	VAL	HG1	0.903	76	ILE	HG13	0.692
72	VAL	HG2	1.094	76	ILE	HG2	0.795
72	VAL	N	119.556	76	ILE	HD1	0.684
73	ILE	CA	62.780	76	ILE	N	120.798
73	ILE	CB	34.990	77	ASN	CA	55.450

Res. Nr.	Res. label	At. name	cs [ppm]	Res. Nr.	Res. label	At. name	cs [ppm]
77	ASN	CB	37.416	81	GLY	HA3	3.859
77	ASN	H	8.503	81	GLY	N	109.062
77	ASN	HA	4.374	82	LEU	CA	52.857
77	ASN	HB2	2.927	82	LEU	CB	44.370
77	ASN	HB3	2.927	82	LEU	CG	25.919
77	ASN	HD21	7.567	82	LEU	CD1	23.773
77	ASN	HD22	6.565	82	LEU	CD2	25.821
77	ASN	N	118.994	82	LEU	H	7.572
77	ASN	ND2	107.083	82	LEU	HA	4.568
78	GLU	CA	58.763	82	LEU	HB2	1.485
78	GLU	CB	29.740	82	LEU	HB3	1.518
78	GLU	CG	35.803	82	LEU	HG	1.401
78	GLU	H	8.058	82	LEU	HD1	0.792
78	GLU	HA	4.005	82	LEU	HD2	0.722
78	GLU	HB2	2.048	82	LEU	N	118.127
78	GLU	HB3	2.131	83	CYS	CA	56.392
78	GLU	HG2	2.144	83	CYS	CB	26.739
78	GLU	HG3	2.144	83	CYS	H	8.133
78	GLU	N	118.887	83	CYS	HA	4.422
79	LYS	CA	58.245	83	CYS	HB2	2.538
79	LYS	CB	33.481	83	CYS	HB3	2.754
79	LYS	CG	25.874	83	CYS	N	119.733
79	LYS	CD	28.872	84	LEU	CA	53.576
79	LYS	CE	41.710	84	LEU	CB	40.359
79	LYS	H	8.392	84	LEU	CG	27.713
79	LYS	HA	4.132	84	LEU	CD1	25.508
79	LYS	HB2	1.751	84	LEU	CD2	24.070
79	LYS	HB3	1.751	84	LEU	H	9.268
79	LYS	HG2	1.518	84	LEU	HA	4.339
79	LYS	HG3	1.638	84	LEU	HB2	1.188
79	LYS	HD2	1.523	84	LEU	HB3	1.818
79	LYS	HD3	1.641	84	LEU	HG	1.795
79	LYS	HE2	2.909	84	LEU	HD1	0.801
79	LYS	HE3	2.965	84	LEU	HD2	0.758
79	LYS	N	116.790	84	LEU	N	127.393
80	ALA	CA	51.368	85	PRO	CA	62.033
80	ALA	CB	19.095	85	PRO	CB	32.567
80	ALA	H	8.655	85	PRO	CG	27.593
80	ALA	HA	4.453	85	PRO	CD	50.512
80	ALA	HB	1.354	85	PRO	HA	4.487
80	ALA	N	118.205	85	PRO	HB2	2.270
81	GLY	CA	46.484	85	PRO	HB3	2.326
81	GLY	H	7.619	85	PRO	HG2	2.101
81	GLY	HA2	3.948	85	PRO	HG3	2.189

Res. Nr.	Res. label	At. name	cs [ppm]	Res. Nr.	Res. label	At. name	cs [ppm]
85	PRO	HD2	3.638	90	GLY	N	101.637
85	PRO	HD3	3.798	91	PHE	CA	60.187
86	GLU	CA	58.749	91	PHE	CB	37.536
86	GLU	CB	29.057	91	PHE	CD1	131.300
86	GLU	CG	35.883	91	PHE	CZ	129.426
86	GLU	H	8.518	91	PHE	H	7.088
86	GLU	HA	3.874	91	PHE	HA	4.610
86	GLU	HB2	1.993	91	PHE	HB2	3.314
86	GLU	HB3	1.993	91	PHE	HB3	3.314
86	GLU	HG2	2.322	91	PHE	HD1	7.320
86	GLU	HG3	2.322	91	PHE	HZ	7.281
86	GLU	N	118.890	91	PHE	N	118.663
87	GLY	CA	48.044	92	ILE	CA	64.630
87	GLY	H	8.703	92	ILE	CB	36.578
87	GLY	HA2	3.803	92	ILE	CG1	29.181
87	GLY	HA3	4.022	92	ILE	CG2	16.763
87	GLY	N	104.863	92	ILE	CD1	11.336
88	GLU	CA	57.143	92	ILE	HB	1.926
88	GLU	CB	28.570	92	ILE	HD1	0.430
88	GLU	CG	34.863	93	ALA	CA	55.694
88	GLU	H	7.915	93	ALA	CB	16.982
88	GLU	HA	4.596	93	ALA	H	8.419
88	GLU	HB2	2.186	93	ALA	HA	3.848
88	GLU	HB3	2.034	93	ALA	HB	1.488
88	GLU	HG2	2.466	93	ALA	N	124.153
88	GLU	HG3	2.402	94	LEU	CA	57.448
88	GLU	N	116.454	94	LEU	CB	41.082
89	ILE	CA	65.124	94	LEU	CG	26.312
89	ILE	CB	37.769	94	LEU	CD1	25.750
89	ILE	CG1	29.609	94	LEU	CD2	22.415
89	ILE	CG2	17.460	94	LEU	H	7.810
89	ILE	CD1	13.914	94	LEU	HA	4.007
89	ILE	H	8.161	94	LEU	HB2	2.276
89	ILE	HA	3.216	94	LEU	HB3	2.276
89	ILE	HB	1.843	94	LEU	HG	2.291
89	ILE	HG12	1.721	94	LEU	HD1	1.391
89	ILE	HG13	0.559	94	LEU	HD2	0.927
89	ILE	HG2	0.030	94	LEU	N	114.534
89	ILE	HD1	0.931	95	HIS	CA	59.911
89	ILE	N	120.145	95	HIS	CB	29.921
90	GLY	CA	47.105	95	HIS	CE1	136.024
90	GLY	H	6.702	95	HIS	H	7.923
90	GLY	HA2	3.611	95	HIS	HA	4.355
90	GLY	HA3	3.737	95	HIS	HE1	7.349



Res. Nr.	Res. label	At. name	cs [ppm]	Res. Nr.	Res. label	At. name	cs [ppm]
95	HIS	N	122.605	99	ALA	HB	1.463
96	ILE	CA	66.218	99	ALA	N	123.251
96	ILE	CB	37.888	100	LEU	CA	55.463
96	ILE	CG1	29.239	100	LEU	CB	41.753
96	ILE	CG2	16.854	100	LEU	CG	26.294
96	ILE	CD1	14.170	100	LEU	CD1	25.152
96	ILE	H	8.857	100	LEU	CD2	21.693
96	ILE	HA	3.425	100	LEU	H	7.525
96	ILE	HB	1.821	100	LEU	HA	3.962
96	ILE	HG12	0.707	100	LEU	HB2	1.360
96	ILE	HG13	0.707	100	LEU	HB3	1.716
96	ILE	HG2	0.810	100	LEU	HG	1.740
96	ILE	HD1	0.742	100	LEU	HD1	0.745
96	ILE	N	119.119	100	LEU	HD2	0.495
97	HIS	CA	60.171	100	LEU	N	114.955
97	HIS	CB	28.072	101	THR	CA	61.267
97	HIS	CD2	123.924	101	THR	CB	69.381
97	HIS	CE1	138.235	101	THR	CG2	20.950
97	HIS	H	8.457	101	THR	H	7.293
97	HIS	HA	4.146	101	THR	HA	4.329
97	HIS	HB2	2.481	101	THR	HB	4.122
97	HIS	HB3	2.790	101	THR	HG2	0.999
97	HIS	HD2	6.462	101	THR	N	110.090
97	HIS	HE1	7.897	102	ASN	CA	55.100
97	HIS	N	116.164	102	ASN	CB	40.356
98	SER	CA	62.103	102	ASN	H	7.605
98	SER	CB	58.048	102	ASN	HA	4.464
98	SER	H	8.089	102	ASN	HB2	2.676
98	SER	HA	3.965	102	ASN	HB3	2.722
98	SER	N	114.306	102	ASN	HD21	7.402
99	ALA	CA	54.012	102	ASN	HD22	6.867
99	ALA	CB	18.514	102	ASN	N	126.978
99	ALA	H	8.370	102	ASN	ND2	112.526
99	ALA	HA	4.031				

**Table 9.2:** Chemical shift list of the non-phosphorylated PRDL.

Hiermit erkläre ich, dass diese Arbeit bisher von mir weder an der Mathematisch-Naturwissenschaftlichen Fakultät der Ernst-Moritz-Arndt-Universität Greifswald noch einer anderen wissenschaftlichen Einrichtung zum Zwecke der Promotion eingereicht wurde.

Ferner erkläre ich, dass ich diese Arbeit selbständig verfasst und keine anderen als die darin angegebenen Hilfsmittel benutzt habe.

Unterschrift des Promovenden

# 10 Curriculum Vitae

Name	Sebastian Himmel
Address	Radinkendorfer Str. 10
City	Beeskow
Postal Code	15848
Country	Germany
E-Mail	sebastian_himmel@gmx.de
City of birth	Beeskow
Date of birth	03/30/1982
Nationality	German
1988-2001	visiting elementary and secondary school
06/29/2001	"Abitur" certificate at the "Gymnasium Beeskow" as qualification for university studies
2001-2006	Biochemistry studies, Ernst-Moritz-Arndt University Greifswald
08/18/2006	Diploma in Biochemistry
	Diploma thesis: Kristallographische und NMR - spektroskopische Charakterisierung des Thiocyanatocobalamins, Advisor Prof. Dr. W. Hinrichs and Prof. Dr. K. Weisz
since 09/2006	PhD student at the Max Planck Institute for Biophysical Chemistry in the group of Prof. Dr. C. Griesinger (NMR based Structural Biology) in Göttingen and under supervision of Prof. Dr. K. Weisz, Ernst-Moritz-Arndt University Greifswald

Göttingen, April 12, 2011

# 11 Acknowledgement

I want to thank a multitude of people that helped me during the last years to finish my PhD thesis. I enjoyed the privilege to be a PhD student of Prof. Dr. Christian Griesinger and to work in Göttingen in his laboratory alongside with PhD students and post-docs from all over the world. He granted me the opportunity to develop and test my own ideas and theories, always open minded for discussions and new directions. Further, I thank Prof. Dr. Klaus Weisz from the University of Greifswald for the supervision during that time although I worked externally in Göttingen. He provided me always the possibility to report about my progress in his group and I feel very thankful for the excellent cooperation.

In the following I want to express my gratitude to all lab members, especially to Dr. Stefan Becker, who shared all the time the same interest in my project as I did, giving fine guidance and support in all directions. I appreciated our discussions and even more the opportunity to work together with a technical assistant, Sebastian Wolff, in order to finish the variety of aspects of my project. Karin Giller deserves a special thank for all the time and effort she spent in the beginning of my thesis to teach me all the basics I needed to manage my laboratory work. I also thank Sebastian Wolff who was a great and reliable help. He prepared dozens of samples for me. Gerhard Wolf sometimes suffered to measure all my phosphorylation samples but, however, we successfully optimized the conditions to obtain great results. Claudia Schwiegk did a great job to produce the RNA to study protein RNA interactions. Furthermore, I want to highlight the priceless effort of Gabriele Roddewig. She is working for the whole laboratory preparing solutions and media and cleaning whatever we have used. She always provided a helping hand. I thank all other members in the lab, e.g. Melanie Wegstroth and Yvonne Laukat, for the nice atmosphere and funny conversations.

Another great and special thank goes to Dr. Donghan Lee. He gave me a lot of high quality supervision. He helped me a lot to organize my projects, to find direction in my scientific goals and all the spectrometer related work. I welcome his fruitful discussions sometimes leading to nice controversies. However, he was always dedicated to my work, sometimes even spending hours till late in the night

apart from his family.

This project mainly originates from our collaboration partners at the University of Göttingen. I want to thank Prof. Dr. Jörg Stülke and Dr. Sebastian Hübner for all the discussions, explanations and practical help. I also thank Christine Diethmaier and Christopher Zschiedrich for generously providing material and support.

Further thanks goes to Dr. Stefan Becker, David Ban and Dr. Donghan Lee for carefully reading the manuscript of this thesis.

I thank Dr. Lukasz Skora and Dr. Min-Kyu Cho for additional help and a pleasant stay in Göttingen. I enjoyed all the time my stay in the "old cubic" among the "most crazy crew" of the department. Thanks to all members that endured me and made it a funny time. Among them I want to thank Dr. Nicolas Coudevylle who took care of me as the first post-doc.

I also want to thank our secretaries Siegrid Silberer and Petra Breiner who made sometimes things possible one could not imagine. Brigitta Angerstein was always a great help in organizing the helium filling. I have appreciated our good communication through the last years.

This entire work is dedicated to my wife Celina. I got all support from her that made it easy for me to enjoy my time in Göttingen but also to finish the PhD successfully.

I, finally, thank my parents, brothers and sisters as well as grandparents for all the support.